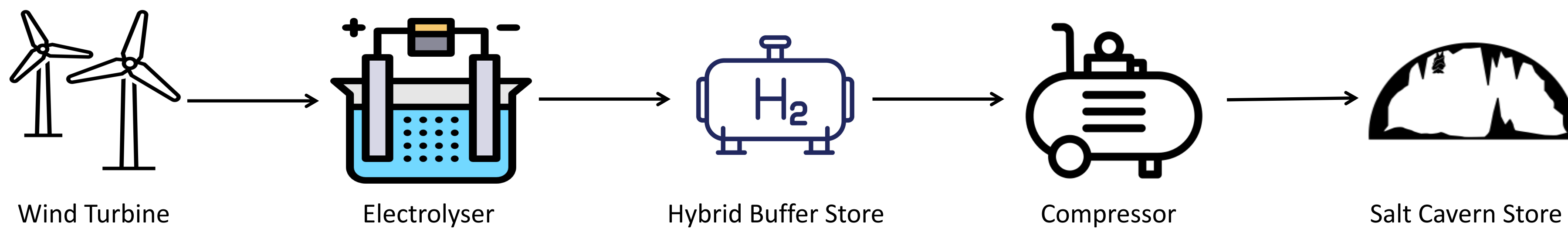


Feasibility Assessment for Metal Hydrides in Buffer Stores

Amelia-Rose Edgley, Marcus Adams, David Grant

1 - Research Context

Hydrogen has the potential to help transition to Net Zero, as a low carbon fuel alternative. Green hydrogen can be produced in an offshore wind connected process. However, power supply is intermittent, so flow rate of hydrogen is not constant. To combat this, a buffer store is employed to smooth the flow rate of hydrogen downstream to a compressor. Given the large amounts of hydrogen to be stored, hybrid tanks comprising a gas and metal hydride system are being considered, as this compacts the buffer tank size.



2 - Terminology

Hydride Gravimetric Density

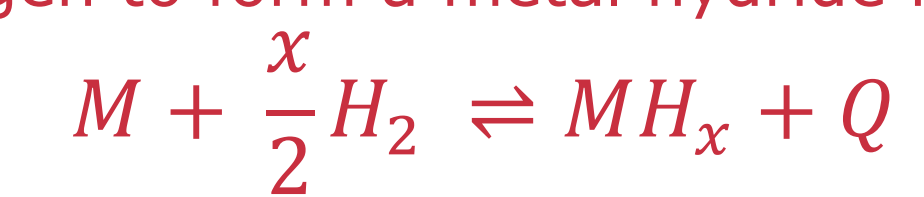
The weight percentage of H₂ that can be stored by a material

Hydride Volumetric Density

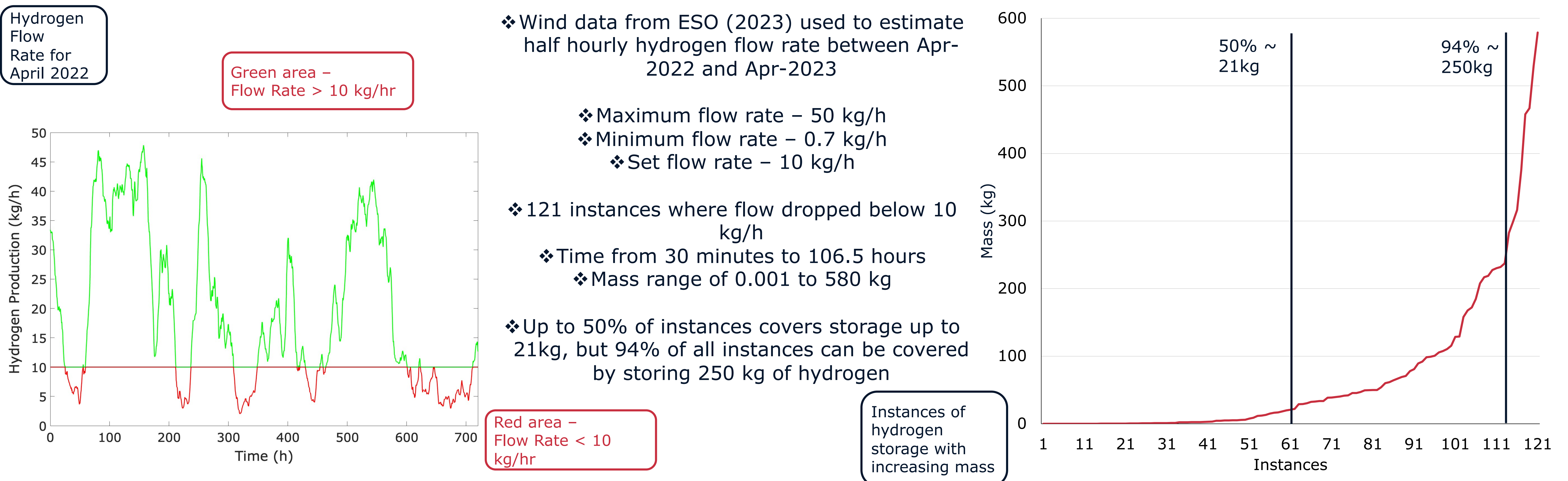
The mass of hydrogen stored per unit volume of an alloy (e.g. kg/m³)

Hydrogenation

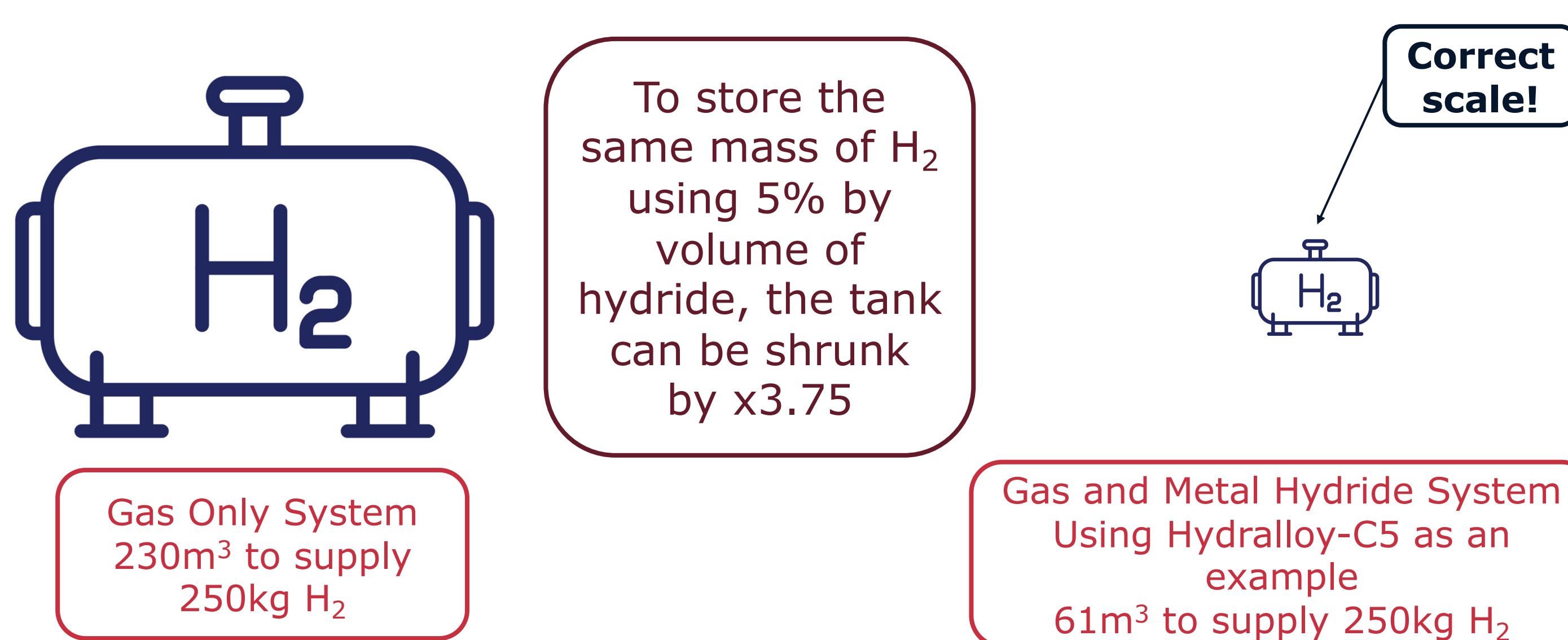
The reaction between a metal/metal alloy and gaseous hydrogen to form a metal hydride material



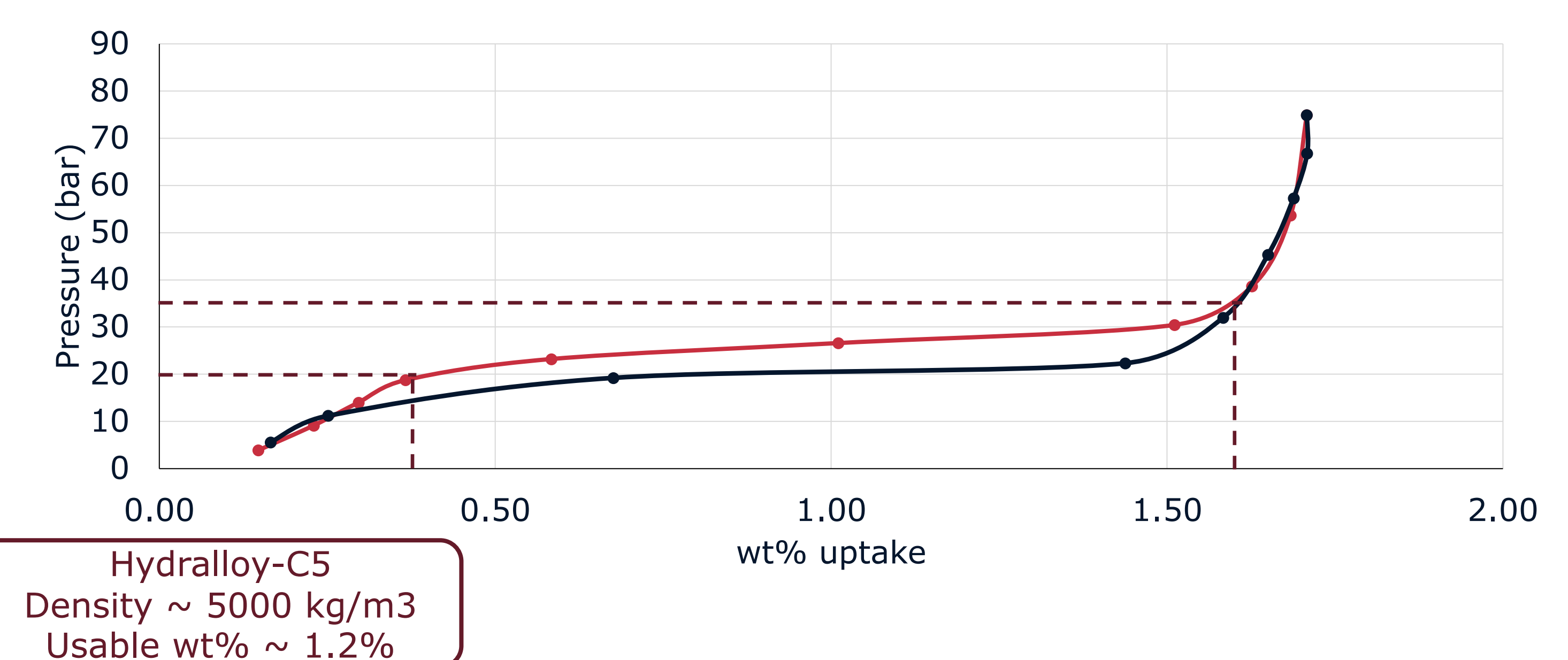
3 - Determining Storage Duration



4 - Tank Comparison



5 - Hydralloy-C5 PCI Data



6 - Future Work

Cost Benefit Analysis

- ❖ A cost benefit analysis will be carried out to determine the optimum amount of hydride to form the hybrid system
- ❖ This will take into account the amount of material cost saved by having a smaller tank overall, compared to the cost of adding the hydride material
- ❖ The benefit stems from having constant flow rate to the compressor. Having less fluctuation in flow means the compressor will be operating in optimal conditions, and will require less maintenance

Material Optimisation

- ❖ (Ti,Zr)(Cr,Fe,Mn,Ni)₂ selected as a material. The research is split into three categories: production, characterisation, and testing.
- ❖ Production will look at optimum manufacturing method, and any post-processing required to provide the best results
- ❖ Characterisation on XRD, SEM, ICP-OES, and other techniques to determine the homogeneity and phase purity of the material
- ❖ Sieverts experiments to determine the kinetics, gravimetric density, volumetric density, and plateau pressure of the material

Resistance to Impurities

- ❖ As the electrolysis will occur in the offshore wind location, desalinated sea water will be used as a source. This may lead to impurities such as oxygen in the hydrogen stream.
- ❖ As such, it is important to understand the effect the impurities have on the hydride material, and how much of an impact this will have on overall performance



Road Detritus

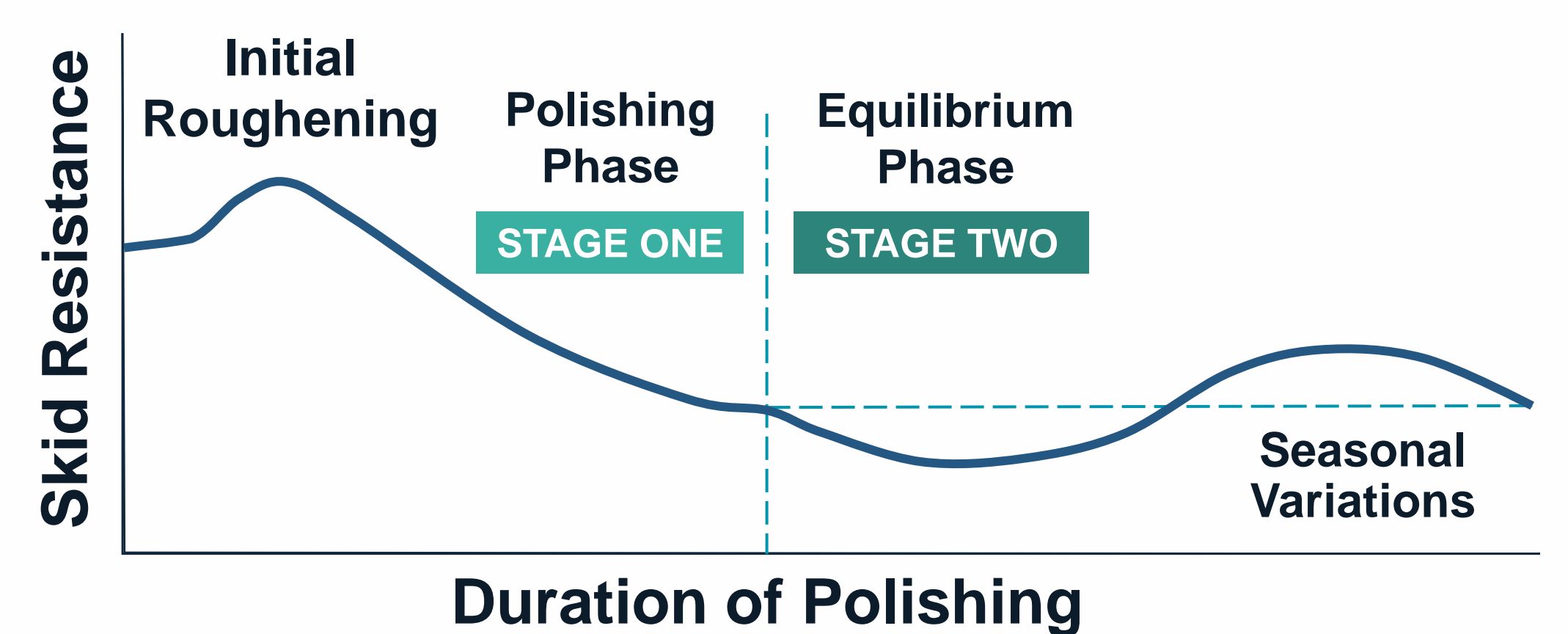
Unveiling Their Effect on Polishing and Texture Changes

Anissa Noor Tajudin

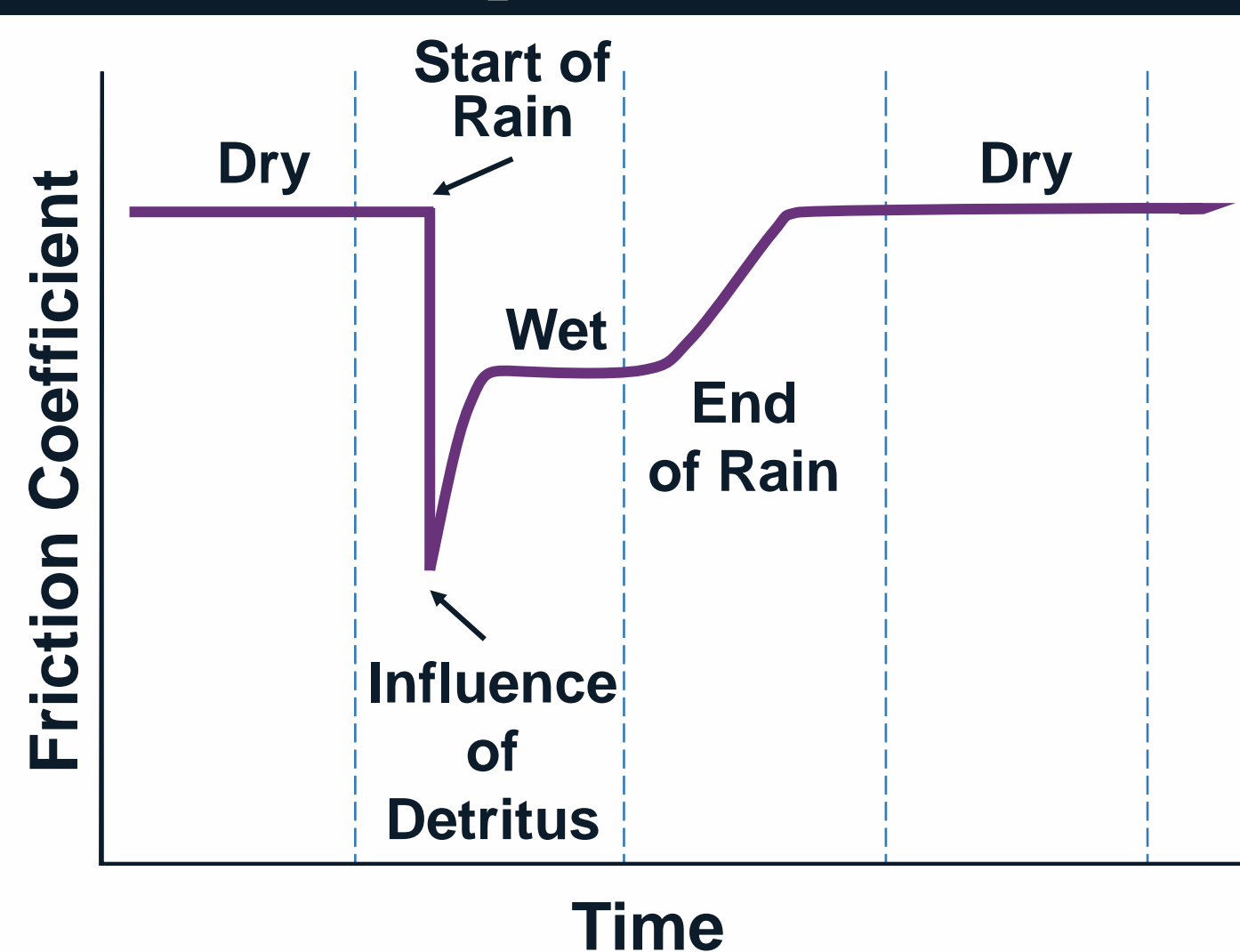
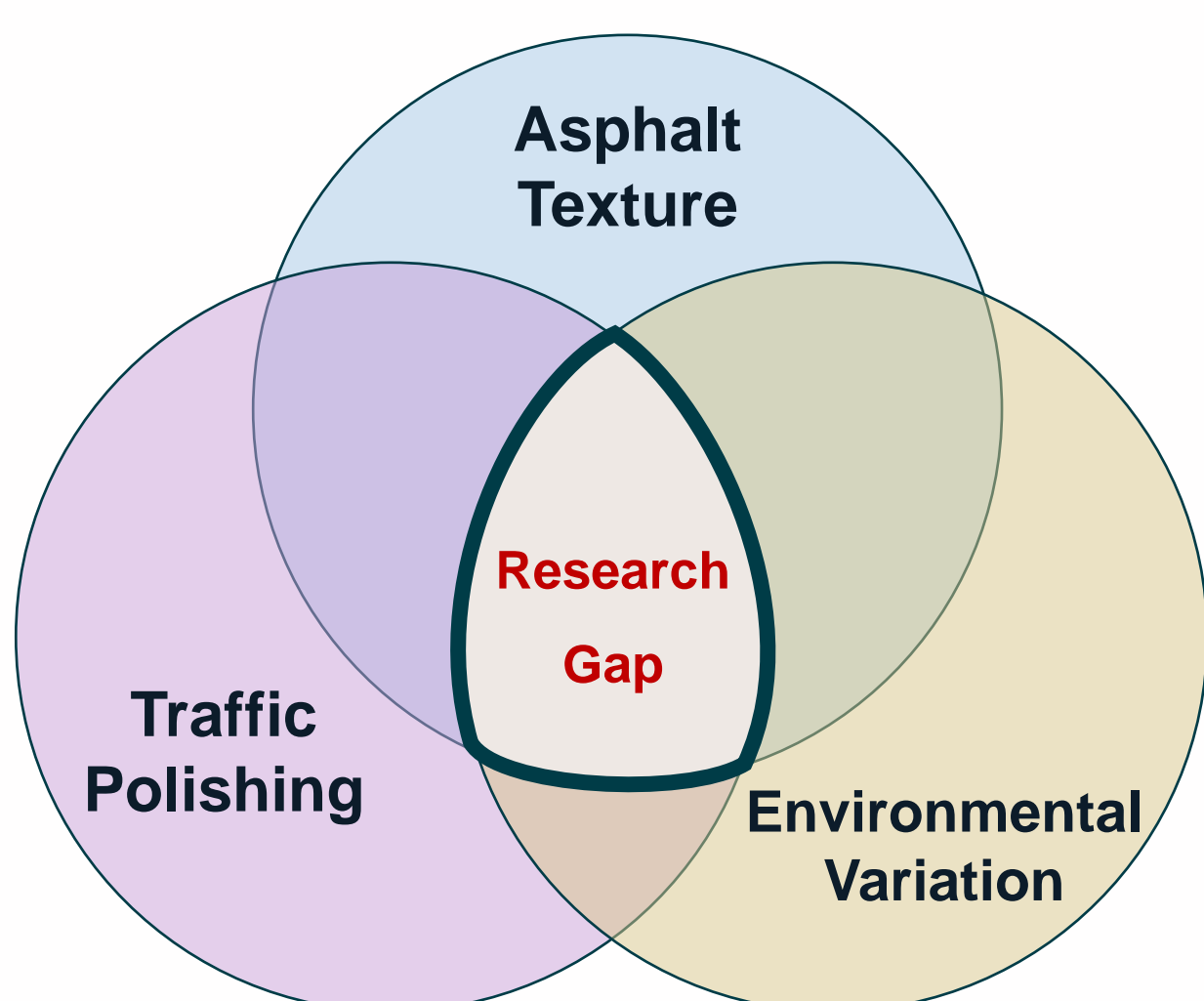
Supervisors: Dr. Nick Thom & Prof. Gordon D. Airey

Introduction

This research investigates the complex dynamics of skid resistance on asphalt surfaces, considering the impact of road detritus and changes in texture from traffic polishing. Through the innovation of an accelerated wearing machine, we aim to simulate traffic effects to examine the transition from initial texture conditions to polished states, enhancing the understanding of pavement performance over time.

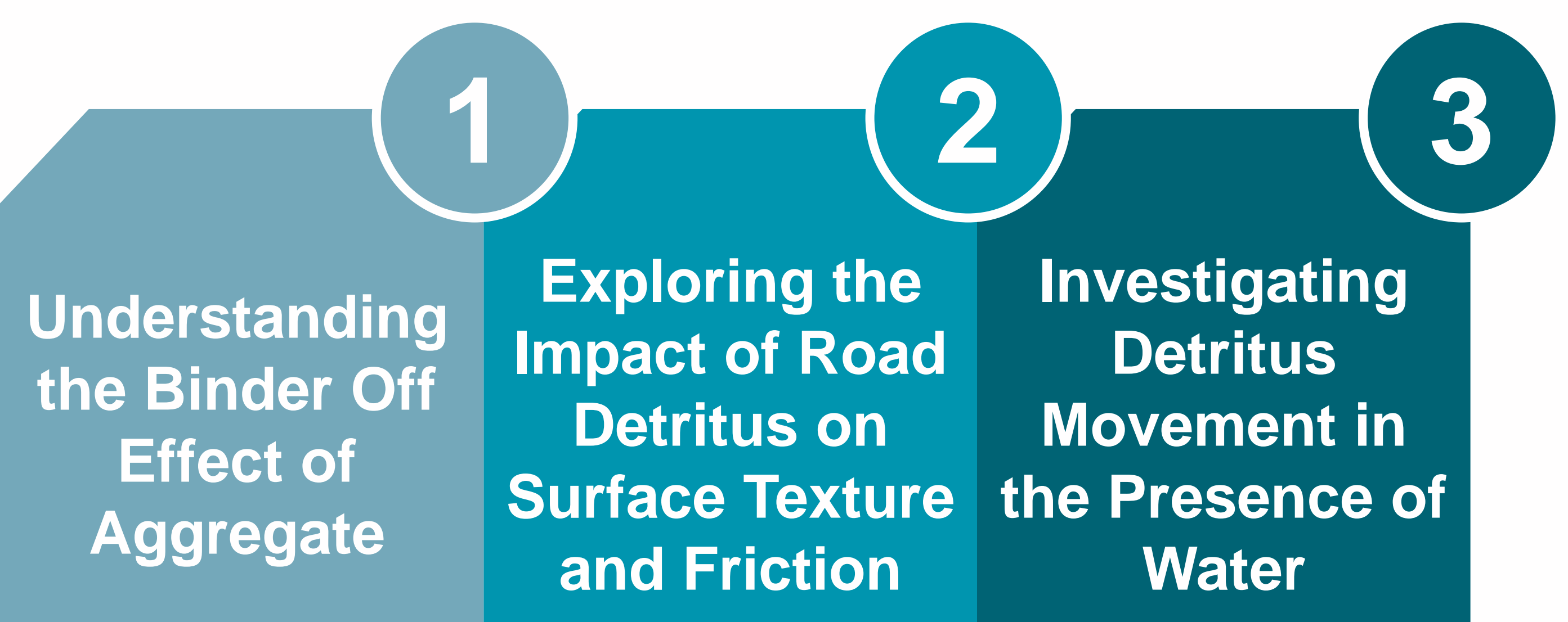


Research Gap

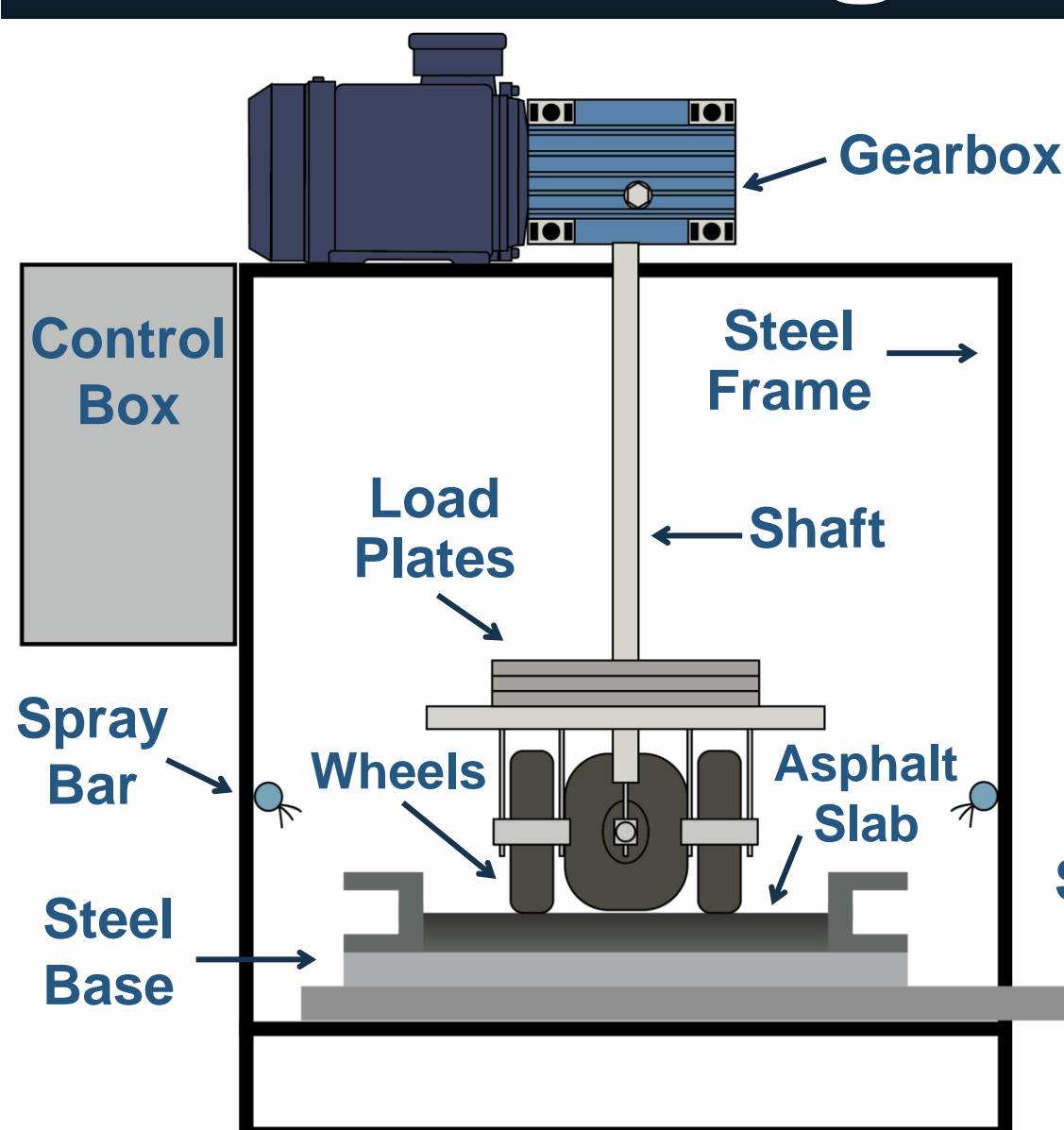


The research specifically addresses unexplored effects of detritus and moisture on asphalt surfaces using an innovative lab-based traffic polishing simulator.

Research Phases



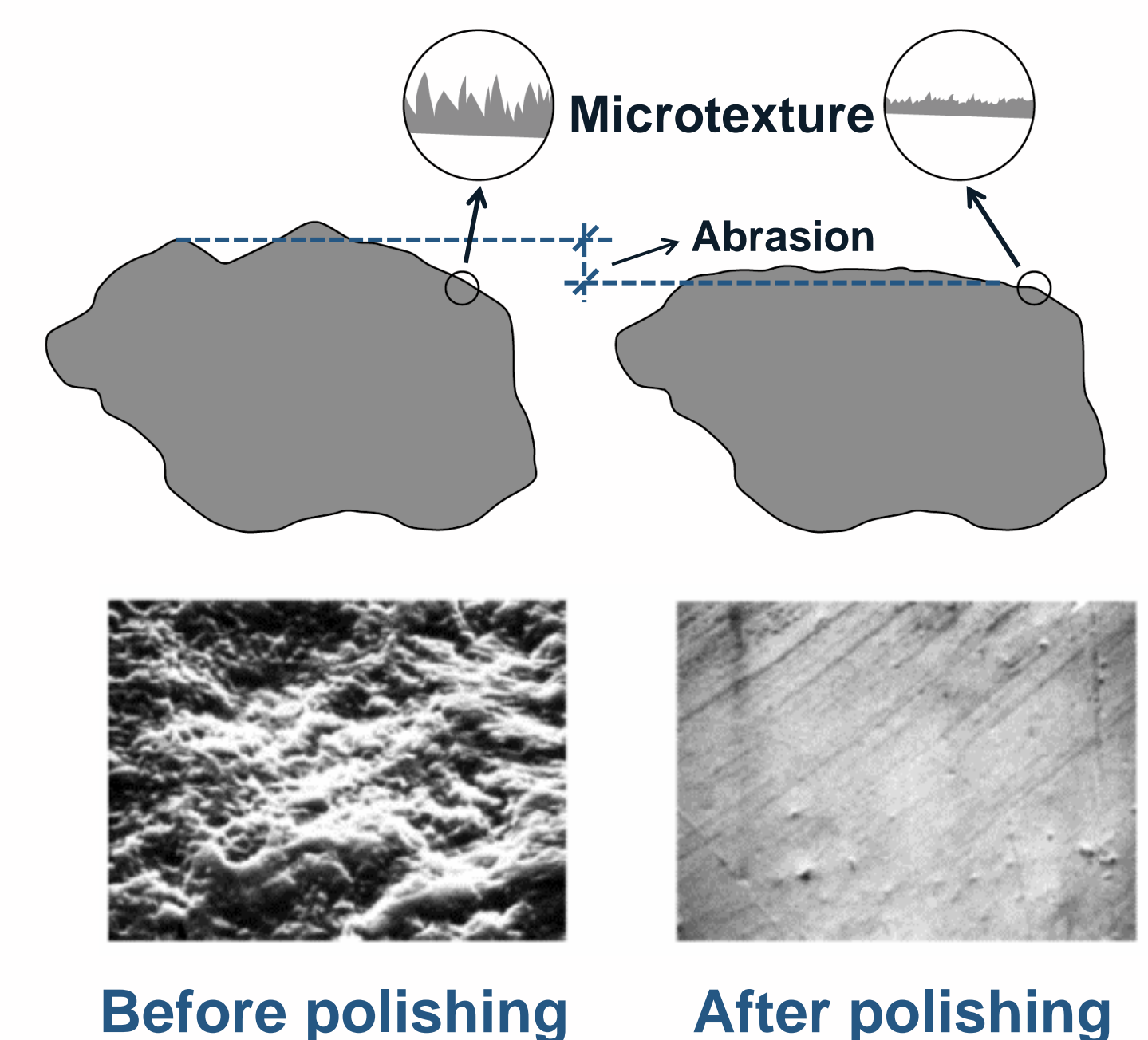
Polishing Machine Assembly



The machine has three motor-driven rubber wheels, adjustable load plate, slider, dry/wet polishing options, and a control box for time and speed settings.



Future Works



Future work will focus on polishing asphalt to equilibrium, adding varied road detritus, and replicating environmental conditions in lab simulations.

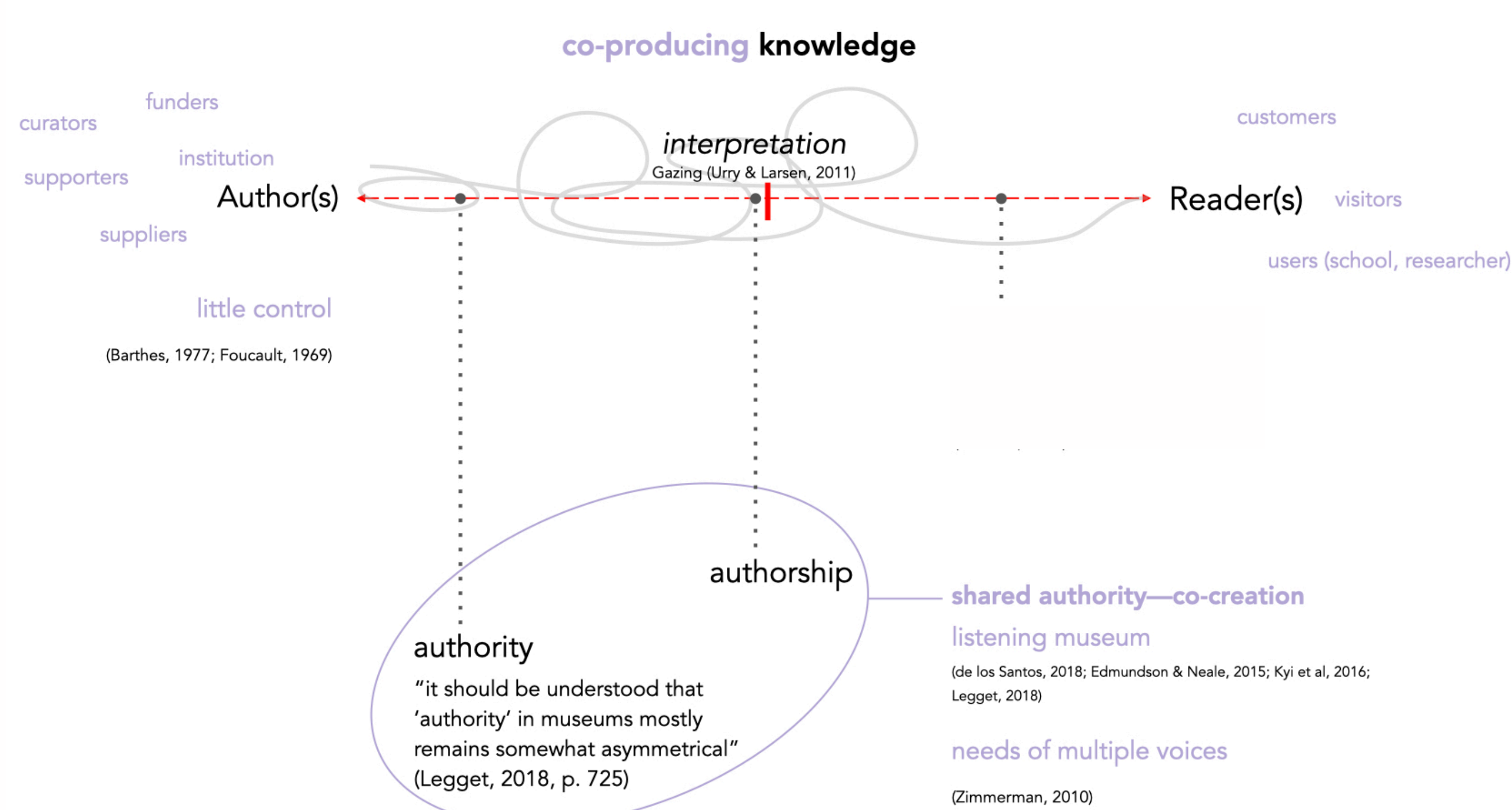


Reinscribing [in] the Art Museum Landscape: Resonating Reader's Voices Towards Post-Museum Paradigm

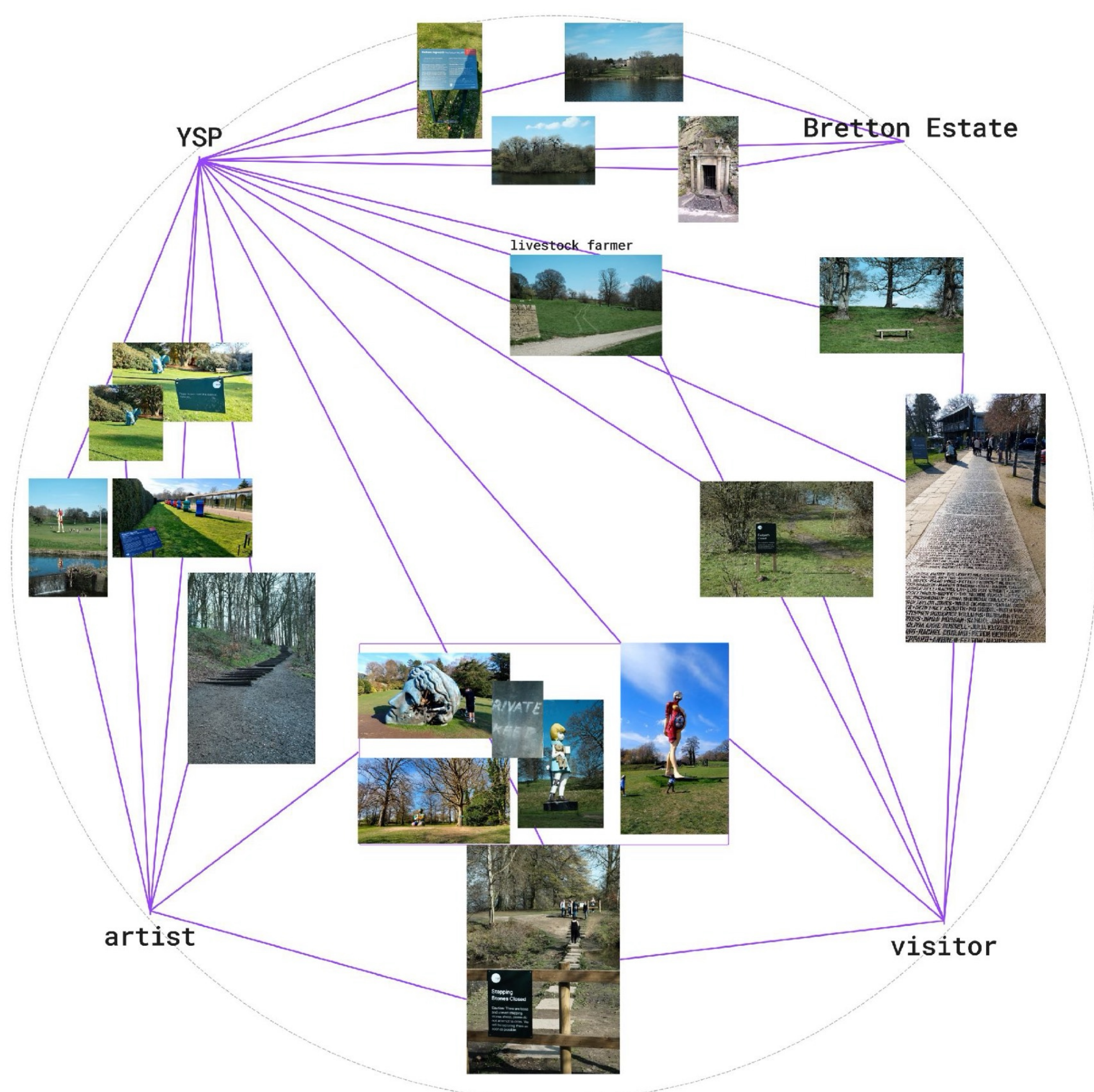
PhD student: Arif Wahid

Supervisors: Prof Jonathan Hale & Dr Laura Hanks

The majority of communication in museums nowadays leaves little room for the visitors to give a meaningful impact on the museum and themselves.



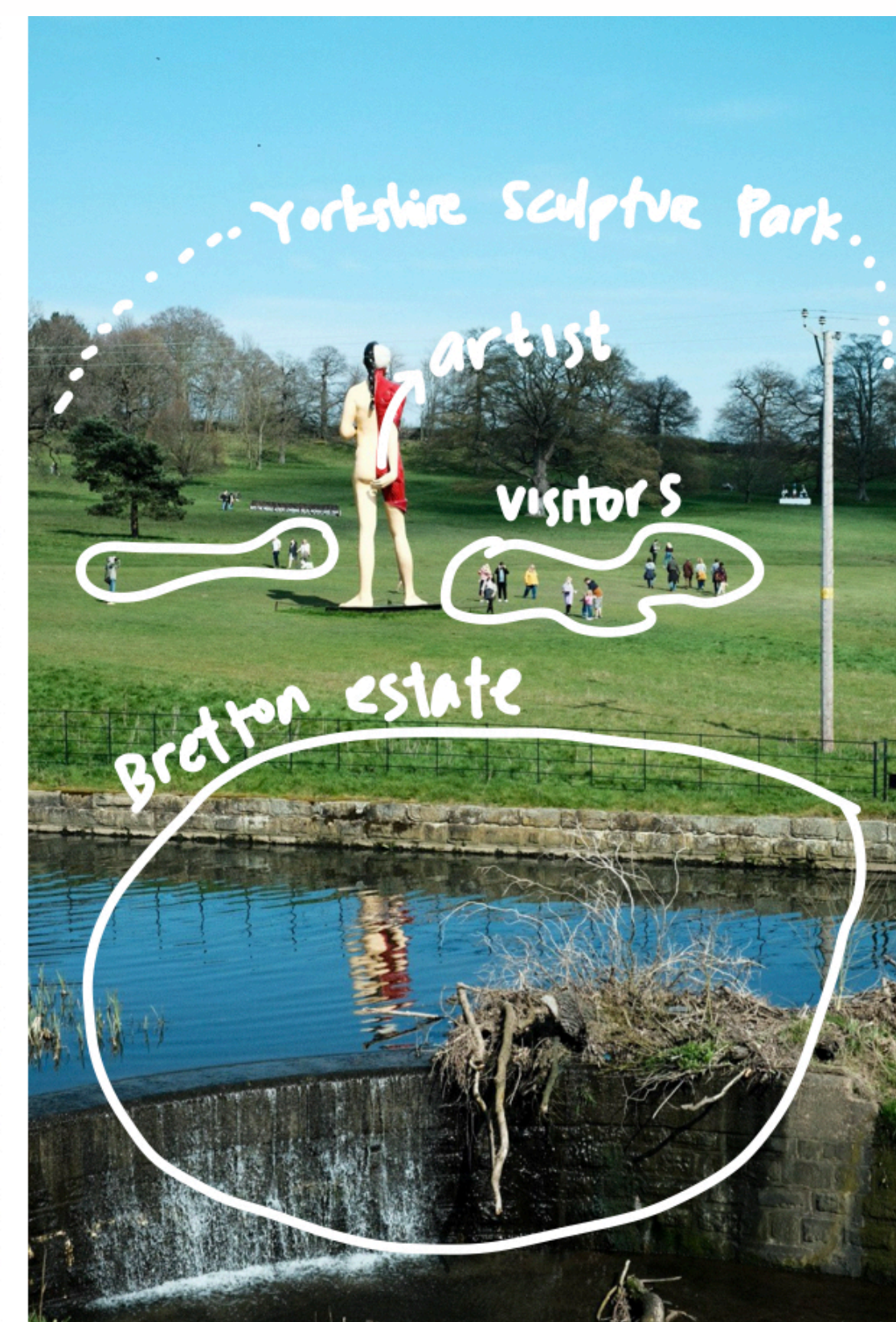
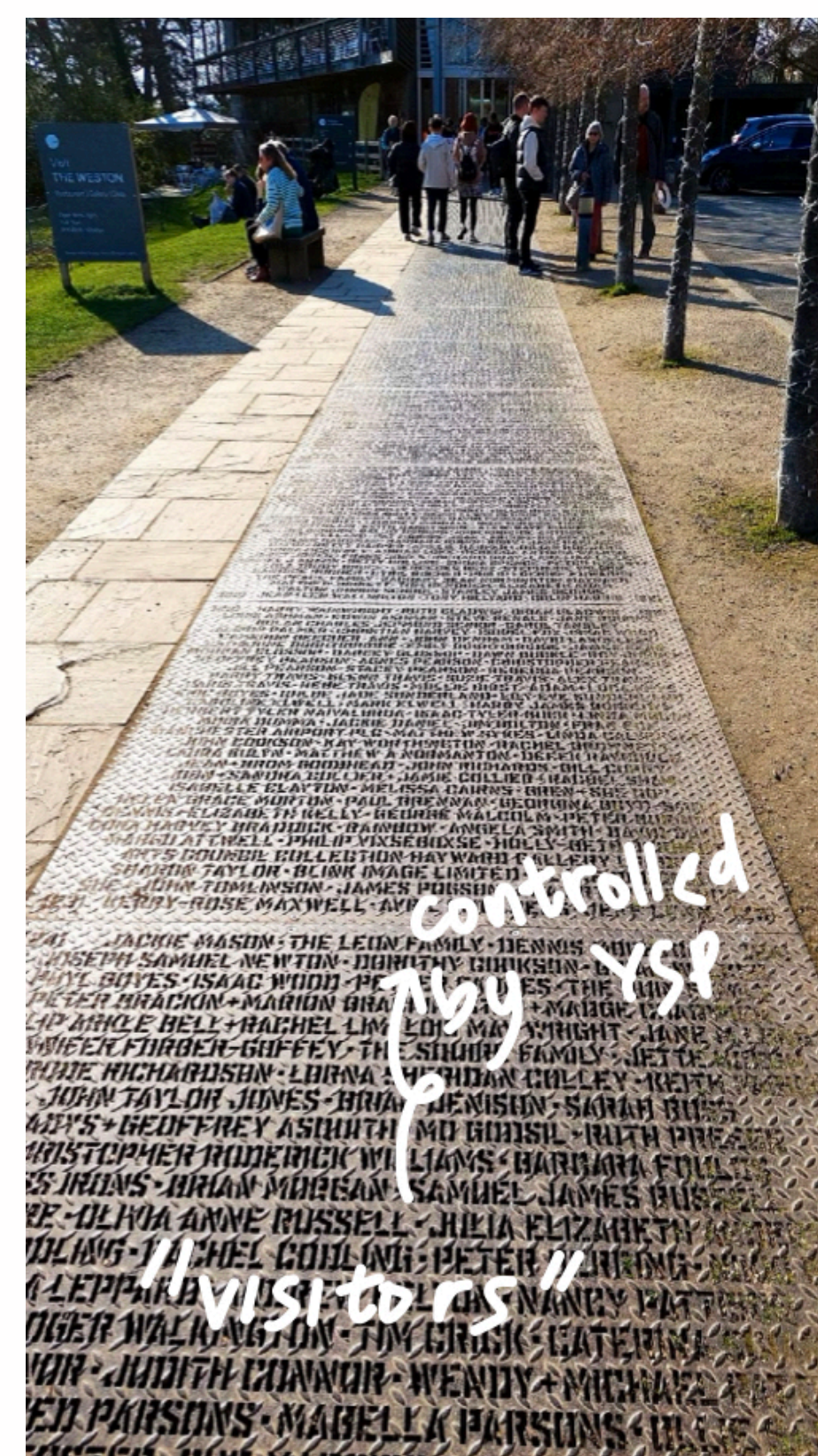
authors-readers continuum on museum experience



tension between characters in the YSP

Summary

This research investigates the potential of **inscriptive practices** to enhance visitor experience in the **art museum** and gallery context. It observes Johnson Chang's 'Yellow Box' model as an alternative to the 'White Cube' to push forward the notion of post-museum. One of the aims is to **advocate museums as a place of co-producing knowledge** instead of letting the museum tell all the stories to us. Inscription here is defined as a perceived human-made marking that leaves traces on a surface. Inscription also appears in many scales—from objects to buildings to nature. When human action interacts with nature, a **landscape** is constructed. Using York Sculpture Park as a case study, this research seeks the rich markings in its mixture of outdoor and indoor galleries, small to large objects, and different stakeholders that influence the park's existence.



various inscriptions found in the YSP ground

Methodology

- Walking is used as a method for the visitor interviews. Walking is a form of inscribing, too, because it leaves more or less semi-permanent traces by movement, and as a collective action, it is indeed creating a continuous line.
- Landscape is seen as an interior. As humans interiorise nature, it becomes a landscape. The landscape is then seen as a continuation of what is inside (interior), and vice versa. This perspective widens the tools for understanding the context.

Future work

- continuing data collection and analysis
- preparing potential workshop with YSP visitors



EVALUATION OF A HYBRID PROCESS TO REPLACE MALT KILNING

Benjamin Wells, Dr D. Cook, Dr C. Dodds, Dr G. Duran-Jimenez

benjamin.wells@nottingham.ac.uk

INTRODUCTION

Malting is one of the world's oldest biotechnologies and it requires innovation to reduce its energy impact. Industrial malting operations use three major processing stages to induce chemical and physical changes within the barley grain. Kilning is the final and most energy intensive stage of malting. This thermal treatment has three functions; to reduce the moisture content of 'green' malt (40%) to a biologically stable 6%, to pause the germination at the required level of modification and to promote the Maillard reactions between amino acids and sugars, producing colour and flavour. The result is a friable malt which can be safely stored for several years.

Malt kilning represents a significant opportunity for increased energy efficiency as it contributes 30% to malted barleys 504 kgCO₂e/t carbon footprint. Electrification, crucial for net zero, can be applied by combining traditional heating with microwave energy in a toroidal fluidised reactor. This process enhances thermal uniformity by generating heat volumetrically within the grain, not just externally, creating a thermal gradient that drives moisture to the surface more efficiently and prolongs the constant drying rate period, significantly accelerating the process and limiting the energy impact. Hybrid microwave kilning has the potential to vastly improve process thermal control and allows for optimization to minimise the degradation of diastatic enzymes and promote other key product quality parameters, essential for the brewing process.

MICROWAVE KILNING

Microwave technology offers significant advantages for malt kilning, including rapid heating rates, far exceeding those of conventional methods, selective heating of moisture within the grain and volumetric heating that ensure a uniform heat distribution throughout the grain. It also provides excellent and instantaneous control over the energy delivery and allows for a shift from natural gas to more sustainably generated electricity. However, applying electromagnetic heating to malt kilning has its associated challenges. Potential issues include: a non-uniform thermal energy distribution within the grain bed, this variance leads to uneven drying or even of burning of the grains, additionally microwave technology often faces scale-up problems caused by penetration depth.

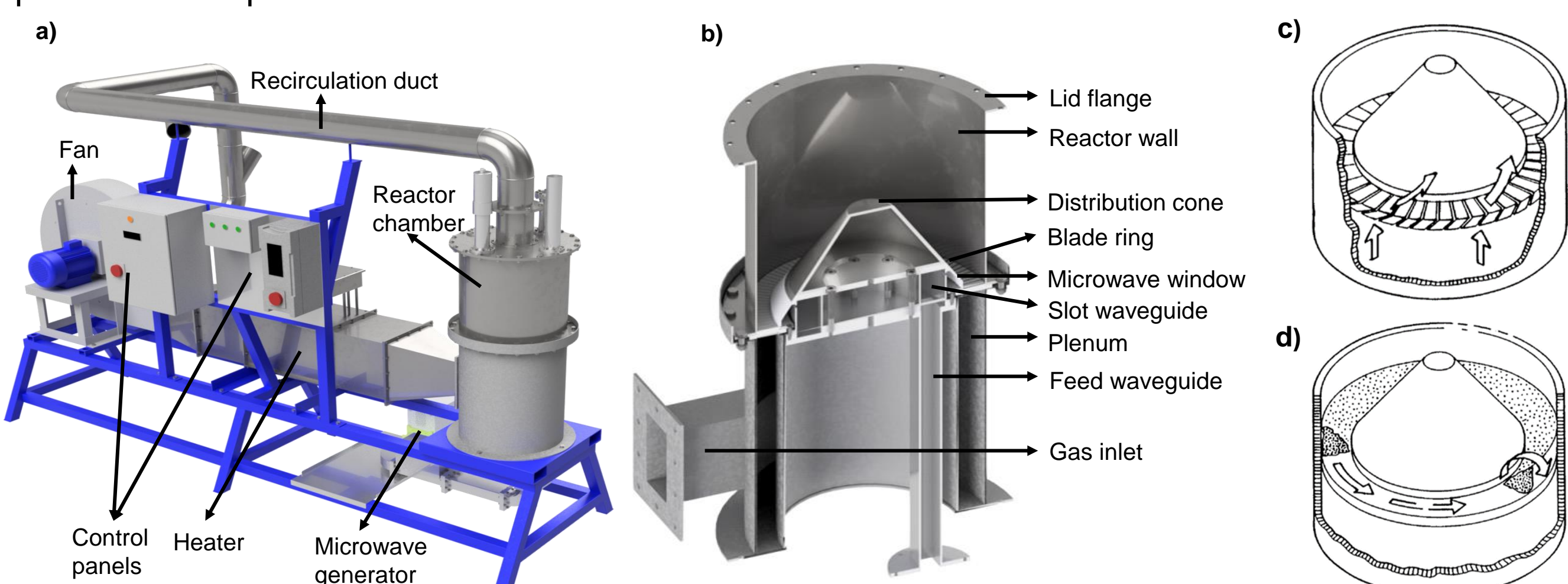


Figure 1. Diagram of TorWave, a toroidal fluidised bed with microwave applicator a-b). (Rodriguez et al. 2024) Fluidising passage of gas through fixed blades c), toroidal movement of grain d). (Lakshmanan 1998)

The introduction of TorWave, developed through a partnership between the University of Nottingham and TorTech, addresses these problems. This innovative toroidal fluidised bed enhanced with a custom microwave applicator, ensures particles are efficiently mixed and continuously exposed to areas of well-defined and concentrated microwave energy. This design promotes uniform treatment and effectively mitigates the common issues of penetration depth and energy distribution in microwave kilning.

MECHANISMS OF DRYING

There are two mechanisms for the migration of water within the grain during thermal drying. The first is liquid migration, as the grain heats up the water inside the grain will move from the hottest areas to the coolest ones, driven by the thermal gradient. The second is vapour migration, as heating continues, the internal moisture begins to vaporise. The vapour is then driven towards the surface by the increased vapour pressure inside the grain. Once the moisture reaches the surface it is evaporated into the surrounding air.

In a traditional malt kiln heat is applied externally, creating a thermal gradient from the surface in, therefore moisture is initially driven inwards to achieve a natural equilibrium for both moisture and temperature within the grains, heating then continues to vaporise the water and drive it to the surface.

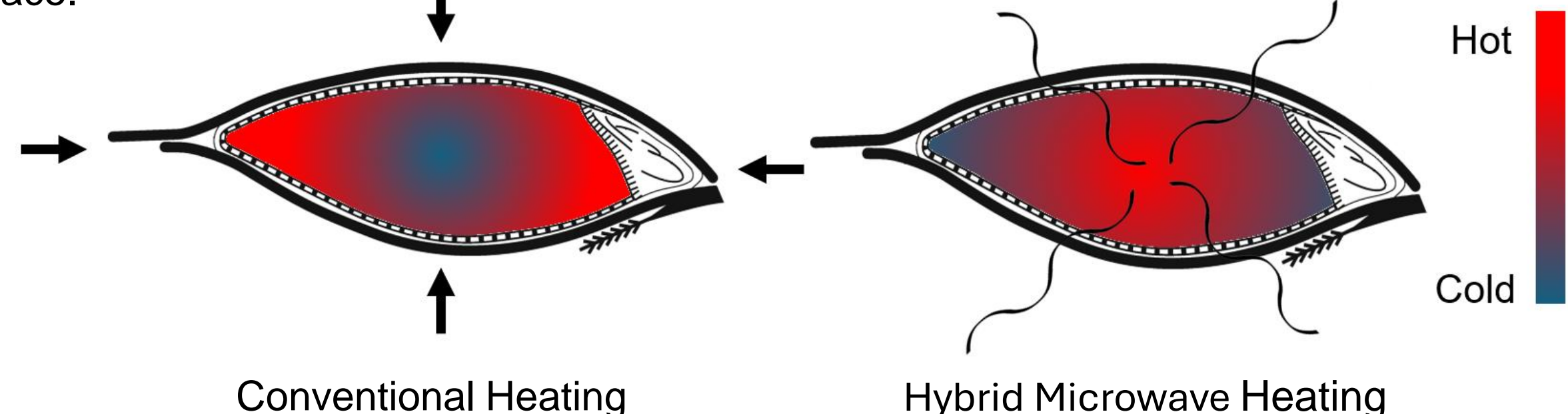


Figure 2. Diagram of thermal gradients in malt grains being heated conventionally and in the TorWave.

Figure 2 shows heat transfer mechanisms in malt kiln process. The thermal gradient in electromagnetic heating is unique as it is reversed.

Microwaves generate heat uniformly through the volume of the grain, high rates of gas to solid heat transfer in the TorWave can then efficiently cool the particle from the outside of the grain. This not only reduces the risk of thermal runaway but induces a thermal gradient where the grain is hottest in the centre cooling towards the surface. In this situation both liquid and vapour migration are in the same direction, and both push the moisture towards the surface, where mass transfer occurs into the gas stream through surface evaporation. This change in drying kinetics can significantly increase the rate of drying and reduce processing time.

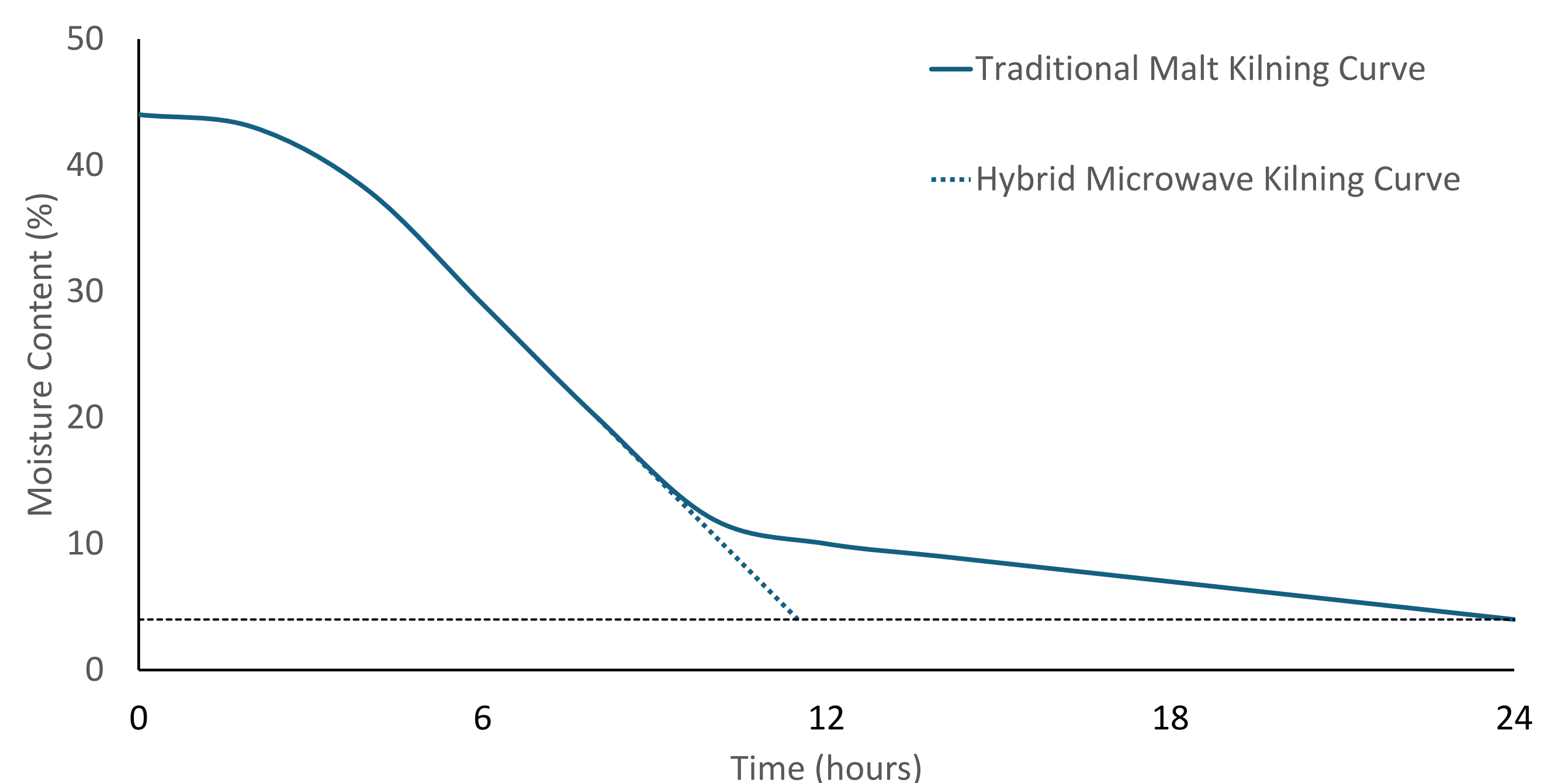


Figure 3. A graph to show the reduction in processing time to drying malted barley in a hybrid microwave process where samples are dried traditionally to 15% moisture and then finished to 6% in the TorWave.

MALT QUALITY

In the brewing industry, malt quality is crucial as it significantly influences the brewing process and the overall characteristics and quality of beer. The challenge of malt kilning is balancing the need to achieve the desired malt characteristics such as moisture content, colour and flavour complexity, which can be enhanced at higher temperatures while preserving as much enzymatic activity as possible.

Two of the most important enzymes that play a role in malt quality are α -amylase and β -amylase. These enzymes are fundamental for the conversion of starch into sugars, which yeast then ferments into alcohol and other components during brewing.

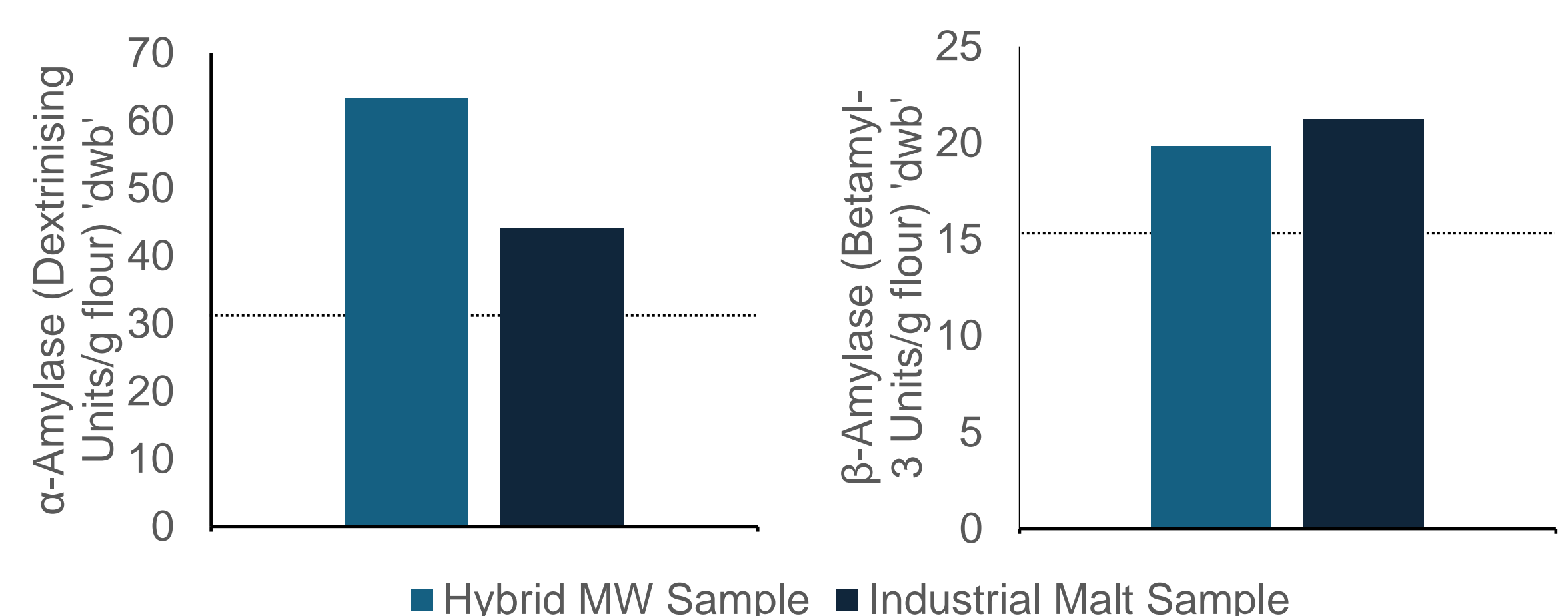


Figure 4. Graphs showing the enzymatic activity levels in hybrid microwave kilned samples vs the same batch kilned industrially. Microwave samples were dried at 80°C from 15% to 6% moisture.

FUTURE RESEARCH & CONCLUSION

When considering the denaturing of diastatic enzymes, α -amylase and β -amylase and the reduction of moisture across the hybrid microwave kilning process, the technology shows impressive potential. Processing time to dry from 15% to a biologically stable 6% can be reduced from hours to minutes while maintaining an acceptable brewing standard in the two enzymes considered.

Amylases, α and β , represent some of the least thermo-sensitive enzymes in malted barley, the research now continues to consider an ever-widening group of enzymes such as the much less temperature resistant endo- β -glucanase, while less critical for sugar production this enzyme is still essential for reducing mash viscosity in the brewing process by breaking down β -glucan.

The temperature and duration of malt kilning plays a pivotal role in developing malt colour through mechanisms such as the Maillard reaction and caramelisation, both of which are non-enzymatic browning reactions. In addition, the flavour of malt is greatly affected by the kilning process, through the thermal decomposition of fatty acids and lipids and the creation of Maillard reaction products. The research will look at the effects of reduced processing time and the reversed thermal gradient in the hybrid microwave process for malt kilning, on malt quality parameters such as enzymatic thermal stability, colour and flavour profile in malted barley.

REFERENCES

Lakshmanan, V.I. and Dodson, C.E. (1998). An Innovative Gas-Solid Torbed Reactor for the Recycling Industries. *Pyrometallurgical Recycling*.
Rodriguez J.M. et al.(2024 in press) *Chem. Eng. Process*.



Enhancing Railway Bridge Life-Cycle Modelling

Chris Taylor, Dr Luis Neves, Prof Richard Wilkinson, Prof John Andrews

Motivation

Bridge condition is the result of two processes: **deterioration** and **intervention**. Incomplete and **sparse intervention records** mask the true condition pathways, with unidentified interventions leading to slower predictions for deterioration rates [1]. This project will develop a comprehensive model of the deterioration-inspection-intervention process of **metallic railway bridges** to enhance predictive modelling by **uncovering the impact of intervention and re-calibrating deterioration rates**.

Methodology

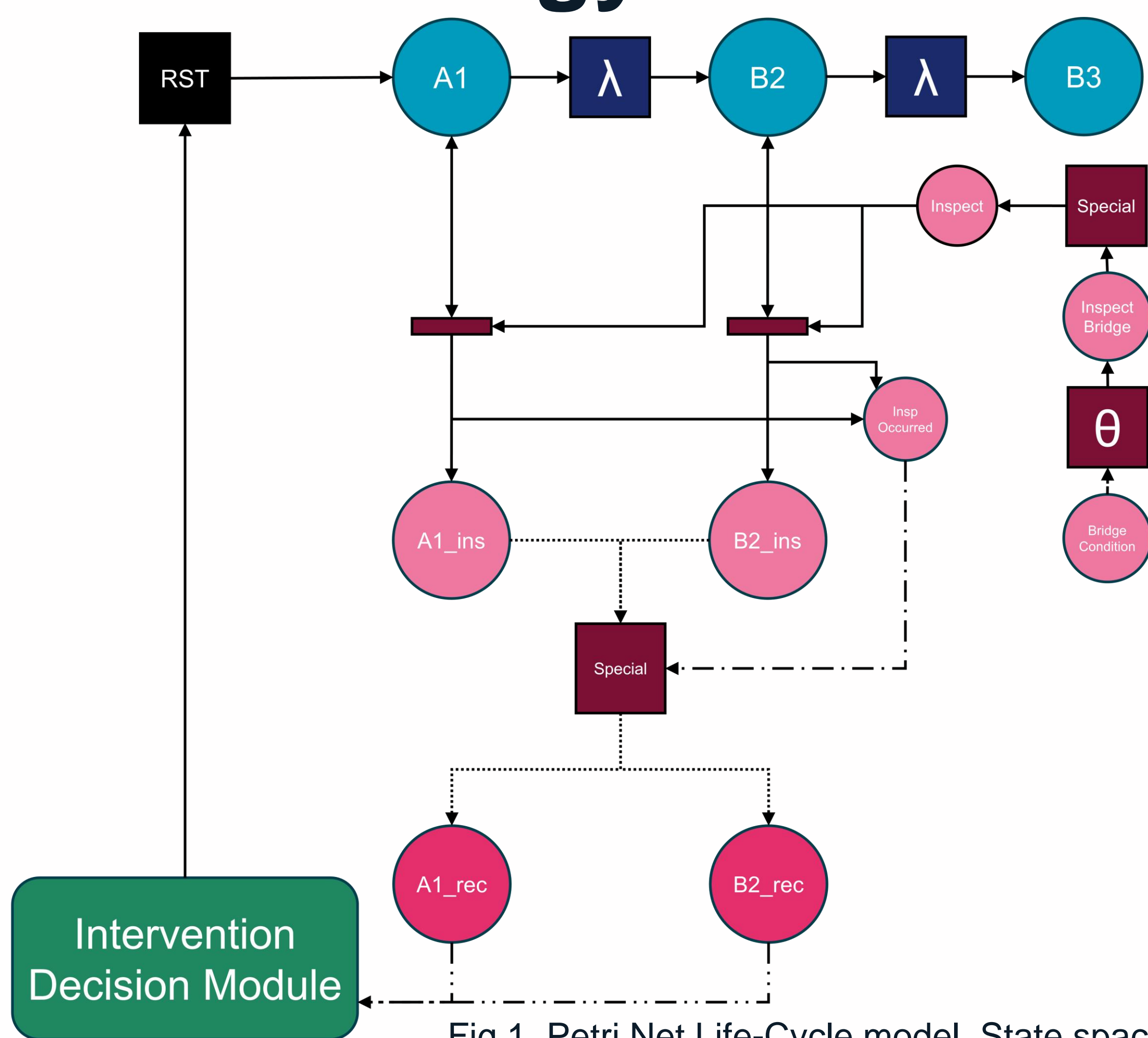


Fig 1. Petri Net Life-Cycle model. State space reduced for clarity

A **Coloured Petri Net** is used to model the life-cycle of bridge elements. **Tokens represent defects** (areas) of components (elements) on a metallic bridge deck.

Deterioration

Defects on an element progress in Severity and Extent. Isomorphic to CTMC. Previous models focus on aggregated element condition [2,3].

Inspection

The worst two defects are recorded for each element as element condition. Inspection interval depends on bridge condition.

Intervention

Relevant defects are restored to AGAN. The element condition then depends on presence of other defects

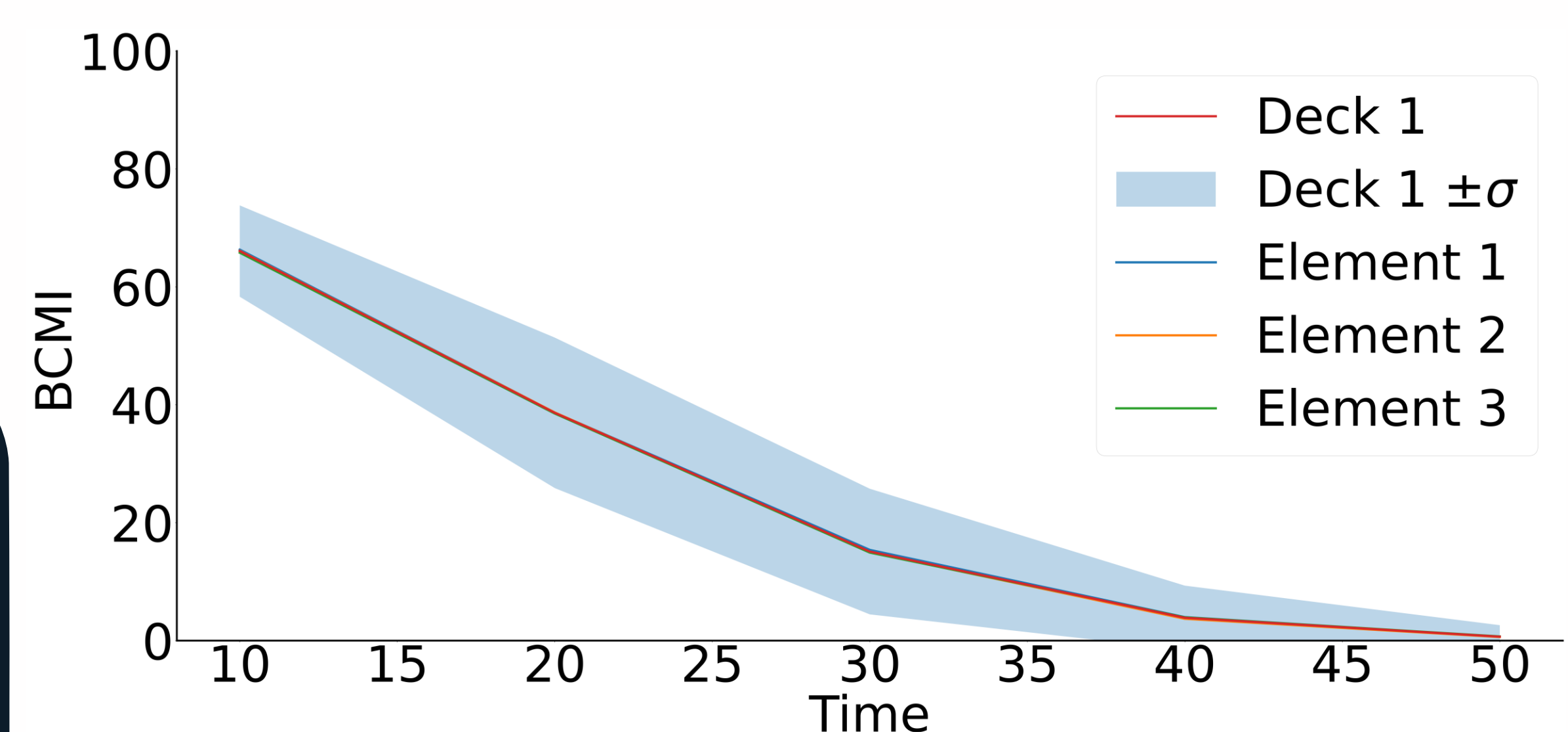


Fig 2. Example simulated condition of a single homogenous deck comprised of 3 generic metallic elements under a 'do-nothing' maintenance strategy.

Future Work

Intervention Decision Module

Planning interviews with NR asset managers to gain insight into real-world decision processes. This will support development of structure and parameter bounds for module.

Parameter Calibration

Deterioration rates and intervention decision parameters will be calibrated using optimisation algorithms, to find the set of parameters which maximise the likelihood of the condition and intervention data.

References

- [1] - Agrawal, A. K., et al. (2010). "Deterioration Rates of Typical Bridge Elements in New York." *Journal of Bridge Engineering* 15(4): 419-429.
- [2] - Le, B., et al. (2017). "A Petri net model for railway bridge maintenance." *Proceedings of the Institution of Mechanical Engineers, Part O: Journal of Risk and Reliability* 231(3): 306-323.
- [3] - Yianni, P. (2017). *A Modelling Approach to Railway Bridge Asset Management*, The University Of Nottingham. PhD: 216.

Introduction

GaN technology holds immense potential to revolutionize power electronics, overcoming the limitations of traditional silicon semiconductors and paving the way for a more sustainable future. By addressing GaN's reliability challenges and implementing predictive maintenance strategies, we can maximize the lifespan of GaN-based devices, minimize electronic waste, and optimize their energy efficiency.

Aim of this Research

- Contributing to eco-friendly technology by designing an energy-efficient and reliable GaN-based power inverter,
- Developing an online health management platform for GaN-based power modules.

Work done to date

- Developing a GaN-based test circuit board to identify various failure indicators.

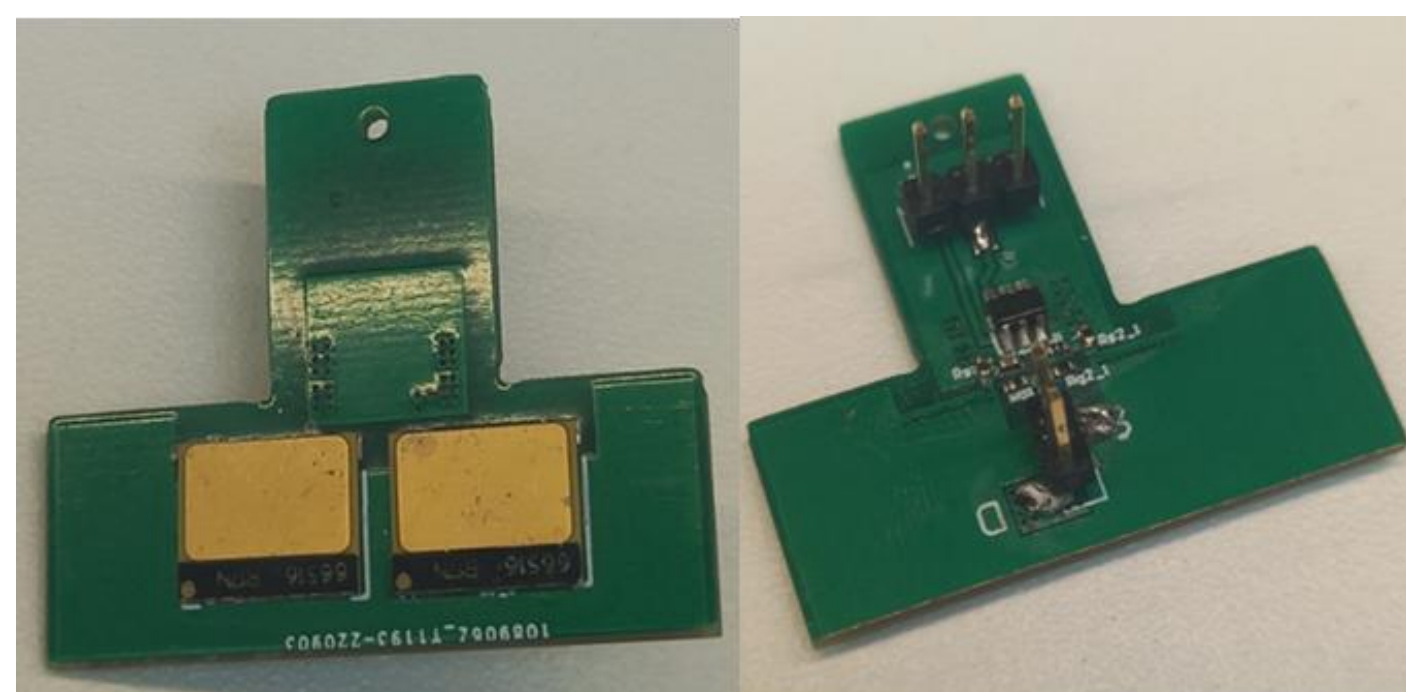


Fig. 1: GaN-based test circuit board

- Thermal Cycling following the JEDEC (Joint Electron Device Engineering Council) standards (up to 200 thermal cycles).

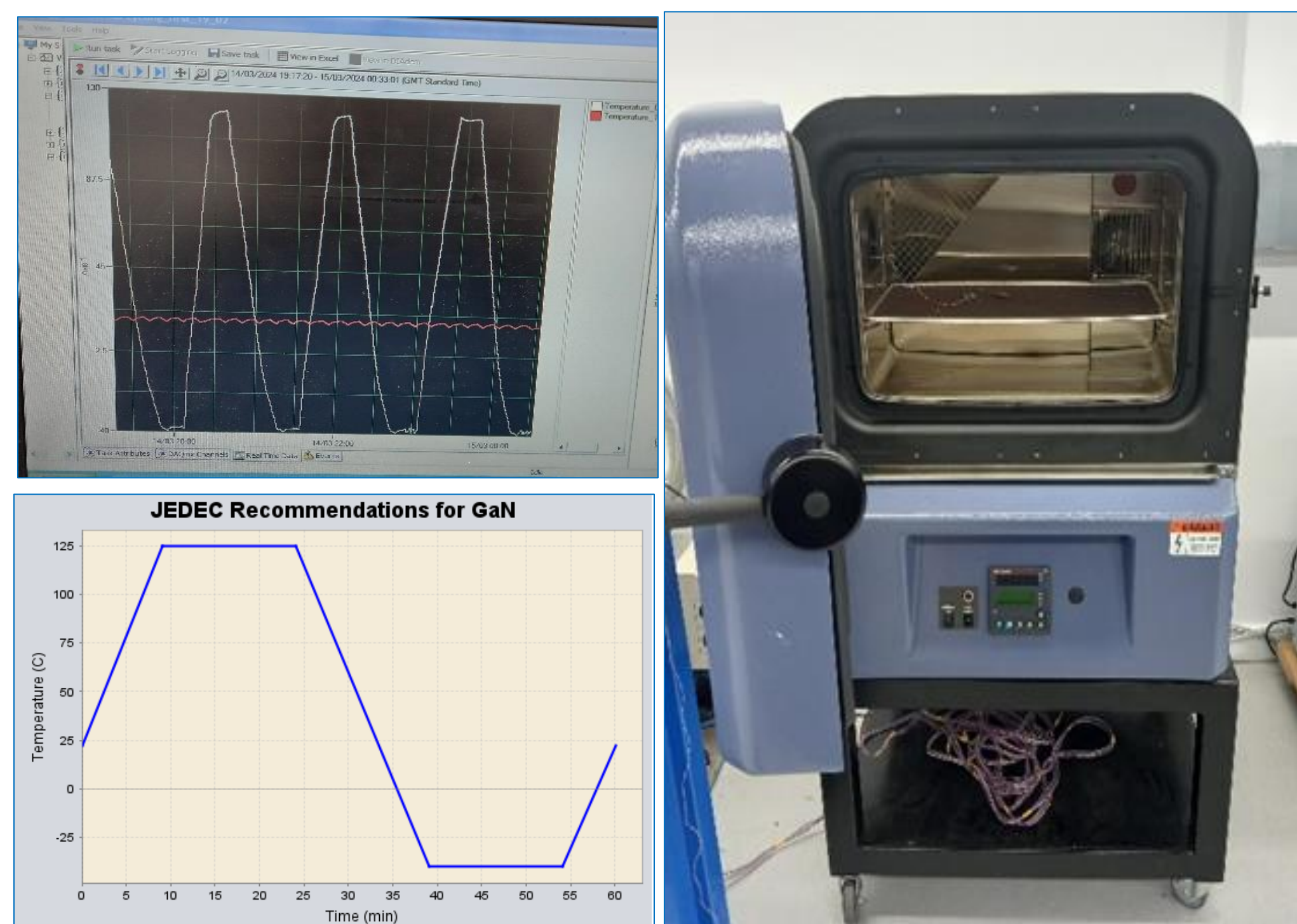


Fig. 2: Thermal cycles (JEDEC Standard) (left). Thermal Chamber with the test circuit board (right)

- Static characteristics after 100 thermal cycles - inconclusive results

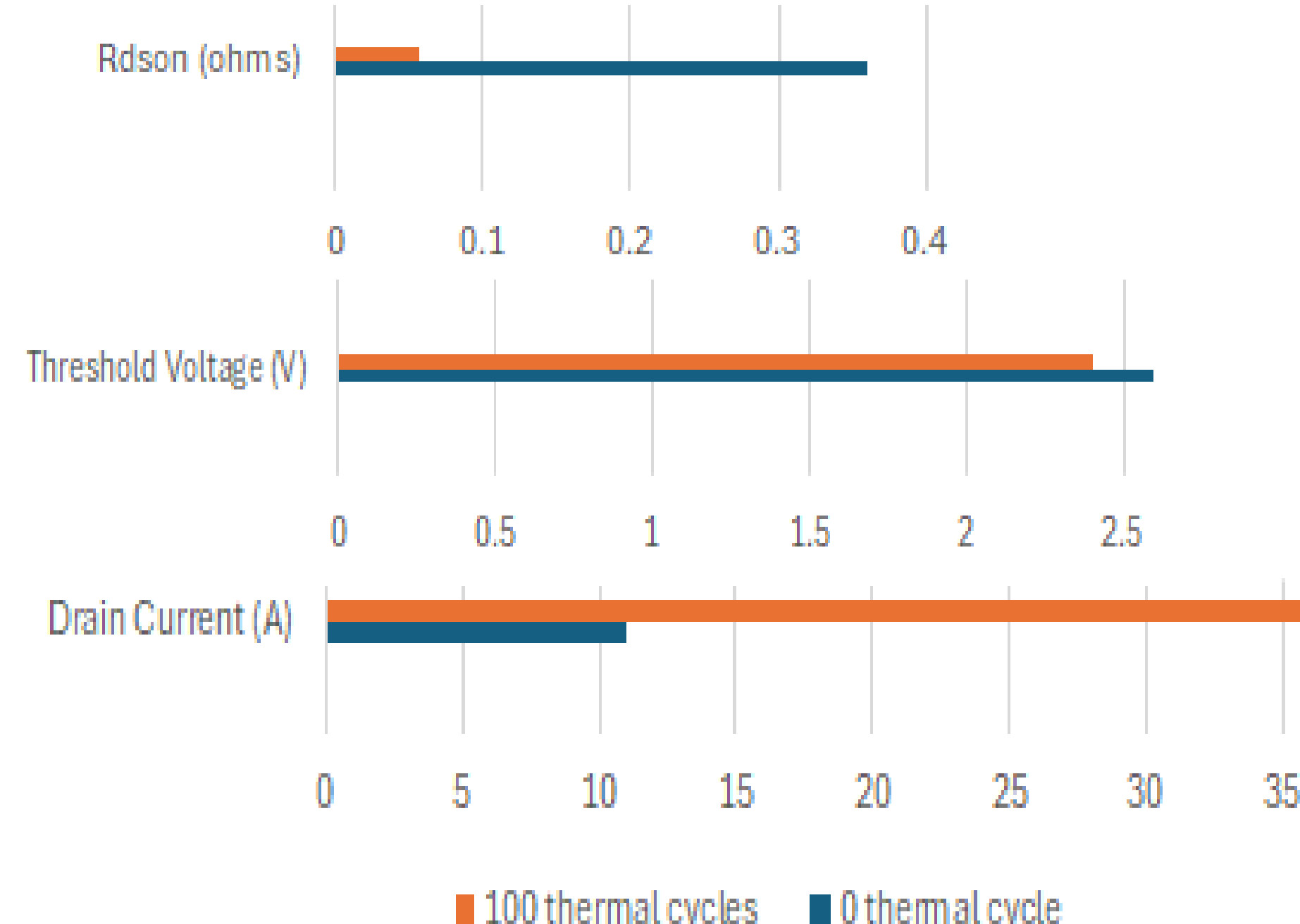


Fig. 3: Static Characterisation test results

- X-ray CT scans – shows the effect of vias under the pad

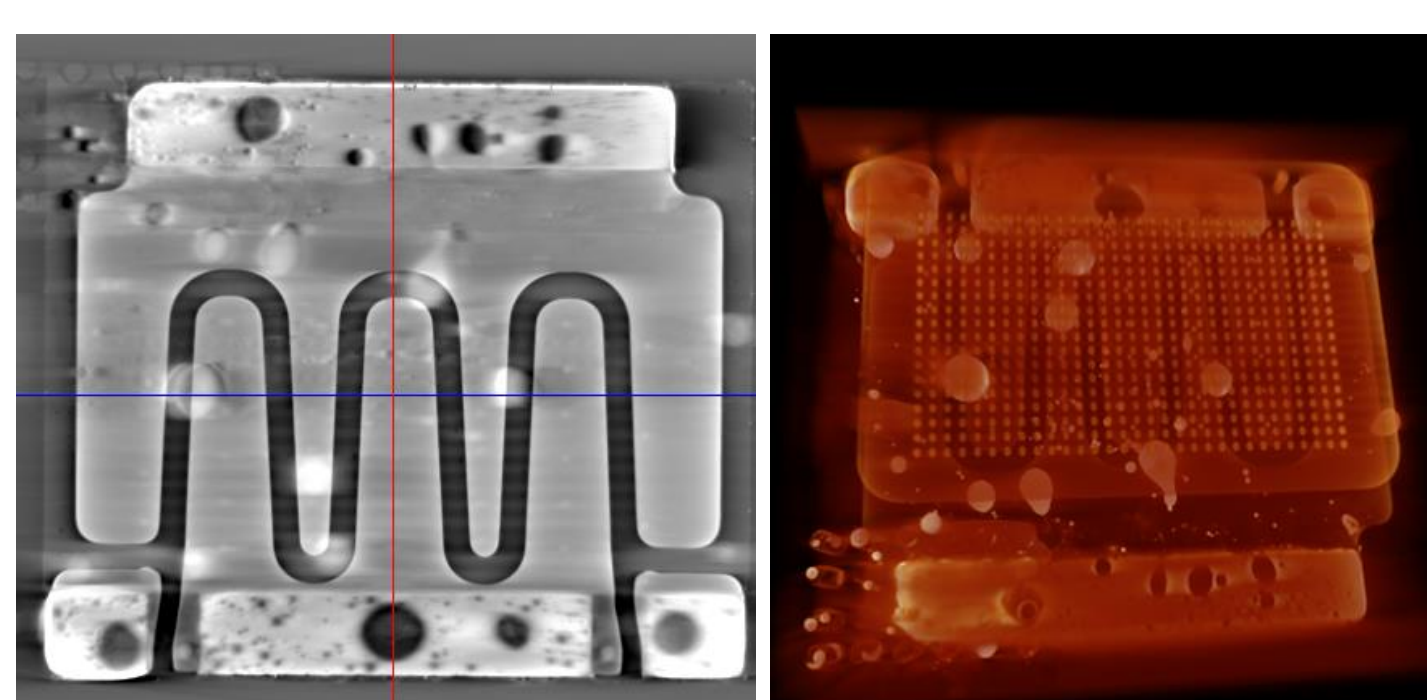


Fig. 4: Solder Layer View and full x-ray CT scans of GS66516T package

- Thermo-mechanical simulation using Ansys Sherlock Simulation

Table 1: Delta Strains for different parts onto the PCB at two different temperatures

RefDes	Package	Part Type	Side	Solder	Max Disp	Delta Strain
Q2_1	GS66516T_1	TRANSISTOR	BOT	SAC305	2.9E-2	1.536.55
Header1	10129380903001..	PLUG CONN.	TOP	PB905N10	2.5E-2	1.663.58
Q1_1	GS66516T	TRANSISTOR	BOT	SAC305	3.0E-2	1.778.45
Header2	10129380902001..	PLUG CONN.	TOP	PB905N10	2.3E-2	1.778.72
Rg1_1	0402	RESISTOR	TOP	SAC305	2.2E-2	1.804.06
C1_1	0402	CAPACITOR	TOP	SAC305	2.2E-2	1.857.46
Rg2_1	0402	RESISTOR	TOP	SAC305	2.3E-2	1.912.54
_Gate_Driver	SOT-23-6	IC	TOP	PB905N10	2.3E-2	2.037.40
Rg3_1	0402	RESISTOR	TOP	SAC305	2.3E-2	2.145.79
Rs2_1	0402	RESISTOR	TOP	SAC305	2.4E-2	2.275.99
Rs1_1	0402	RESISTOR	TOP	SAC305	2.2E-2	2.291.96
R1_1	0402	RESISTOR	TOP	SAC305	2.3E-2	2.343.03

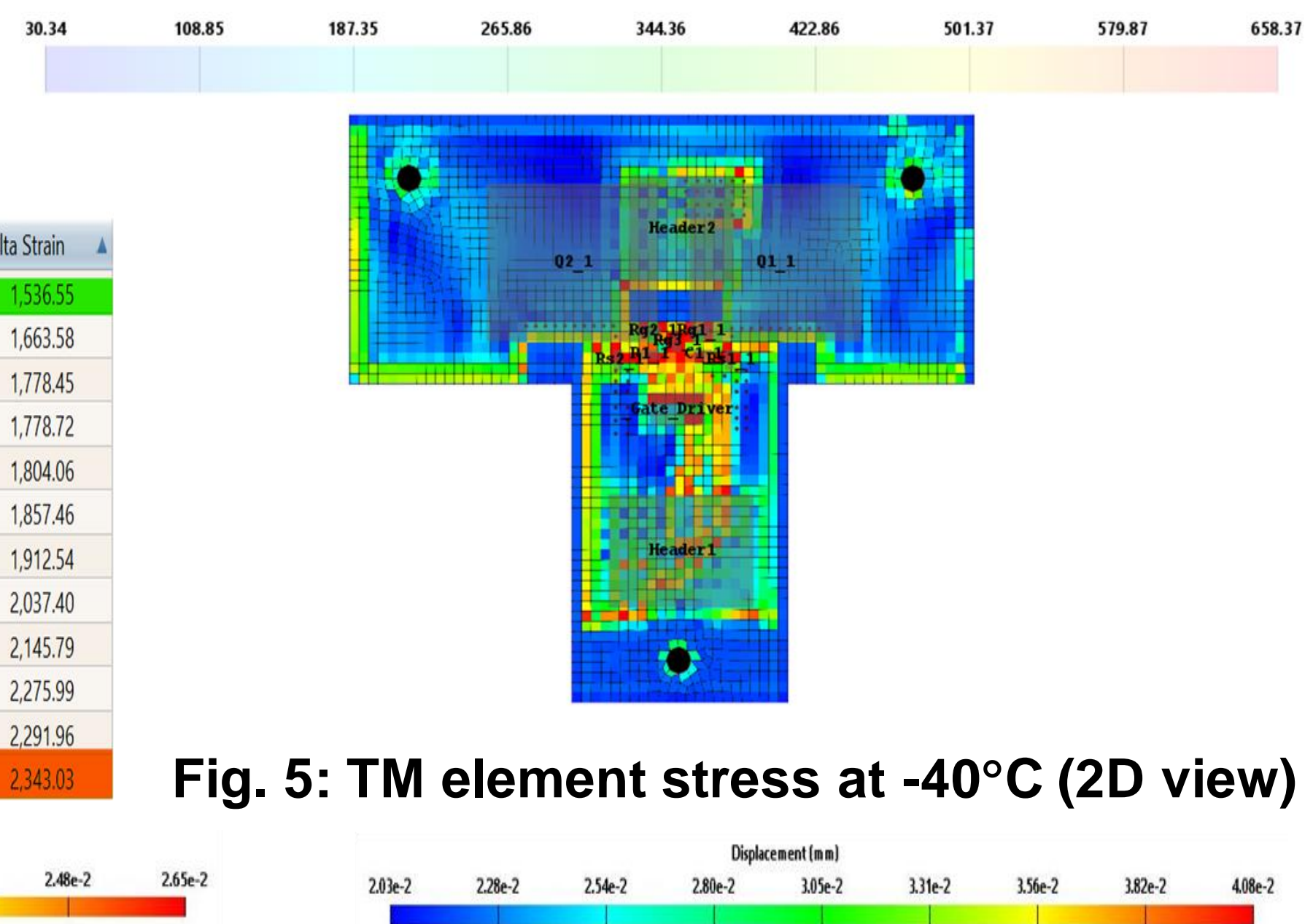


Fig. 5: TM element stress at -40°C (2D view)

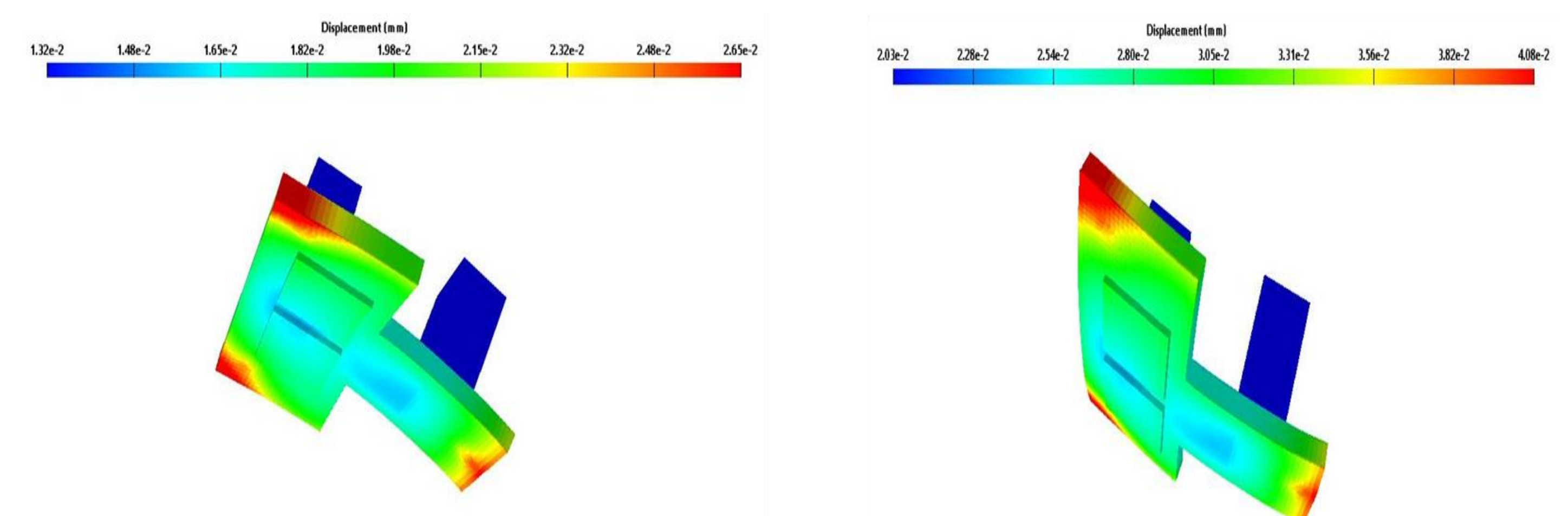


Fig. 6: Thermo-mechanical displacement at -40°C (left) and 125°C (right)

Table 2: Solder Fatigue Analysis for 0.10mm solder thickness

RefDes	Package	Part Type	Model	Side	Material	Solder	Max dT (C)	Damage	TTF (years)	Cycles To Fail	Score
R1_1	0402	RESISTOR	CC	TOP	ALUMINA	SAC305	165.0	4.3E0	2.32	20.305	0.0
Rg1_1	0402	RESISTOR	CC	TOP	ALUMINA	SAC305	165.0	4.3E0	2.32	20.305	0.0
Rg2_1	0402	RESISTOR	CC	TOP	ALUMINA	SAC305	165.0	4.3E0	2.32	20.305	0.0
Rg3_1	0402	RESISTOR	CC	TOP	ALUMINA	SAC305	165.0	4.3E0	2.32	20.305	0.0
Rs1_1	0402	RESISTOR	CC	TOP	ALUMINA	SAC305	165.0	4.3E0	2.32	20.305	0.0
Rs2_1	0402	RESISTOR	CC	TOP	ALUMINA	SAC305	165.0	4.3E0	2.32	20.305	0.0
_Gate...	SOT-23-6	IC	Leaded	TOP	OVERMOLD-LEADED	PB905N10	165.0	3.0E0	3.32	29.059	0.0
C1_1	0402	CAPACITOR	CC	TOP	BARIUMTITANATE	SAC305	165.0	2.0E0	4.93	43.202	0.0
Q1_1	GS66516T	TRANSISTOR	QFN	BOT	EPOXYENCAPSULANT	SAC305	165.0	1.8E0	5.41	47.448	0.0
Q2_1	GS66516T_1	TRANSISTOR	QFN	BOT	EPOXYENCAPSULANT	SAC305	165.0	1.8E0	5.41	47.448	0.0
Header1	10129380903001ALF	PLUG CONNECTOR	Leaded	TOP	BRASS	PB905N10	165.0	3.1E-3	>100	27.983.240	10.0
Header2	10129380902001ALF	PLUG CONNECTOR	Leaded	TOP	BRASS	PB905N10	165.0	2.1E-3	>100	42.066.072	10.0

Next Plan

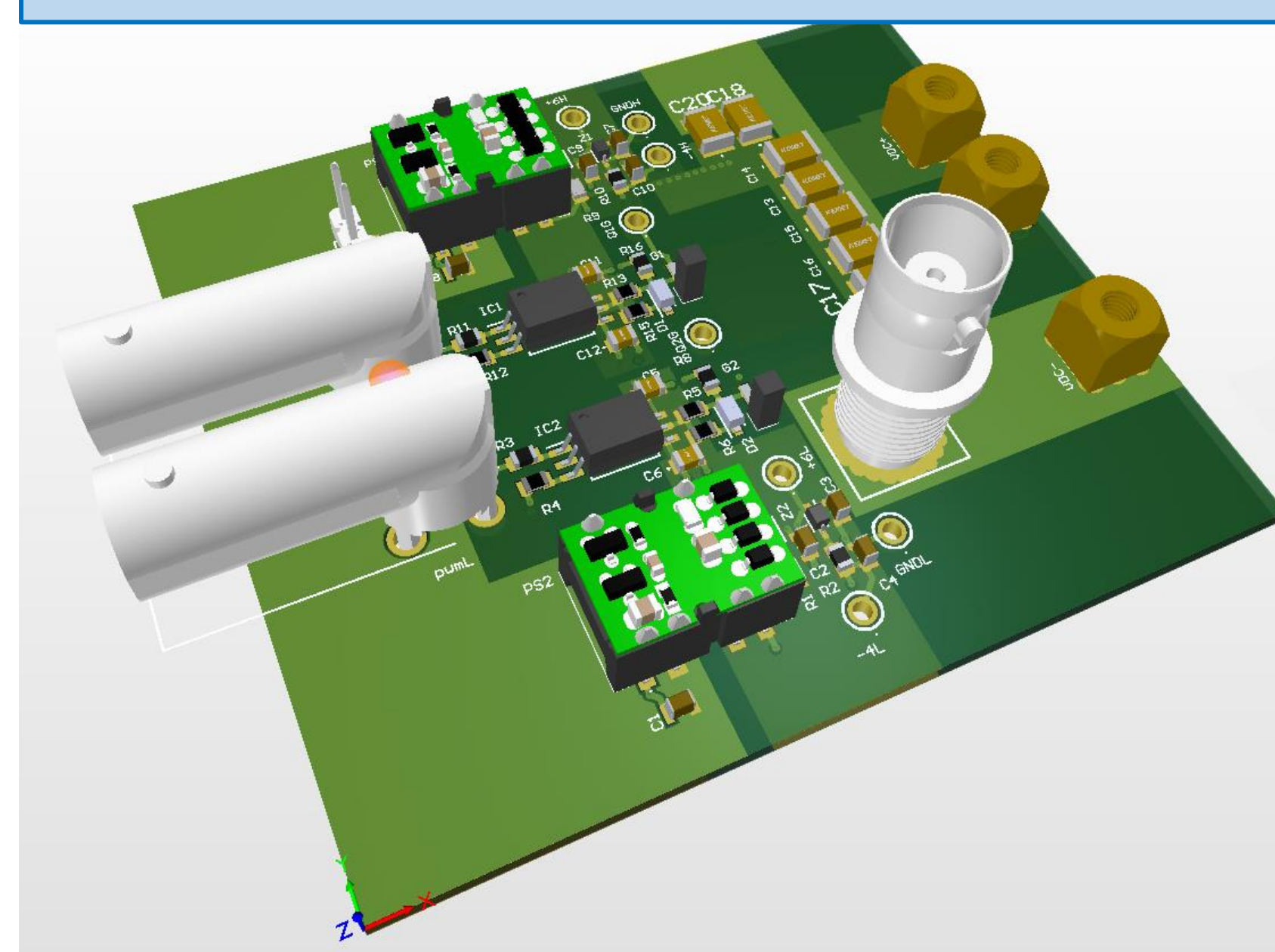


Fig. 7: A printed circuit board developed for DPT test

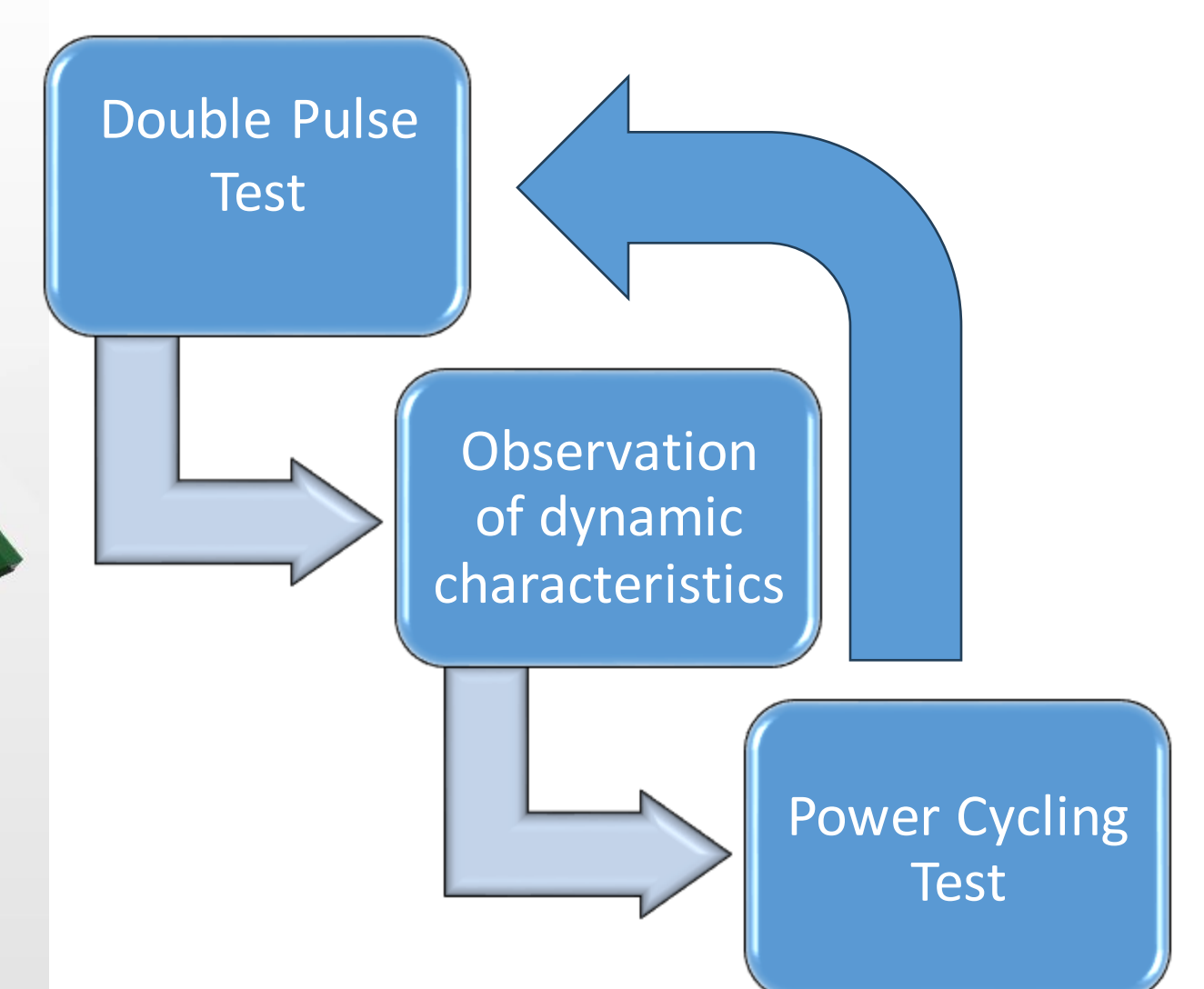
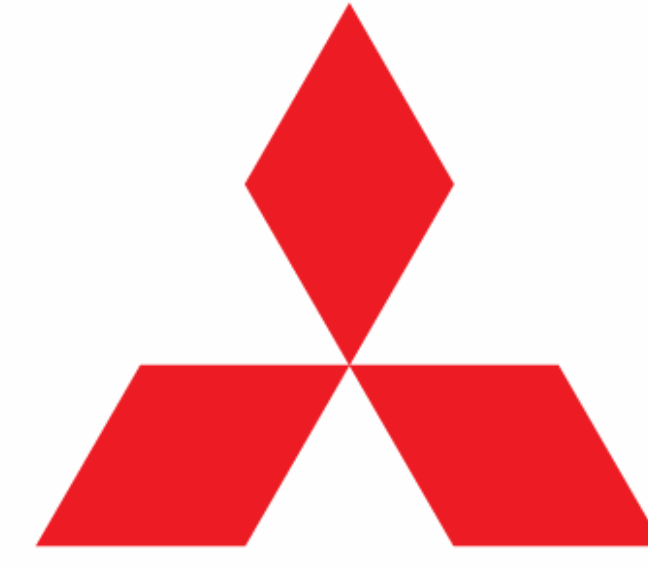


Fig. 8: Comparison of dynamic characteristics before and after power cycling test

Conclusion

- Thermo-mechanical simulation shows solder fatigue will cause failure to all components except the headers.
- The health indicators of GaN devices ($R_{ds,ON}$, V_{th} , Drain Current etc.) will be identified through thermal and power cycling tests.
- Monitoring circuits will be developed for detecting anomalies of the health indicators during the operation of GaN power module.
- Collected data will be used to extrapolate over time to define decision support for condition-based maintenance, aiming to detect present state and future failure of the GaN devices.
- It will help prevent catastrophic system failures & maximize lifespan.



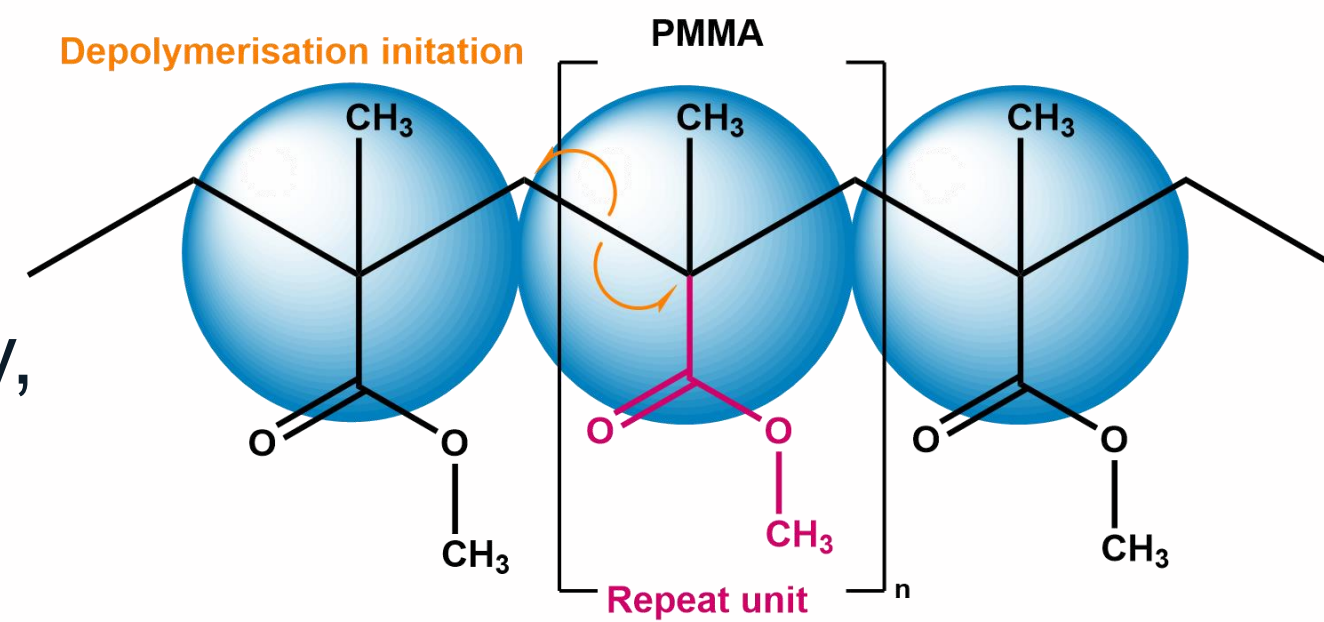
Impact of reaction temperature on the liquid crude purity of pyrolysed commercial poly(methyl methacrylate)

Michelle Duong¹, Josh Walton², Derek Irvine¹, Mohamed Adam¹, Eleanor Binner¹

1. Faculty of Engineering, University of Nottingham, NG7 2RD, United Kingdom
2. Mitsubishi Chemicals UK, Wilton Centre, Wilton, Redcar TS10 4RF, United Kingdom

INTRODUCTION

- Projected global market of 2.8Mt by 2028, therefore there is interest to recycle poly(methyl methacrylate) (PMMA) and reclaim the monomer¹, methyl methacrylate (MMA), through depolymerisation.
- Depolymerisation** of PMMA occurs via a series of radical directed reactions triggered by heat², however % monomer recovery is dependent on the degradation temperature and mechanistic pathway³. Chemical recycling can reach > 95% MMA recovery².
- PMMA has poor heat transfer properties therefore conventional depolymerisation techniques suffer processing challenges.
- Repeating unit of PMMA is polar therefore can move under the influence of microwaves allowing dielectric heating. **Microwave processing** can heat volumetrically, overcoming conventional processing challenges, and provide better product purity.
- Aim: investigate whether the observed differences in liquid crude purity was due to processing differences or changes in the depolymerisation pathway.**



METHODOLOGY

- PMMA was depolymerised using a microwave pyrolysis (MP) system, and a tube furnace (conventional) system via a batch based **stepwise pyrolysis – whereby each run is progressively processed at higher conversion**
- Conventional pyrolysis (CP) of PMMA was conducted at various reaction temperatures until depolymerisation finished – **when no more pyrolytic vapours are observed passing through the condensate collection system**
- Key impurities in the liquid crude were characterised using gas chromatography

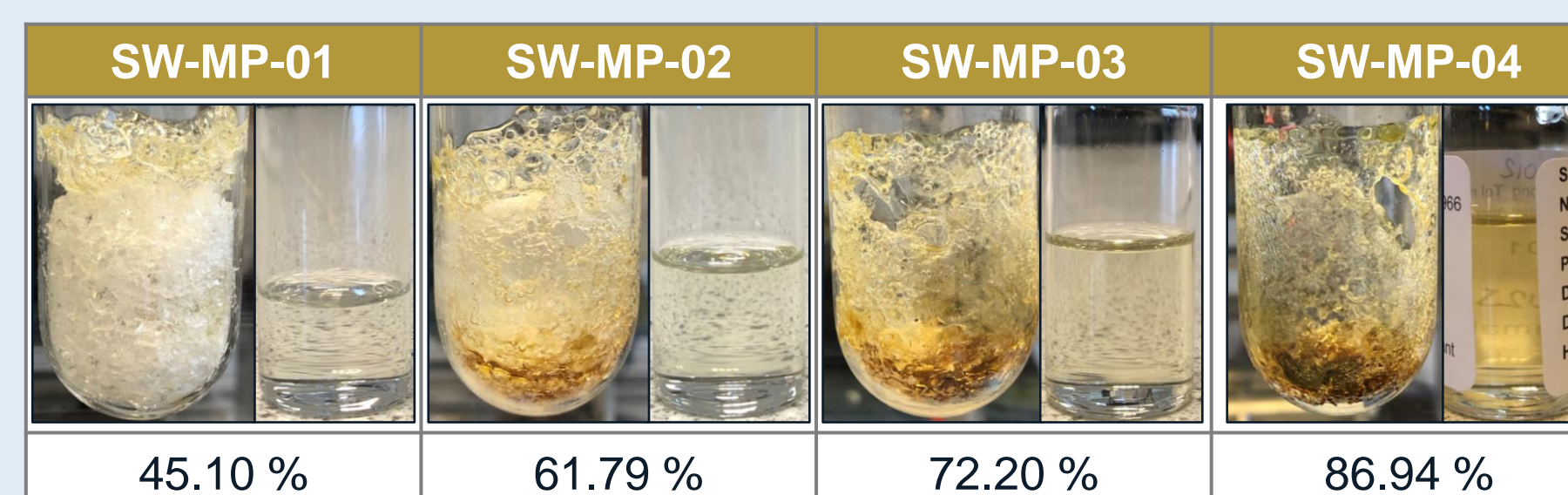
RESULTS & DISCUSSION

- Under **MP**, liquid crude was less discoloured, less char formed in remaining undepolymerised solid crude, and **lower wt. % of impurities observed at higher conversion** compared to conventional pyrolysis.
- Reducing reaction temperatures under CP reduced char formation on reactor walls at the expense of reduced PMMA conversion.
- Select **key impurities** increased with conversion and reaction temperature suggesting these were dependent on processing parameters whilst other impurities were formed in equal wt. % despite changes in reaction temperature.
- Thermally stable structures formed at higher conversion⁴** required higher temperatures for complete degradation promoting further impurities.

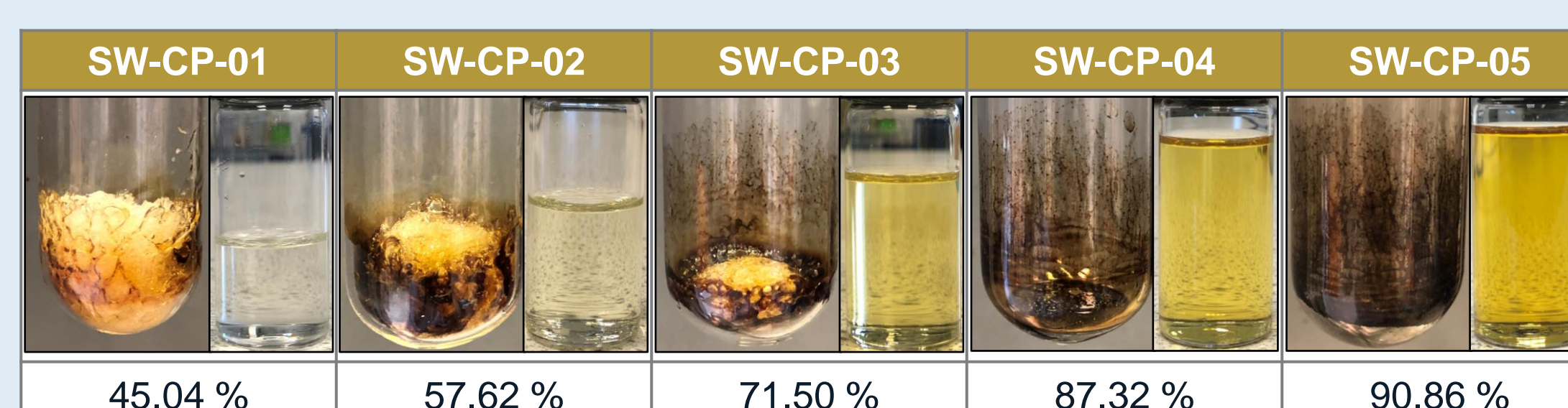
CONCLUSION

- Conventional pyrolysis required higher processing temperatures for complete PMMA conversion due to formation of thermally stable structures resulting from changes in the depolymerisation mechanistic pathway, thus forming more impurities.
- For the same conversion, microwave pyrolysis produced a liquid crude with better product purity.

A) STEPWISE MICROWAVE PYROLYSIS



B) STEPWISE CONVENTIONAL PYROLYSIS



C) DEPOLYMERISATION AT DIFFERENT REACTION TEMPERATURES

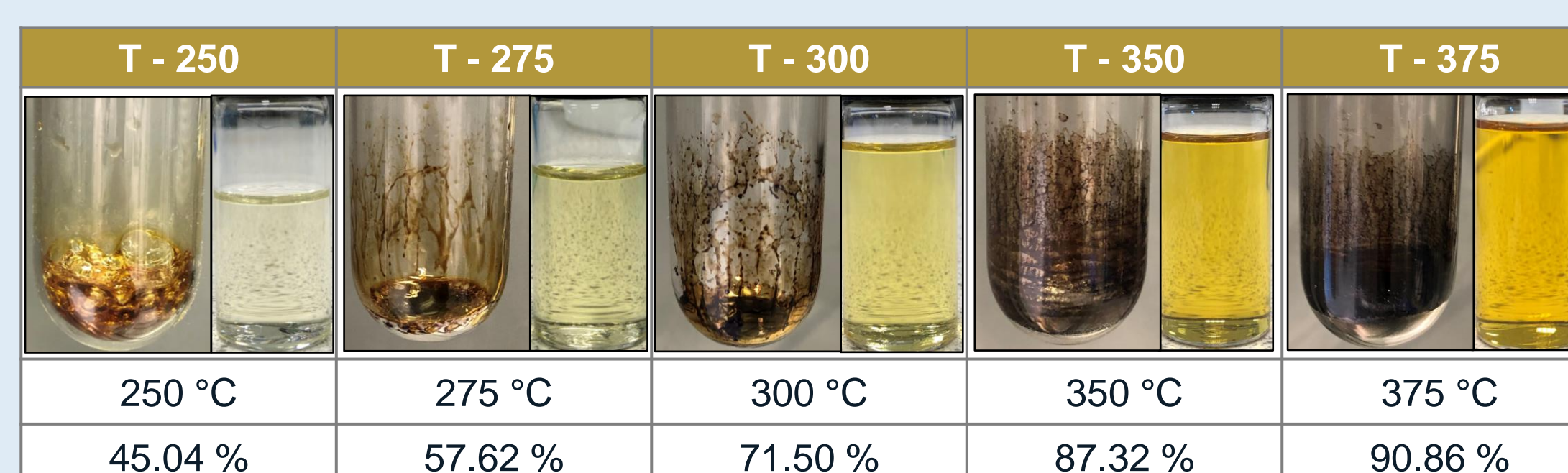


Figure 1 – Images of pyrolysed solid (left) and liquid (right) crude product for each experimental run in set A, B and C. PMMA conversion for each run shown and is defined as wt. % liquid crude. Microwave pyrolysis was conducted at 800 W with processing temperatures ranging between 350 – 400 ° C (A). Conventional pyrolysis was conducted at 450 ° C set temperature with processing temperatures ranging between 300 – 400 ° C. Average reaction temperatures for set C displayed in figure.

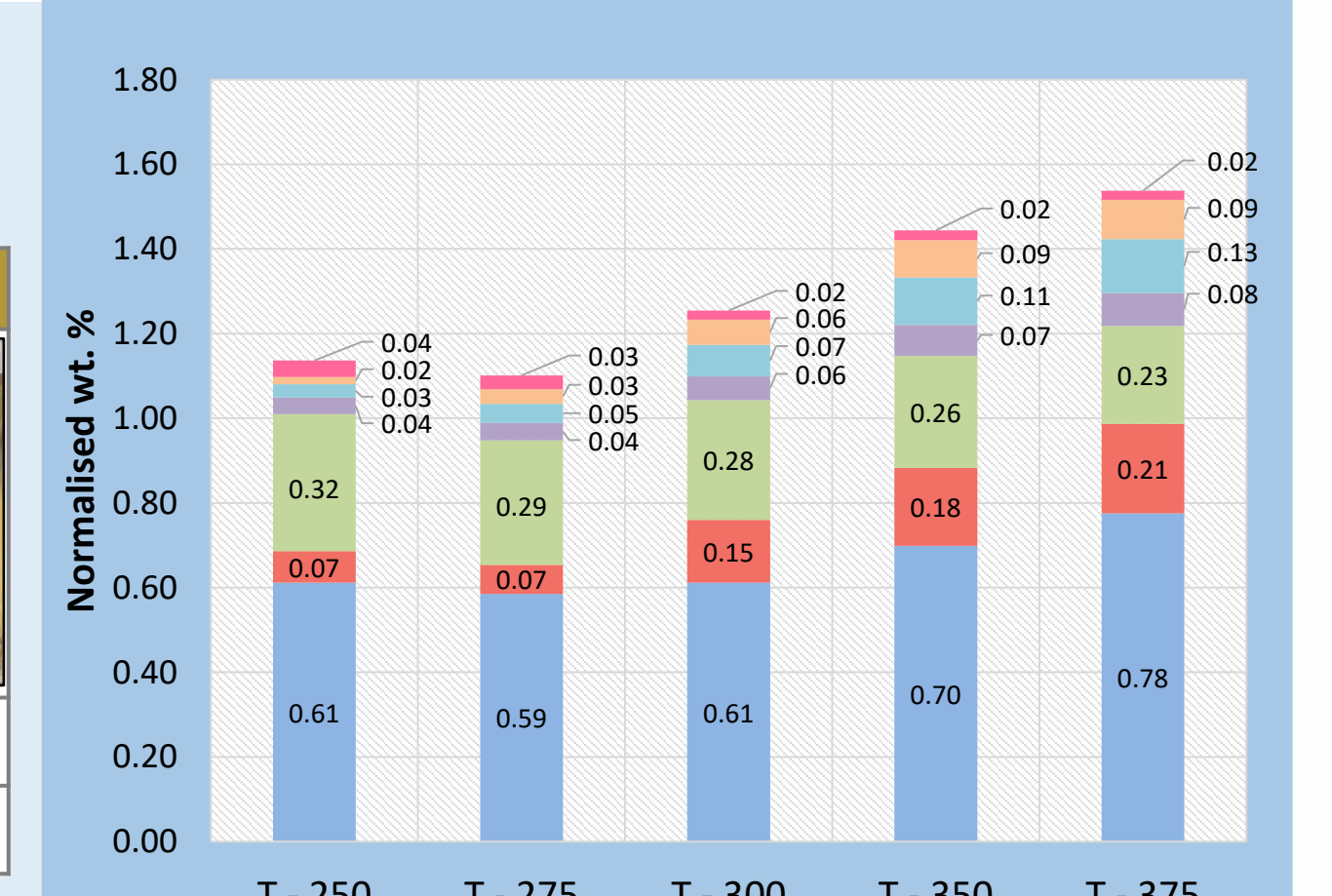
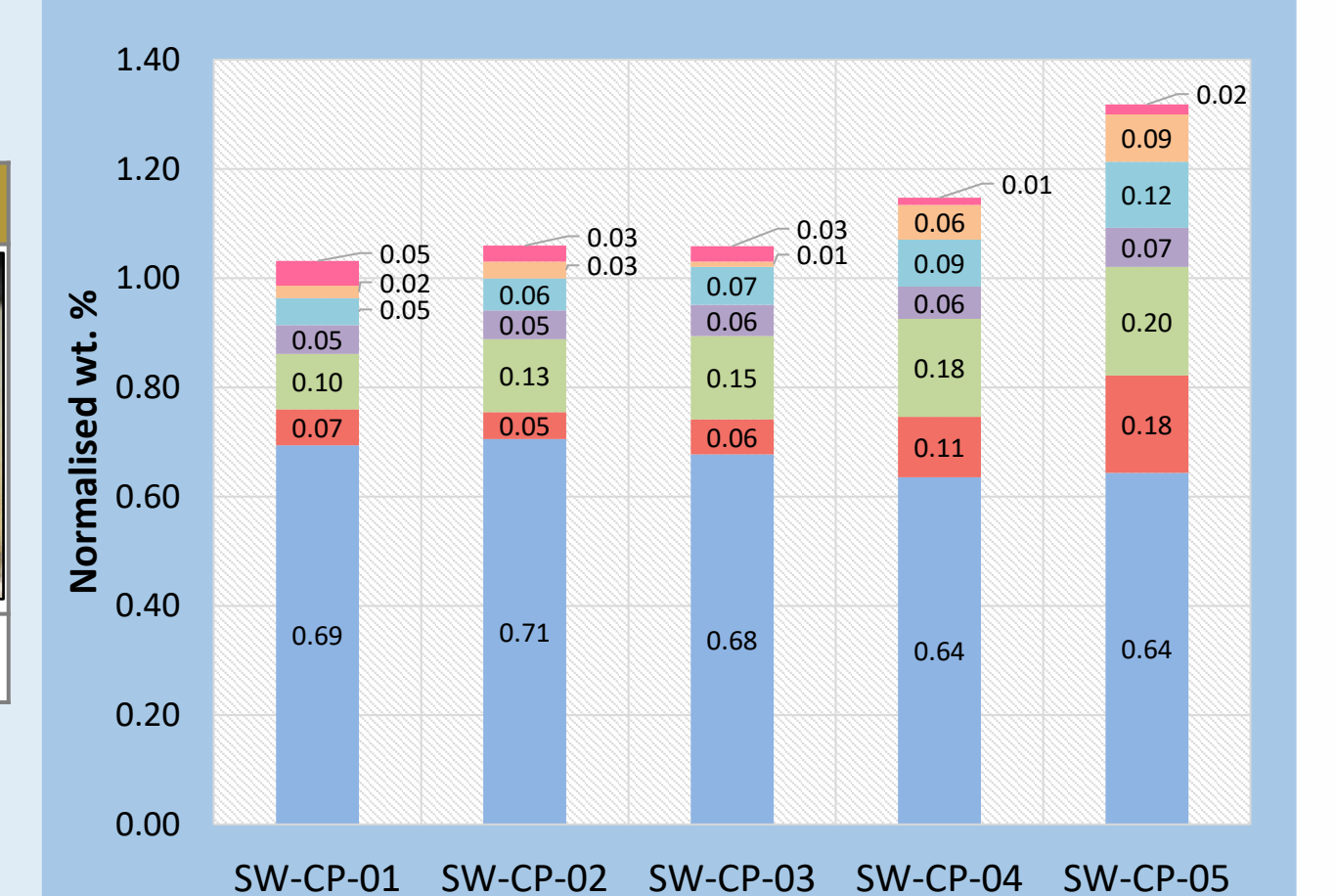
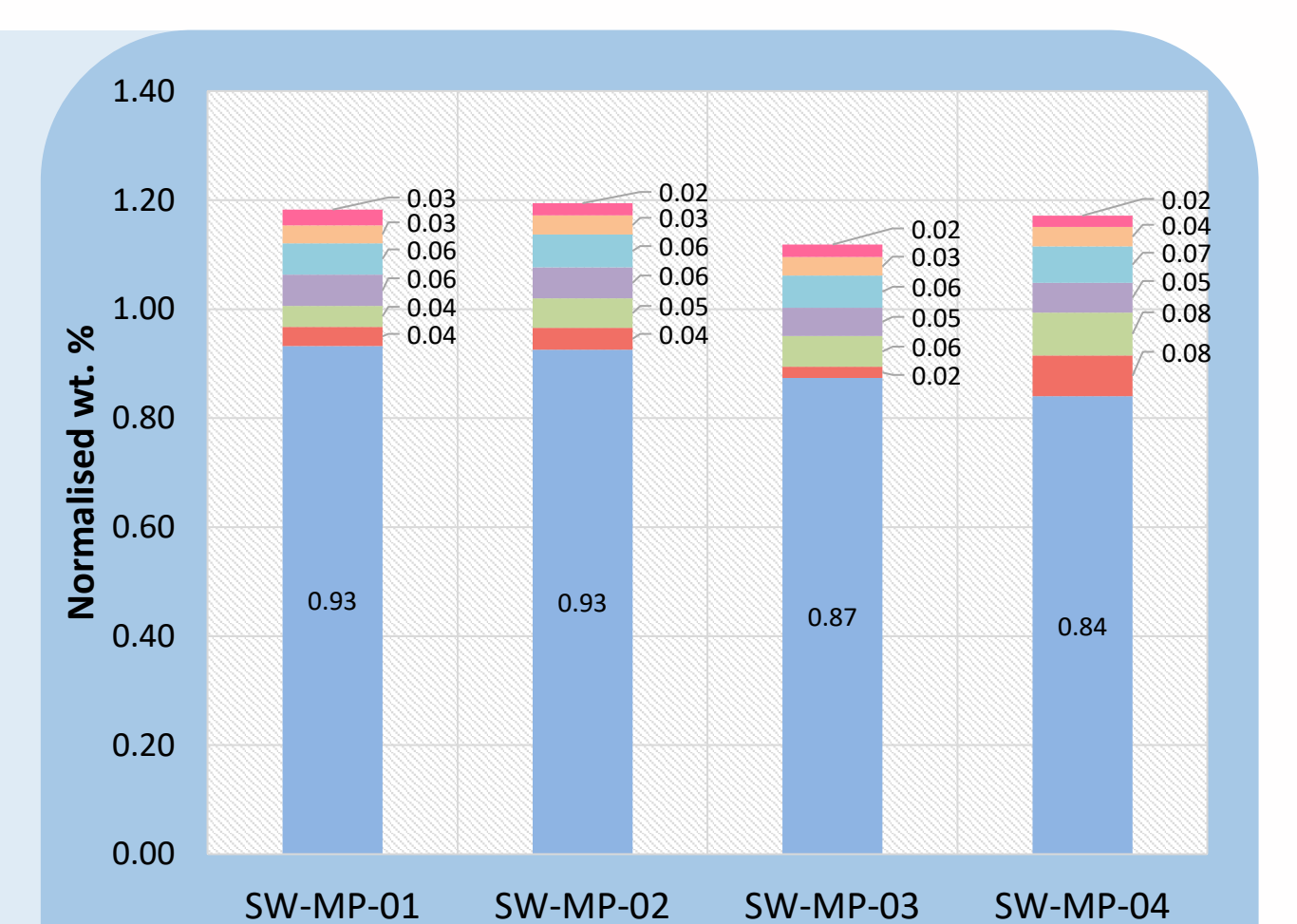
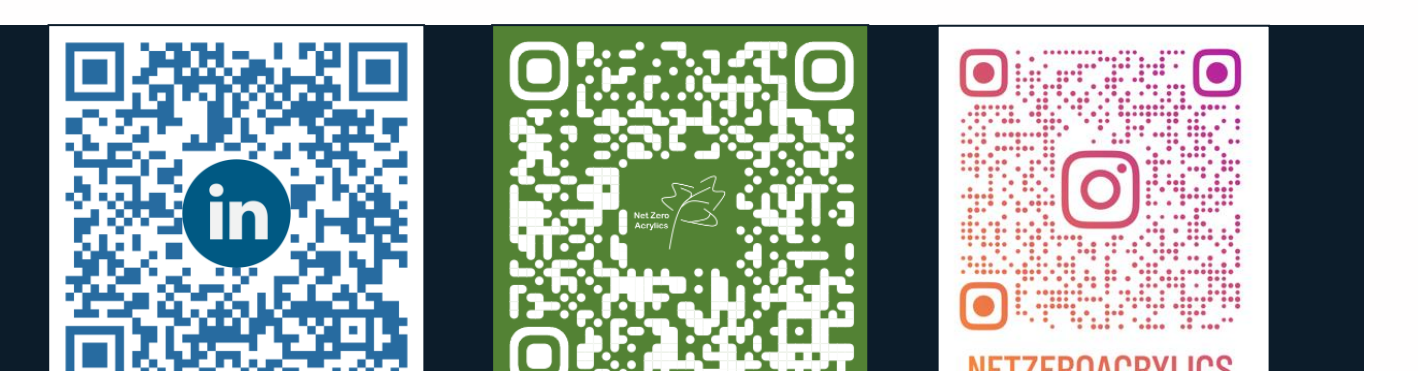


Figure 2 – normalised wt. % of MMA close boilers, identified as key impurities produced in pyrolysed liquid crude.

References:

- J. De Tommaso and J. L. Dubois, *Polymers* 2021, Vol. 13, Page 2724, 2021, 13, 2724.
- E. K. C. Moens, K. De Smit, Y. W. Marien, A. D. Trigilio, P. H. M. Van Steenberghe, K. M. Van Geem, J. L. Dubois and D. R. D'hooge, *Polymers* 2020, Vol. 12, Page 1667, 2020, 12, 1667.
- B. J. Holland and J. N. Hay, *Polym Degrad Stab*, 2002, 77, 435–439.
- F. M. Uhl, G. F. Levchik, S. V. Levchik, C. Dick, J. J. Ligat, C. E. Snape and C. A. Wilkie, *Polym Degrad Stab*, 2001, 71, 317–325.



Machine learning techniques for the development of a smart photogrammetric system

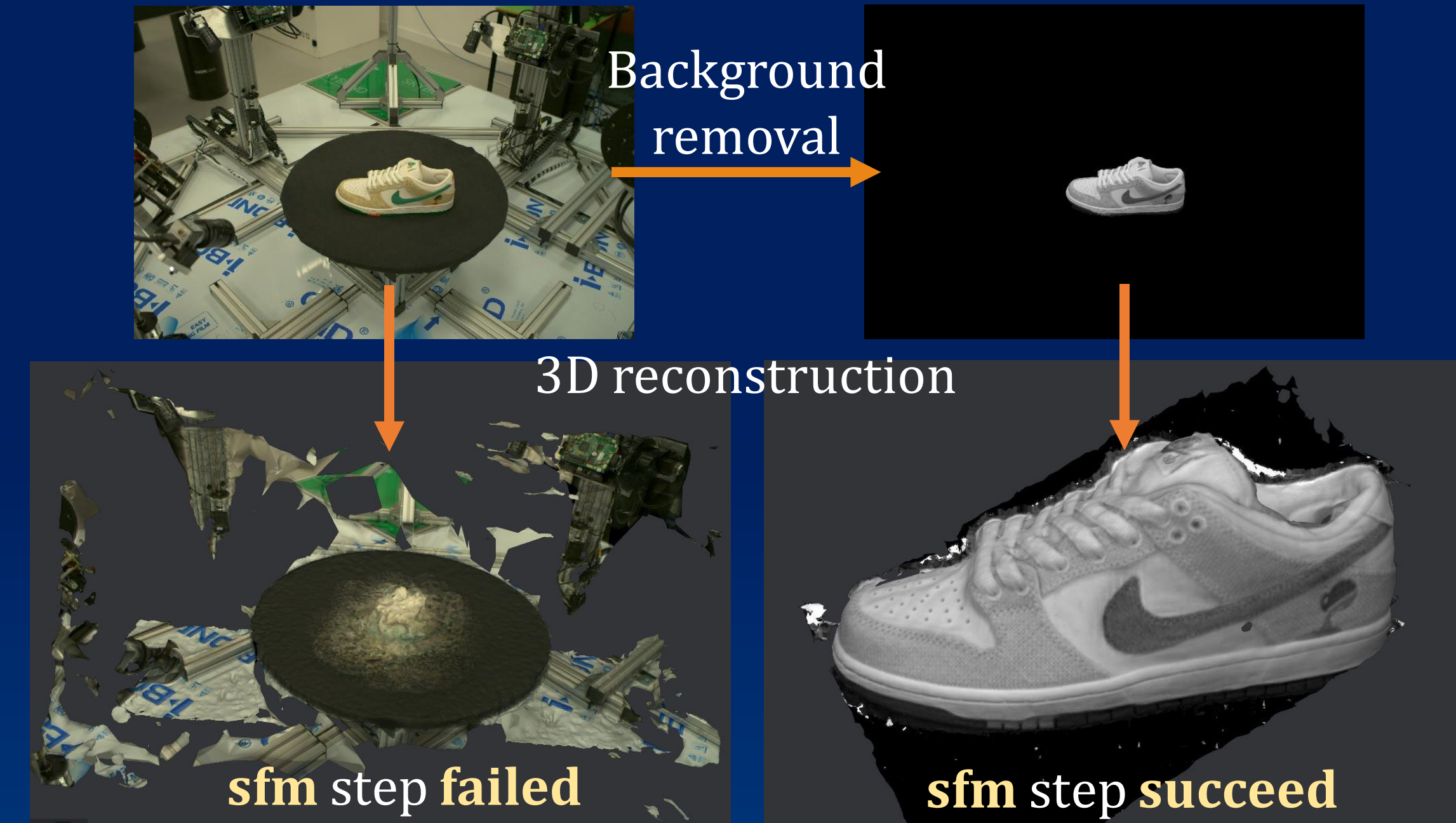
Mingda Harvey Yang

mingda.yang@nottingham.ac.uk

Introduction

In the manufacturing industry, photogrammetry involves acquiring images of parts from chaotic manufacturing environments, thereby analysing the geometric properties and relationships between multiple images and creating 3D reconstructions of objects or scenes. While photogrammetry can be used to reconstruct a point cloud with relative ease, the **structure-from-motion (sfm)** step of the reconstruction process can **fail** when the background of the images is complex or changing. To solve this problem, a background removal operation of the measurand is often necessary before performing reconstruction. The goal of this project is to make a **fully autonomous** photogrammetry pipeline by integrating machine learning to provide accurate measurements with **minimal user intervention**.

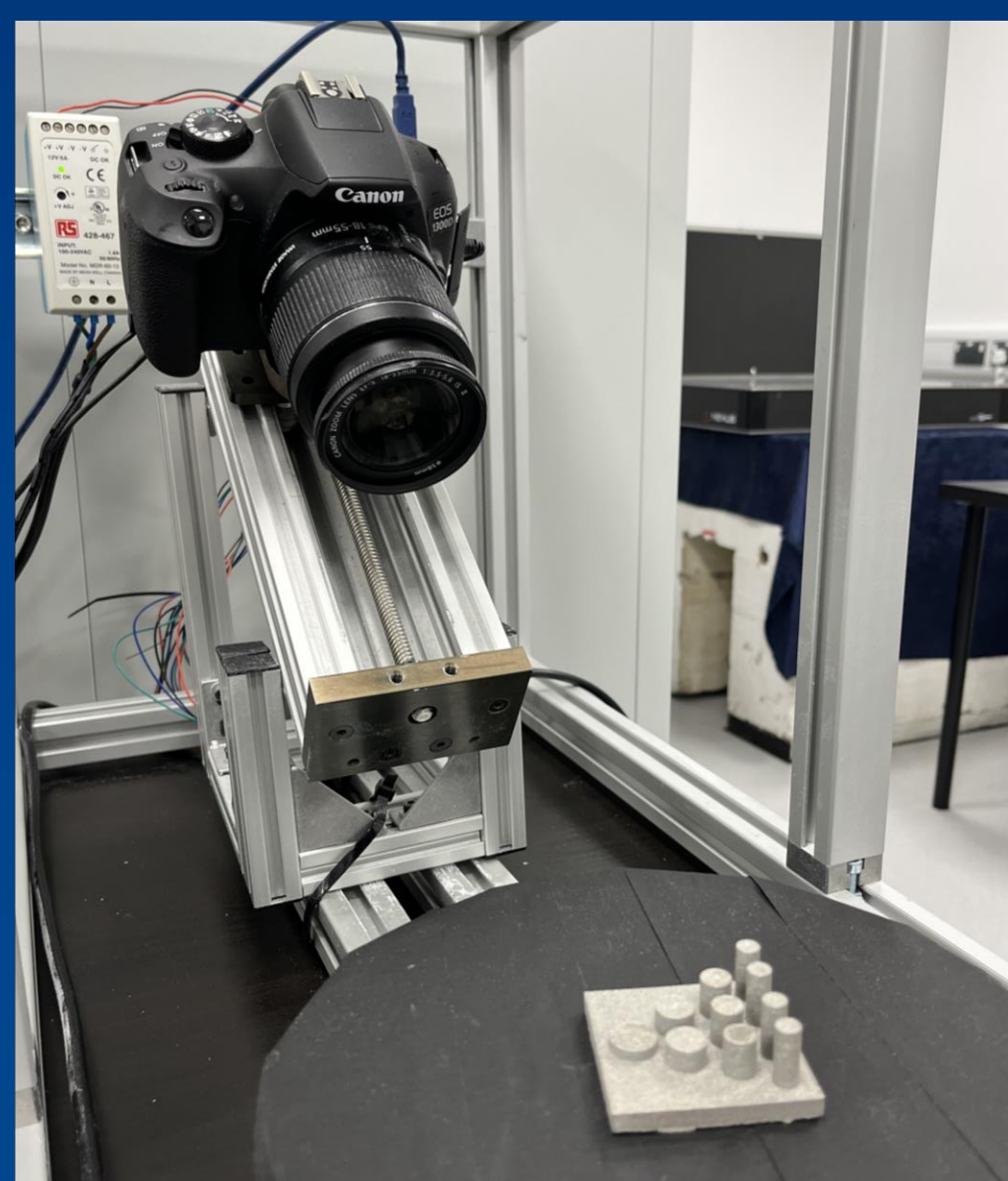
Image acquisition of measurand placed on a rotary stage



Difference of reconstruction between with/without background

Latest progress of photogrammetry pipeline

Preliminary results for the proposed photogrammetry pipeline within a DSLR camera setup.



Monocular photogrammetry system with a static DSLR camera

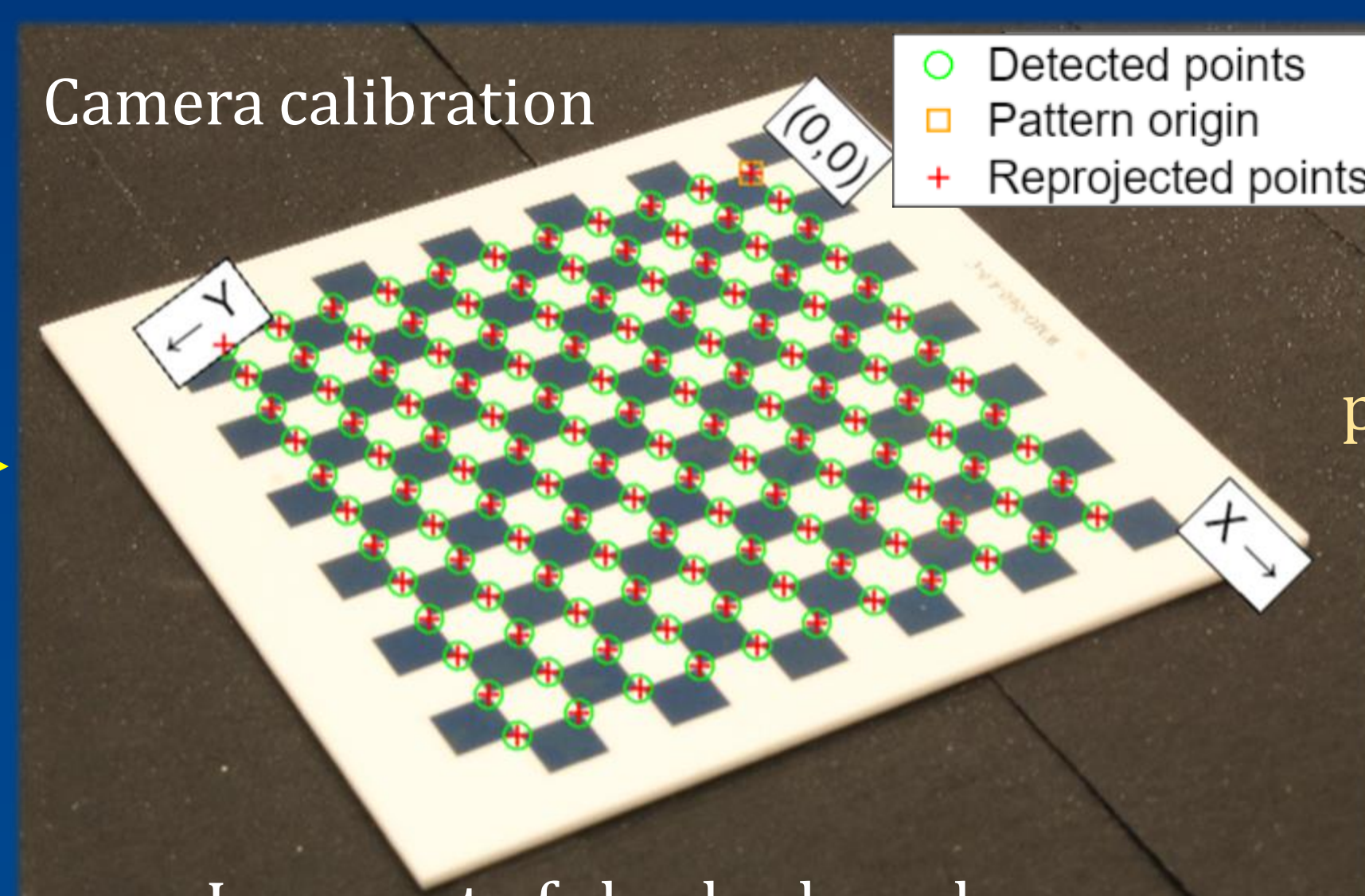
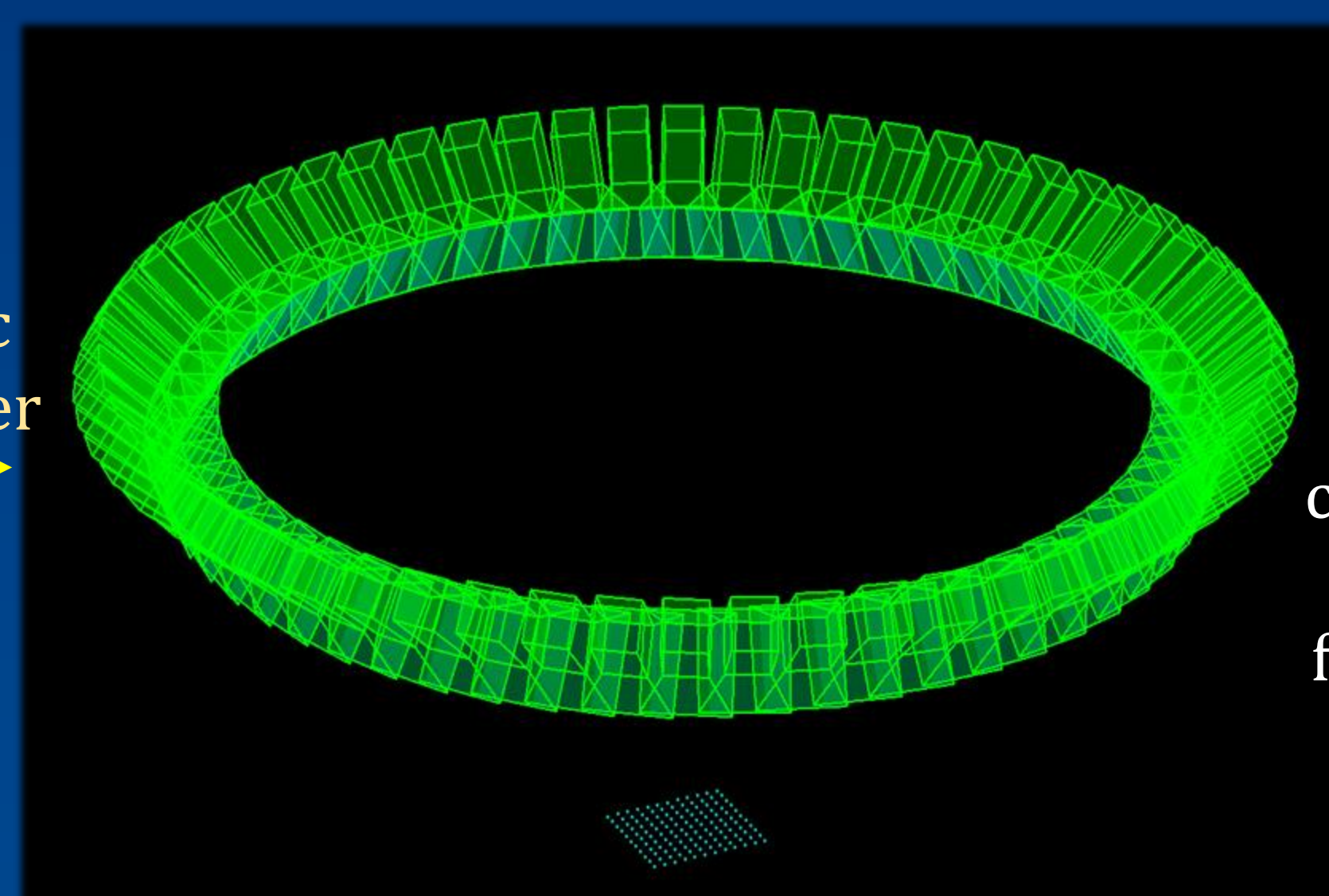
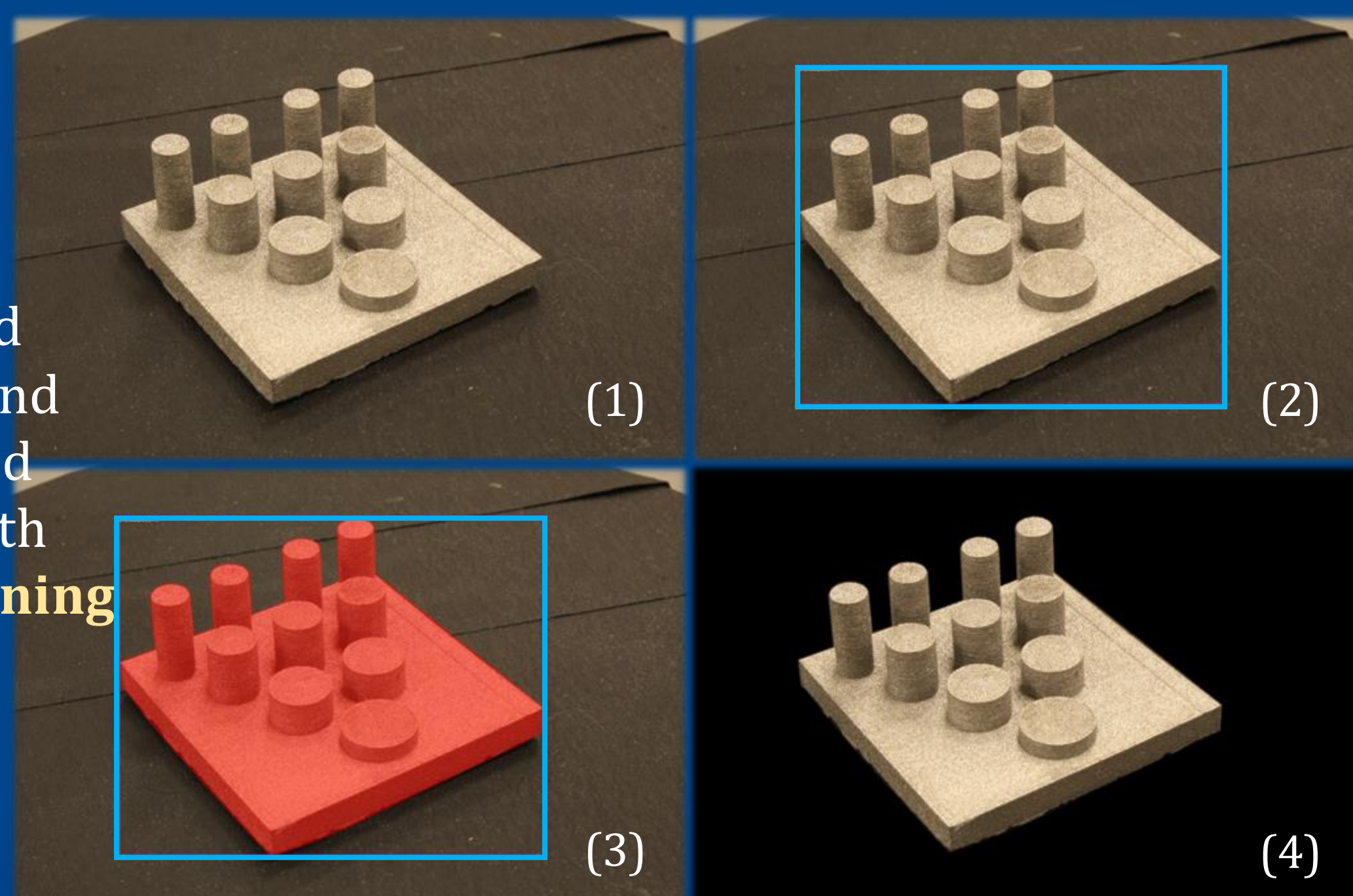


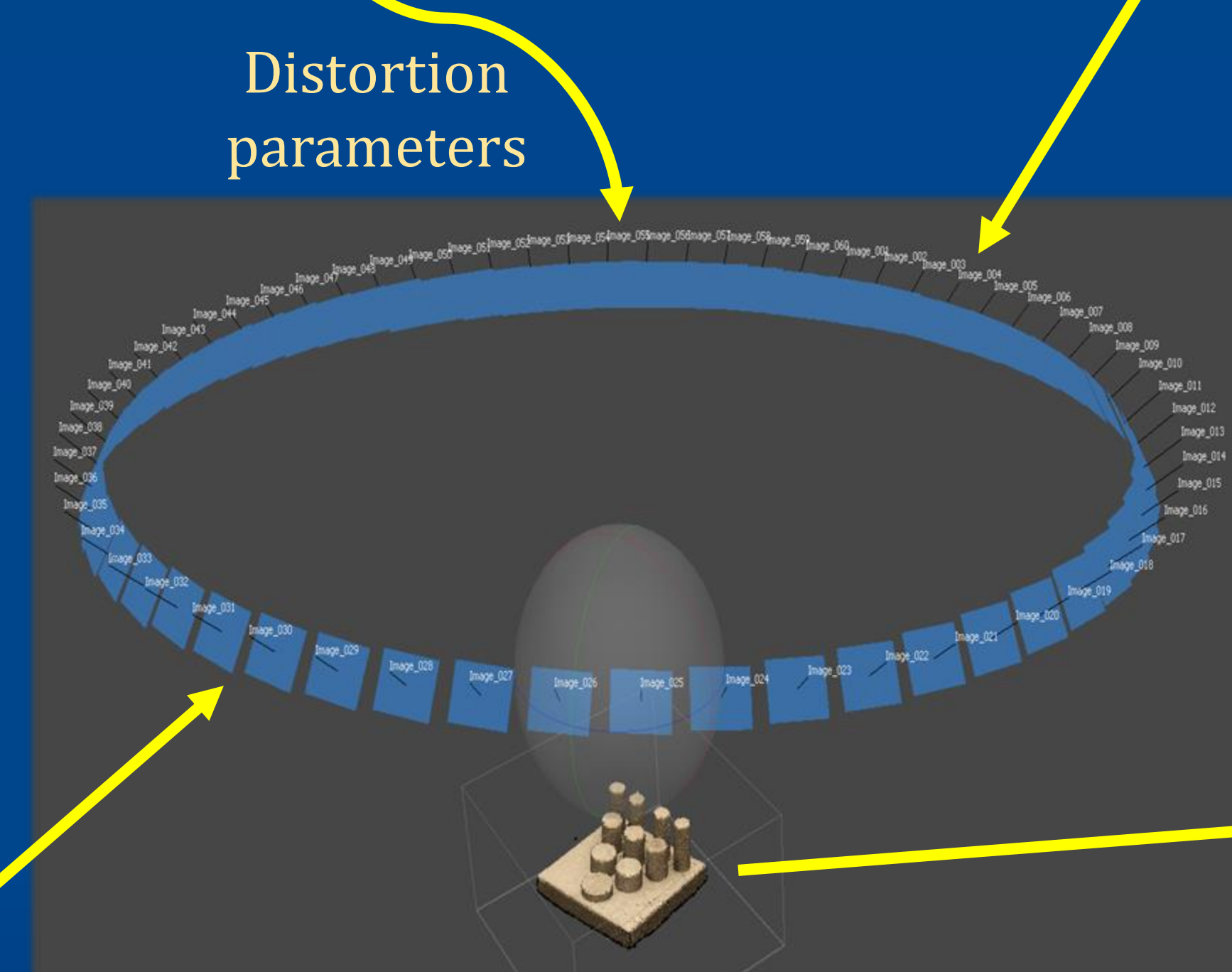
Image set of checkerboard (one image taken every 6° for a total of 60 images)



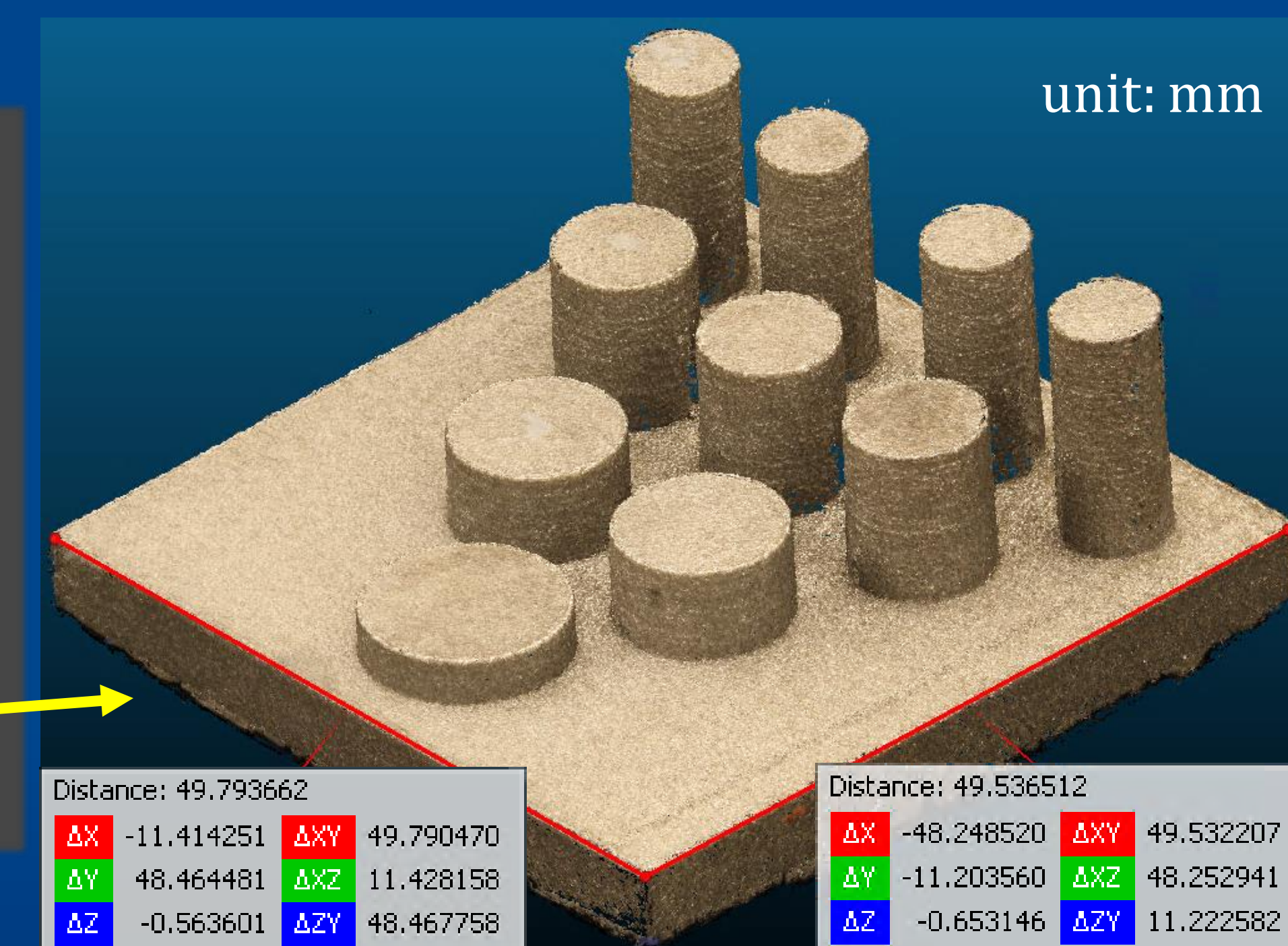
Calculate each camera position and orientation for point cloud **scale-calibration** (extrinsic parameters from total 60 positions)



1. Initial image set of measurand (one image taken every 6° for a total of 60 images)
2. Use **Grounding DINO** [1] for object **detection**
3. Use **Segment Anything Model** [2] for object **segmentation**
4. Background-removed image set generation



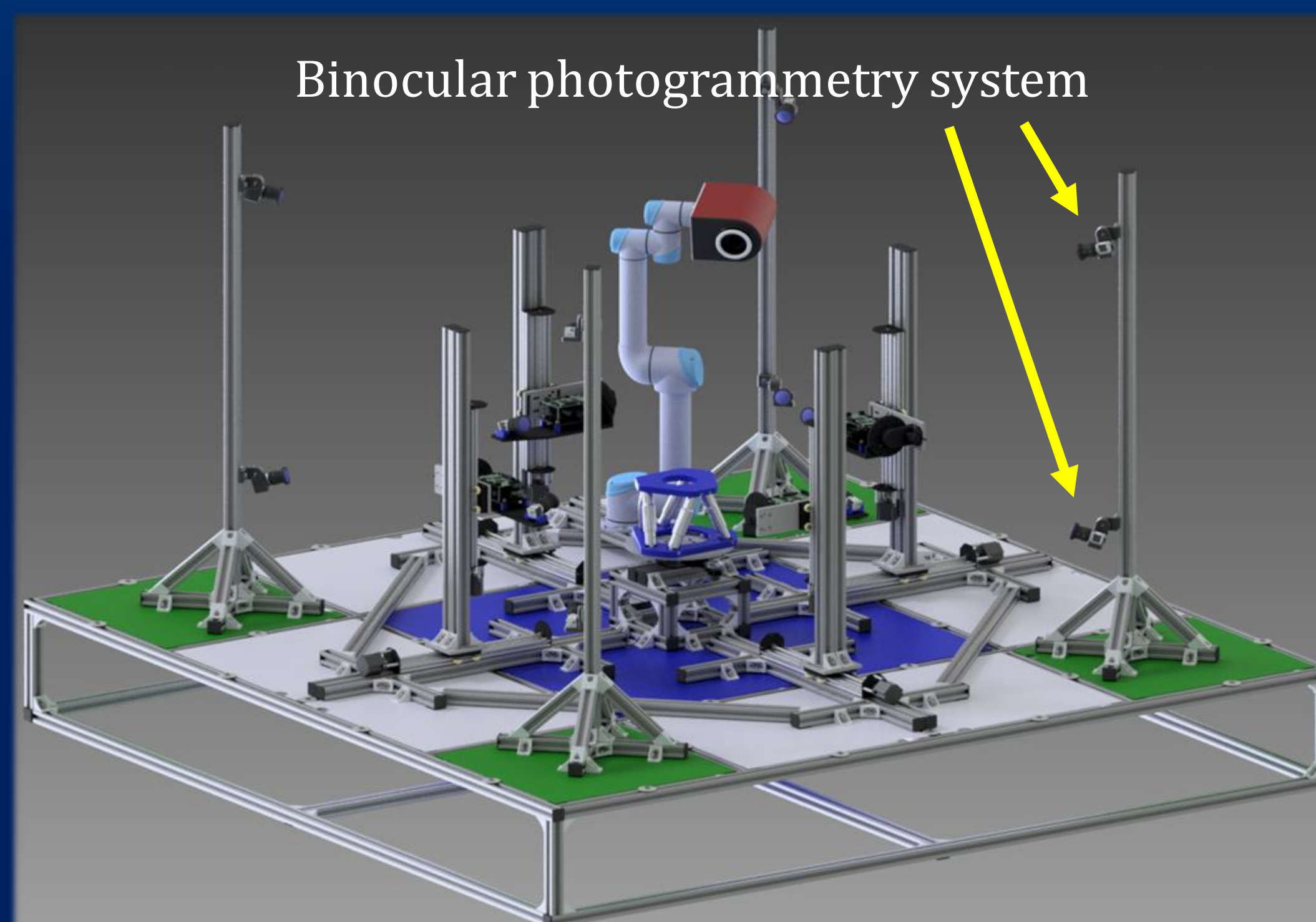
3D reconstruction with visualized camera positions



Scale-calibrated dense point cloud (18M points to compare with 73M points reconstructed with background)

Future work

1. Investigate the compatibility of the pipeline above in different measurement scenario (MCDDM demonstrator, etc.)
2. Compare the reconstructed point cloud with the corresponding **CMM** data to determine the accuracy.
3. Use **CAD** model for algorithm training to replace the language model by Grounding DINO in object detection branch.
4. Implement **Neural Radiance Fields** [3] for reconstruction, **Gaussian splatting** [3] for data smoothing and noise reduction.



CAD model for the Midlands Centre for Data-Driven Metrology (MCDDM) demonstrator



Acknowledgement

The authors would like to thank the UKRI Research England Development (RED) Fund for funding this work via the Midlands Centre for Data-Driven Metrology.

Reference

- [1] Liu S, Zeng Z, Ren T, Li F, Zhang H, Yang J, ... & Zhang L 2023 Grounding DINO: Marrying DINO with grounded pre-training for open-set object detection. arXiv preprint arXiv: 2303.05499
- [2] Kirillov A, Mintun E, Ravi N, Mao H, Rolland C, Gustafson L, ... & Girshick R 2023 Segment anything. arXiv preprint arXiv: 2304.02643
- [3] Kerbl B, Kopanas G, Leimkühler T, & Drettakis G 2023 3D Gaussian Splatting for Real-Time Radiance Field Rendering. ACM Transactions on Graphics, 42(4)



Background

New operational conditions in power plants accelerate the degradation of materials due to:

- Higher operational temperatures for increased efficiency (see Figure 1).
- Flexible operation modes.
- More start-up and shut-down cycles

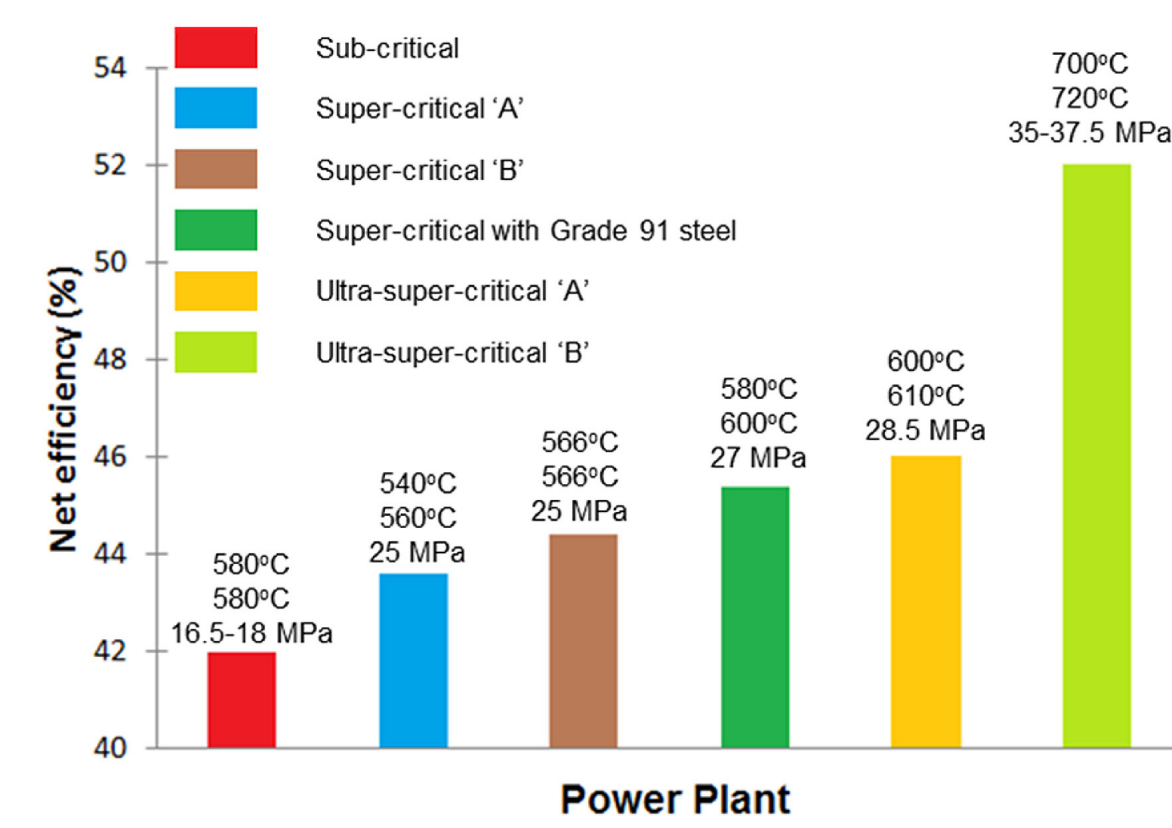


Figure 1. Comparison of net efficiencies in power plants cited by [2].

Failure Mechanisms

Table 1. Common, time dependent and cyclic, life reducing mechanisms found in gas turbine components caused by different types of stress. The influence is symbolically presented as: ● major contribution, ○ local effect, ✗ insignificant [1].

Components	Oxidation, corrosion, erosion	Creep	LCF	HCF
Turbine blades	●	●	●	●
Compressor blades	✗	✗	○	●
Inner casing	●	●	○	○
Rotor structure (except blades)	✗	●	●	✗
Outer casing	✗	●	○	✗
Pipework	✗	○	●	●

Aim and objectives

The project aims to enhance gas turbine component lifetime prediction through:

- Experimental Work:** Testing 26 NiCrMoV 115 (St 572 S) Steel.
- Life Prediction Models:** Developing viscoplastic models to include non-local damage and life prediction.
- ANNs Model:** Using Artificial Neural Networks (ANNs) to predict material lifetimes.

Methodology

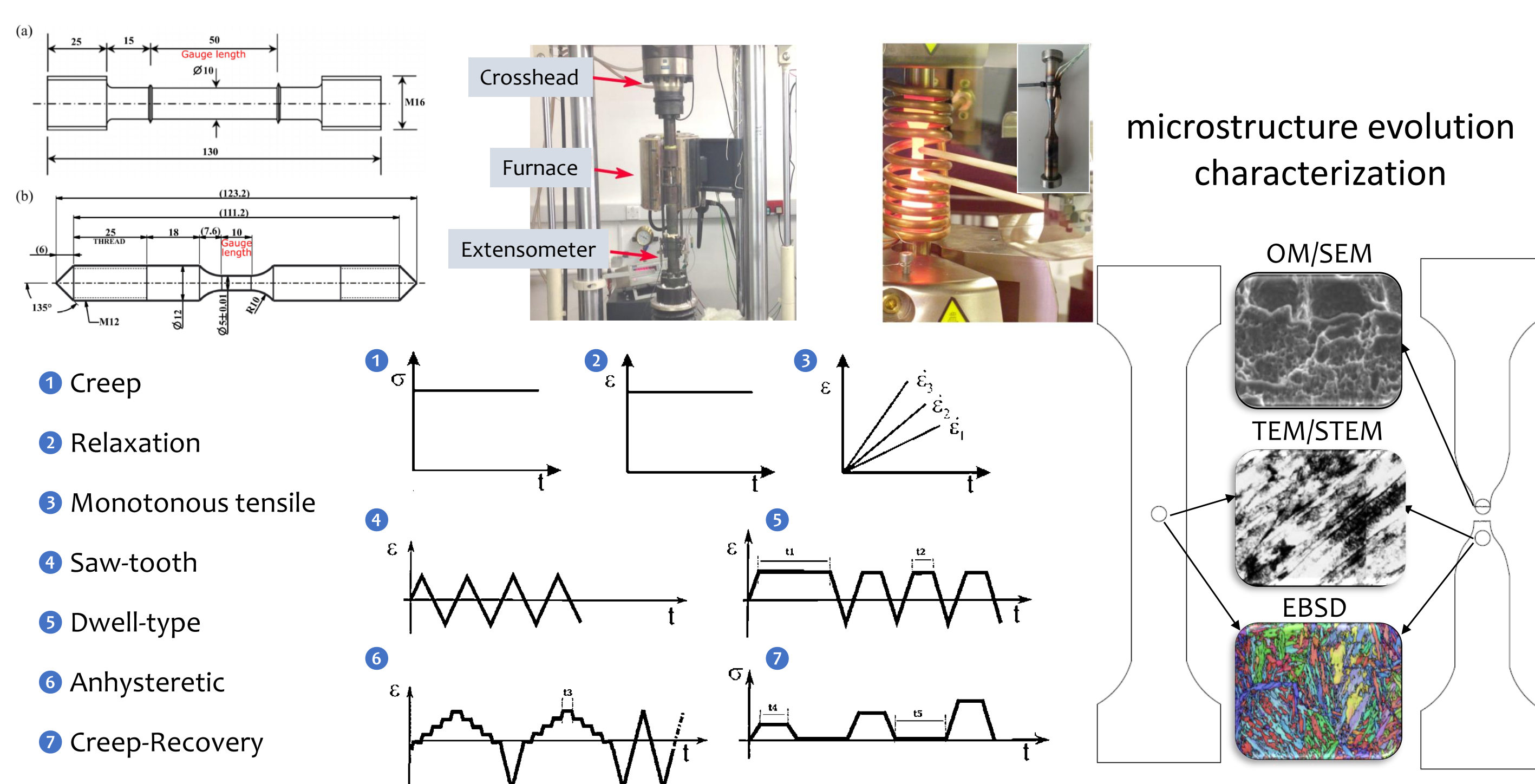


Figure 2. Creep-Fatigue at high temperature conditions

Modelling using TIP and GSM for constitutive equations, considering non-local state variables → calibration with experimental data → UEL subroutine → FEA simulations.

similar works and expected results

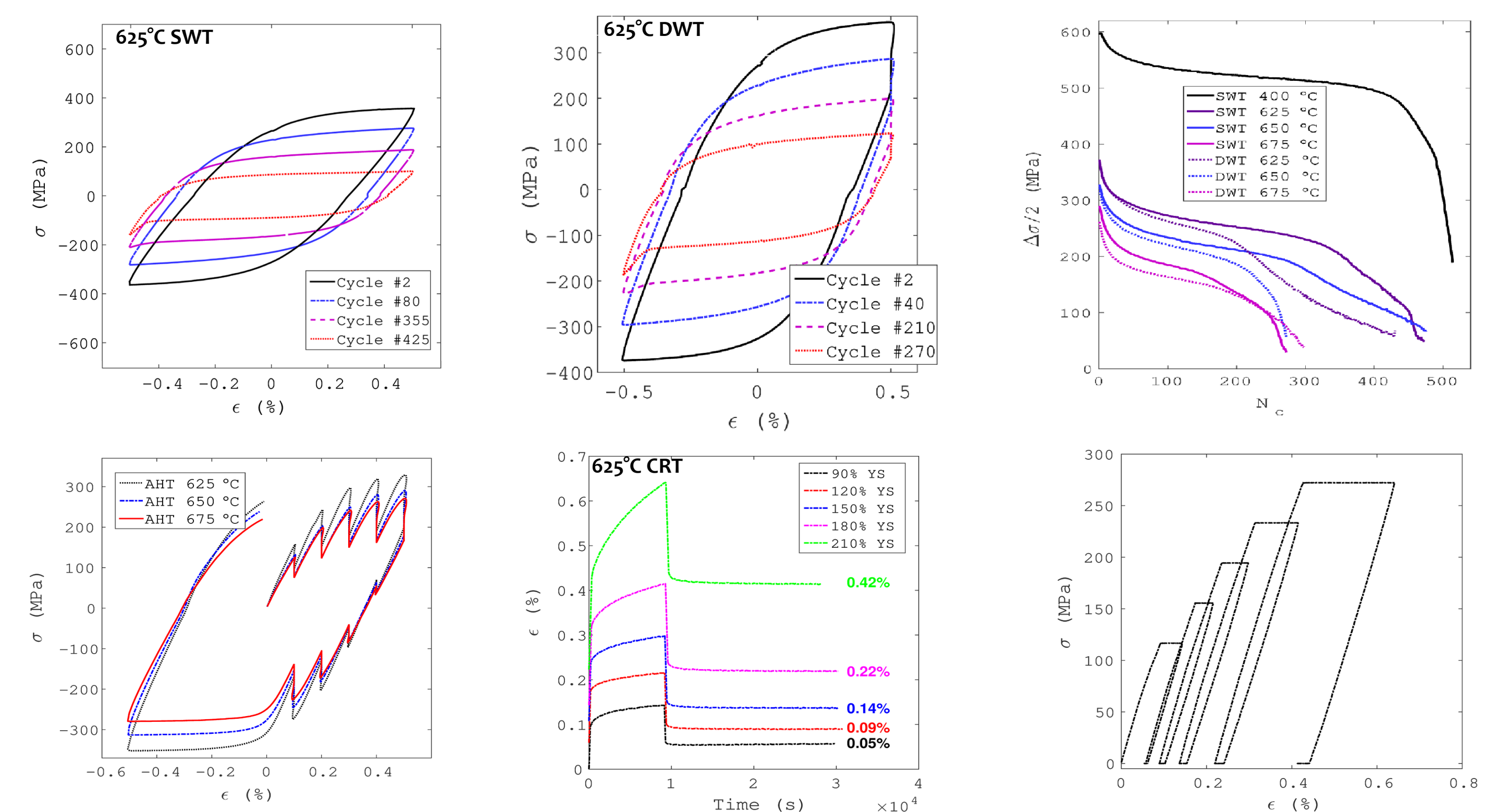


Figure 3. Mechanical responses for various tests: cyclic softening, stress relaxation, fatigue life, creep-fatigue interaction, creep recovery, and cyclic ratcheting during fatigue testing [3].

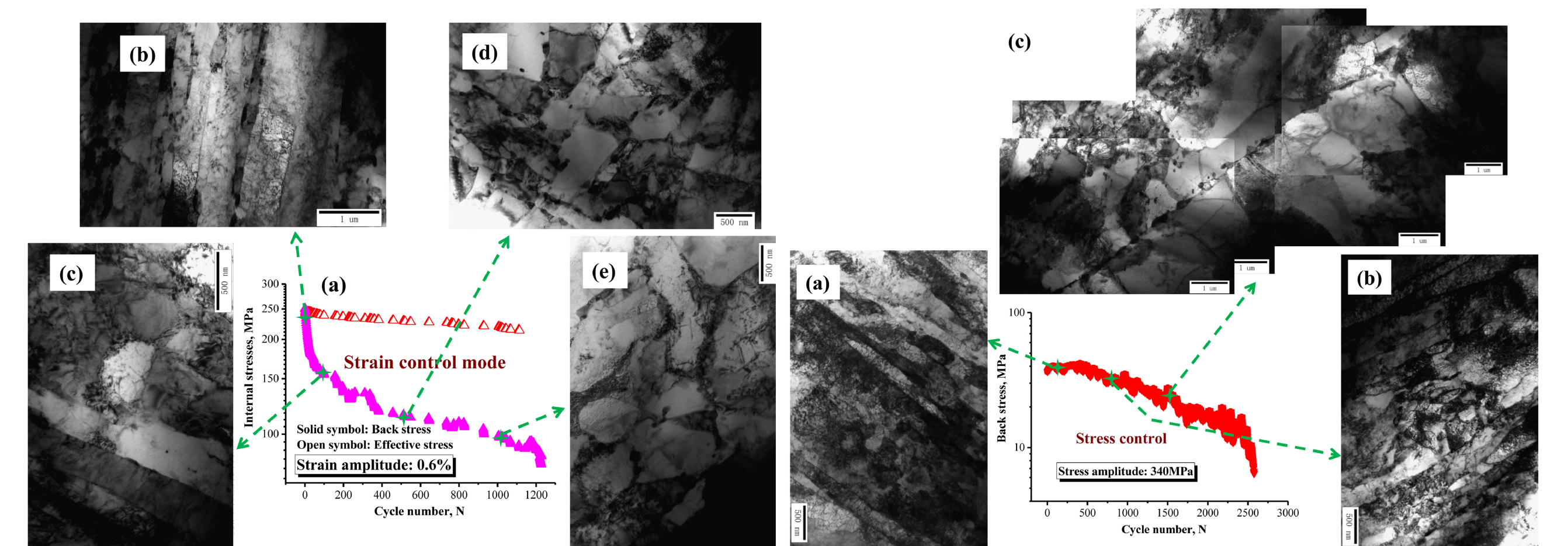


Figure 4. Microstructural evolution of laths illustrating cyclic softening mechanisms under different loading modes: (left) strain-controlled and (right) stress-controlled[5].

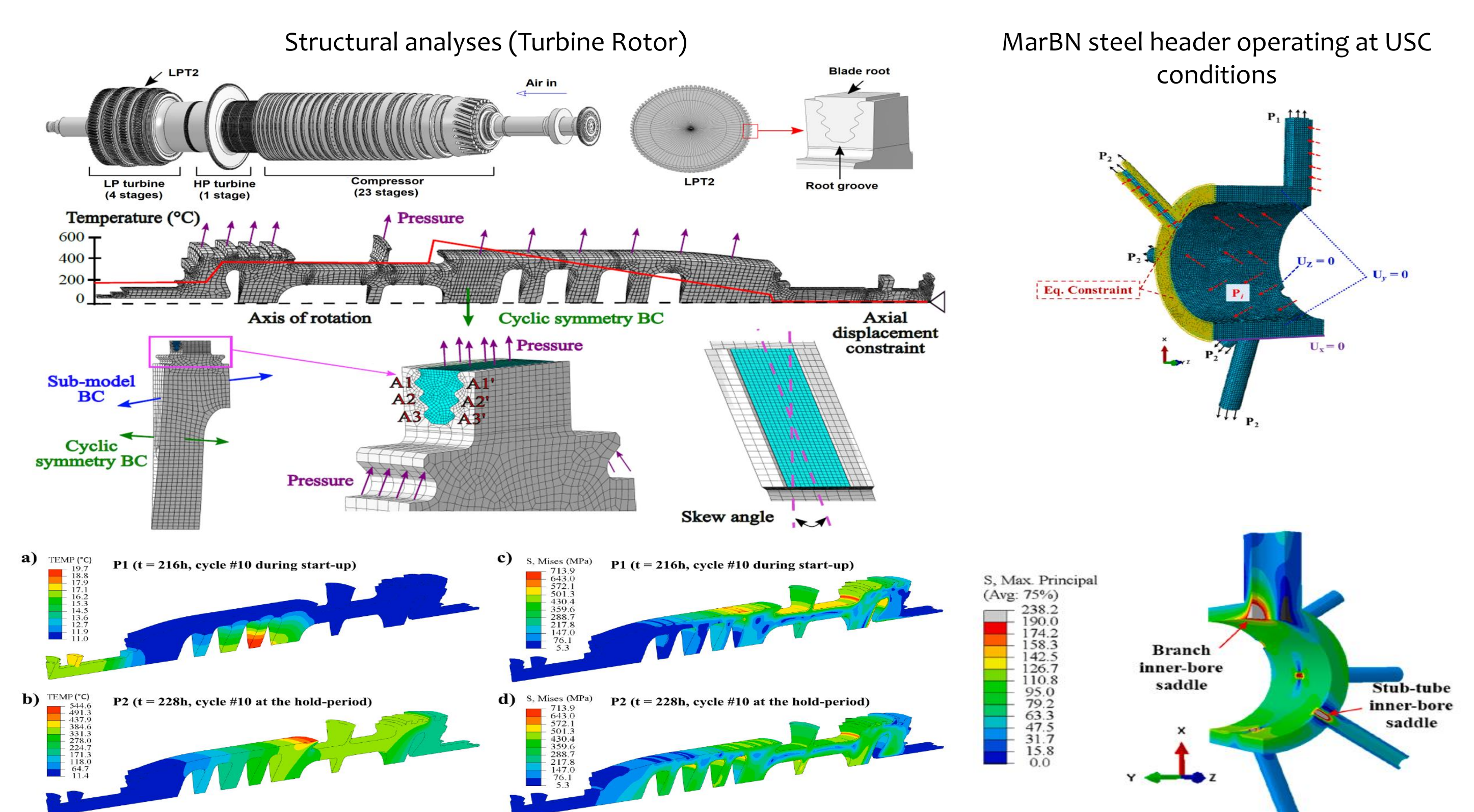


Figure 5. FEM simulation of a turbine rotor using a unified viscoplastic model that accounts for both time-independent fatigue plasticity and time-dependent creep deformations (left image) and header (right image) [3, 4].

References

[1] Lifetime extension for siemens gas turbines. 2020.
 [2] P. Mac Ardghail, S.B. Leen, and N.M. Harrison. A review of thermal, microstructural and constitutive modelling of 9cr steel for power plant applications: Towards a through-process model for structural integrity of welded connections. *International Journal of Pressure Vessels and Piping*, 180:104037, February 2020.
 [3] M. Li, A. Benaarbia, A. Morris, and W. Sun. Assessment of potential service-life performance for marbn steel power plant header under flexible thermomechanical operations. *International Journal of Fatigue*, 135:105565, June 2020.
 [4] Y. Rae, A. Benaarbia, J. Hughes, and W. Sun. Experimental characterisation and computational modelling of cyclic viscoplastic behaviour of turbine steel. *International Journal of Fatigue*, 124:581–594, July 2019.
 [5] Peng Zhao, Fu-Zhen Xuan, and Cheng Wang. A physically-based model of cyclic responses for martensitic steels with the hierarchical lath structure under different loading modes. *Journal of the Mechanics and Physics of Solids*, 124:555–576, March 2019.



Strengthening of Concrete Columns with Sustainable High Tensile-Strength Strain Hardening Cementitious Composites (HTS-SHCCs)

Osamah Karaghool, Osamah.Karaghool@nottingham.ac.uk

Supervisors: Dr Georgia Thermou, Dr John Owen, and Dr Fangying Wang

Introduction

Strengthening of existing structural members is crucial in the case of:

- Deterioration of aged concrete structures.
- Whole function can change.
- Loads can increase.
- Nature disasters like earthquakes.



Why it's important to strengthening of RC columns:

- To increase resilience of existing structures.
- Extend service life of the structures.
- Cost-effectiveness (alternative to complete demolition and reconstruction)

Sustainable HTS-SHCC for strengthening is prepared by replacing a partial of cement with Limestone powder Calcined Clay (LC2):

Sustainable HTS-SHCC mix's ingredients					
Portland cement	Limestone powder	Calcined clay	Fine sand	Polyethylene fibre (PE)	Water & Superplasticizer

The HTS-SHCC has excellent :

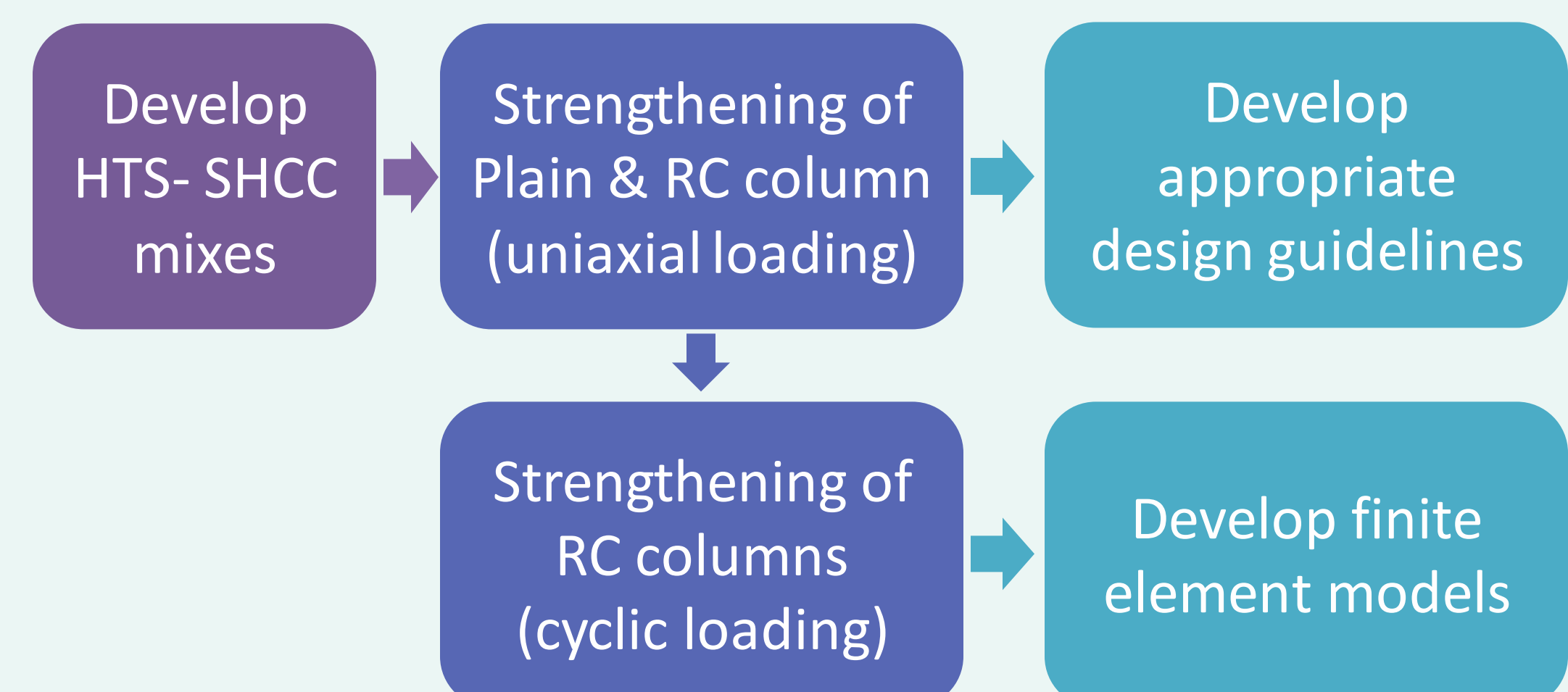
- Durability
- Toughness
- Deformation capacity
- Good bond property with concrete



Which makes it an excellent choice for strengthening concrete structures

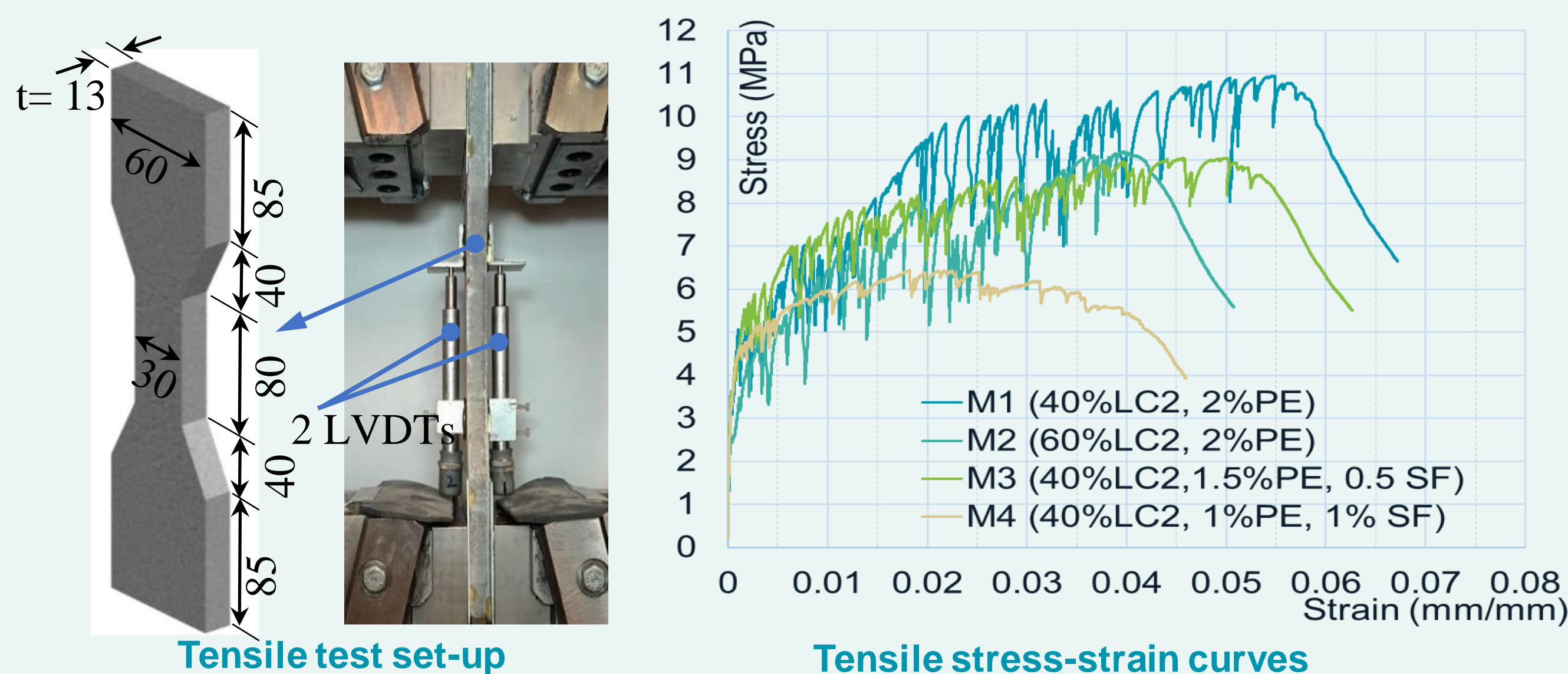
Aim To assess the effectiveness of using sustainable HTS-SHCC for the strengthening of reinforced concrete (RC) columns under uniaxial and cyclic loading

Objectives

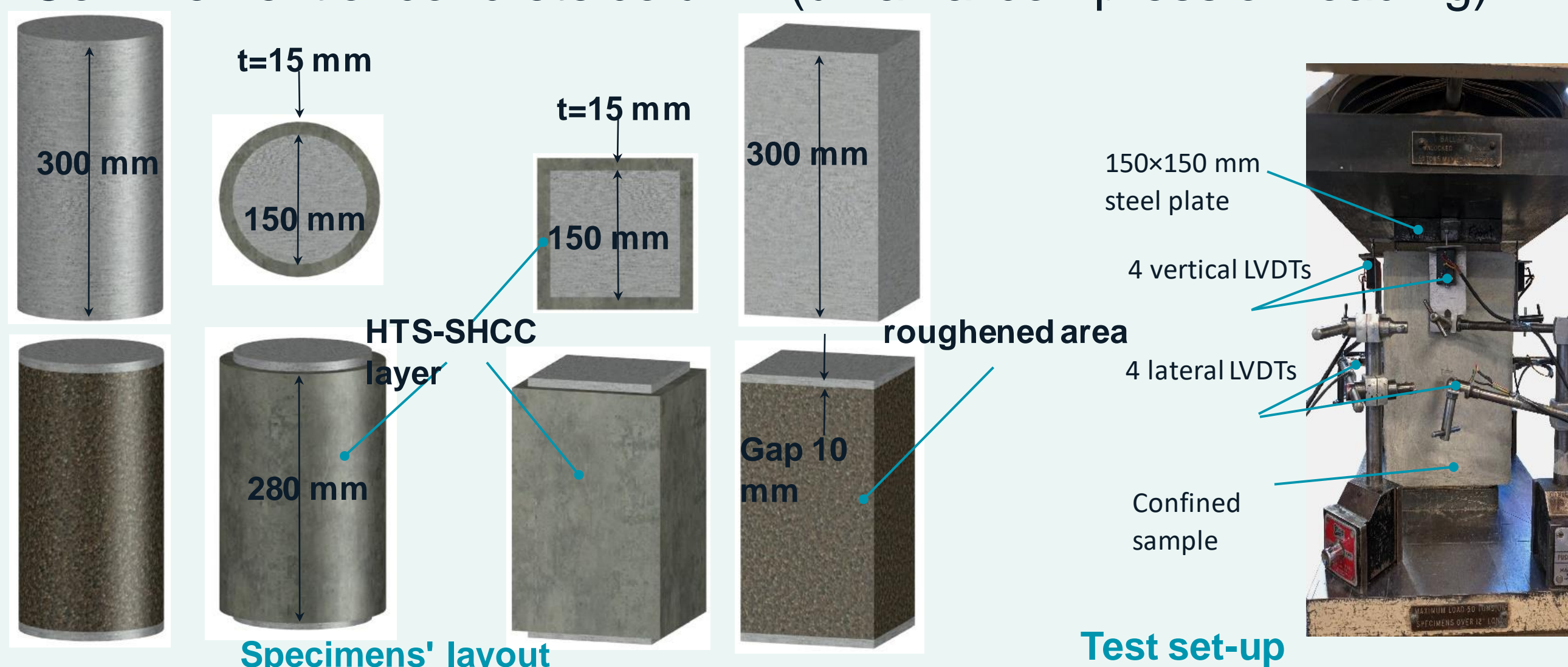


Experimental programme

1- Develop HTS-SHCC mixes



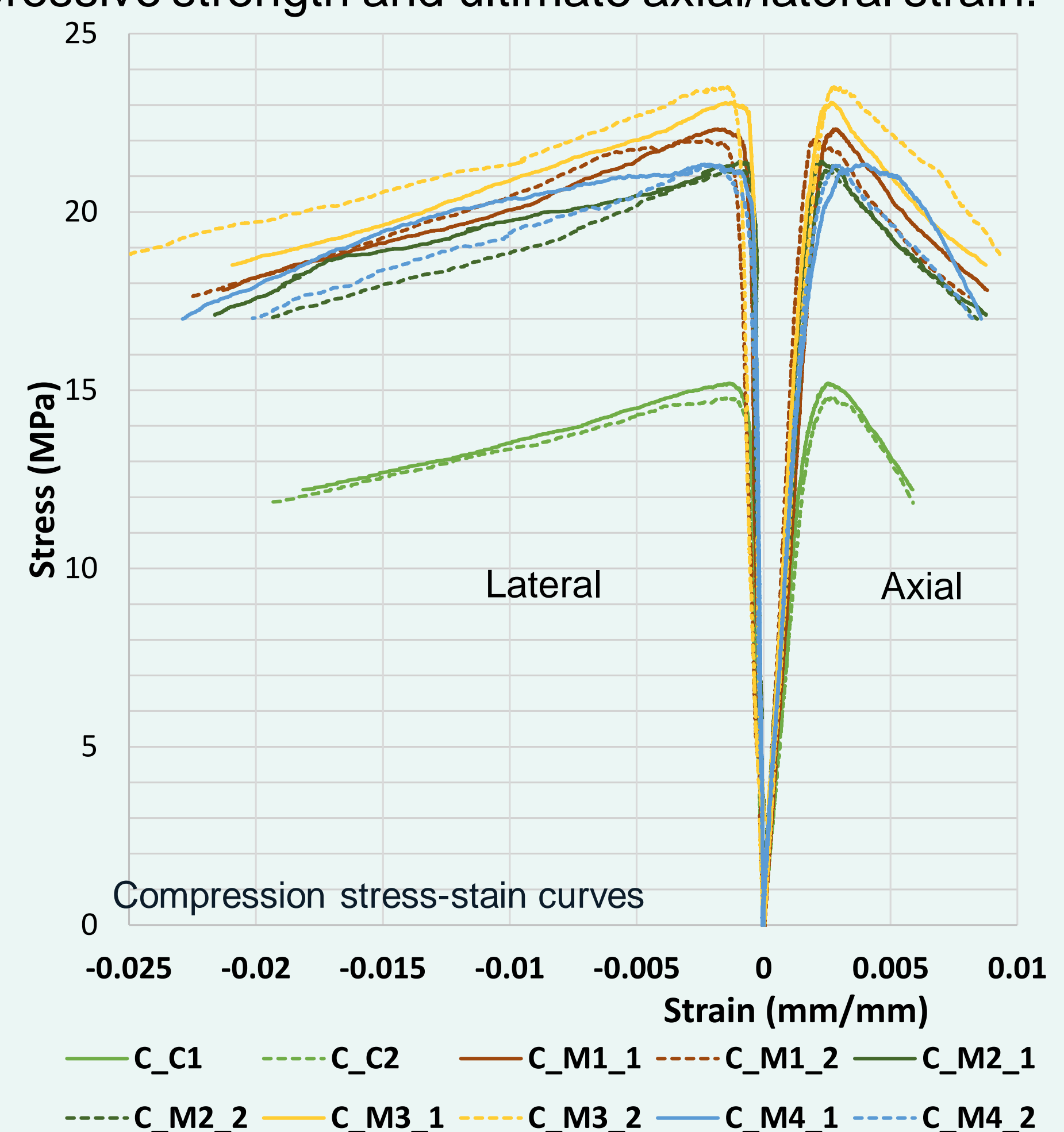
2- Confinement of concrete column (uniaxial compression loading)



Results

Confinement of concrete column with HTS-SHCC under uniaxial compression load test:

- The HTS-SHCC jacketing system significantly increased both the peak compressive strength and ultimate axial/lateral strain.



Can InSAR Coherence be Used to Assess the Hydrology of a Peatland?

R.Z.Walker

Supervisors: Prof D.J.Large and Prof D.Boyd

In blanket peatland, wetter peat is healthier.
If radar data can be used to monitor soil moisture/groundwater level, then monitoring can cover whole peatlands and demonstrate changes over time.

What is InSAR Coherence?

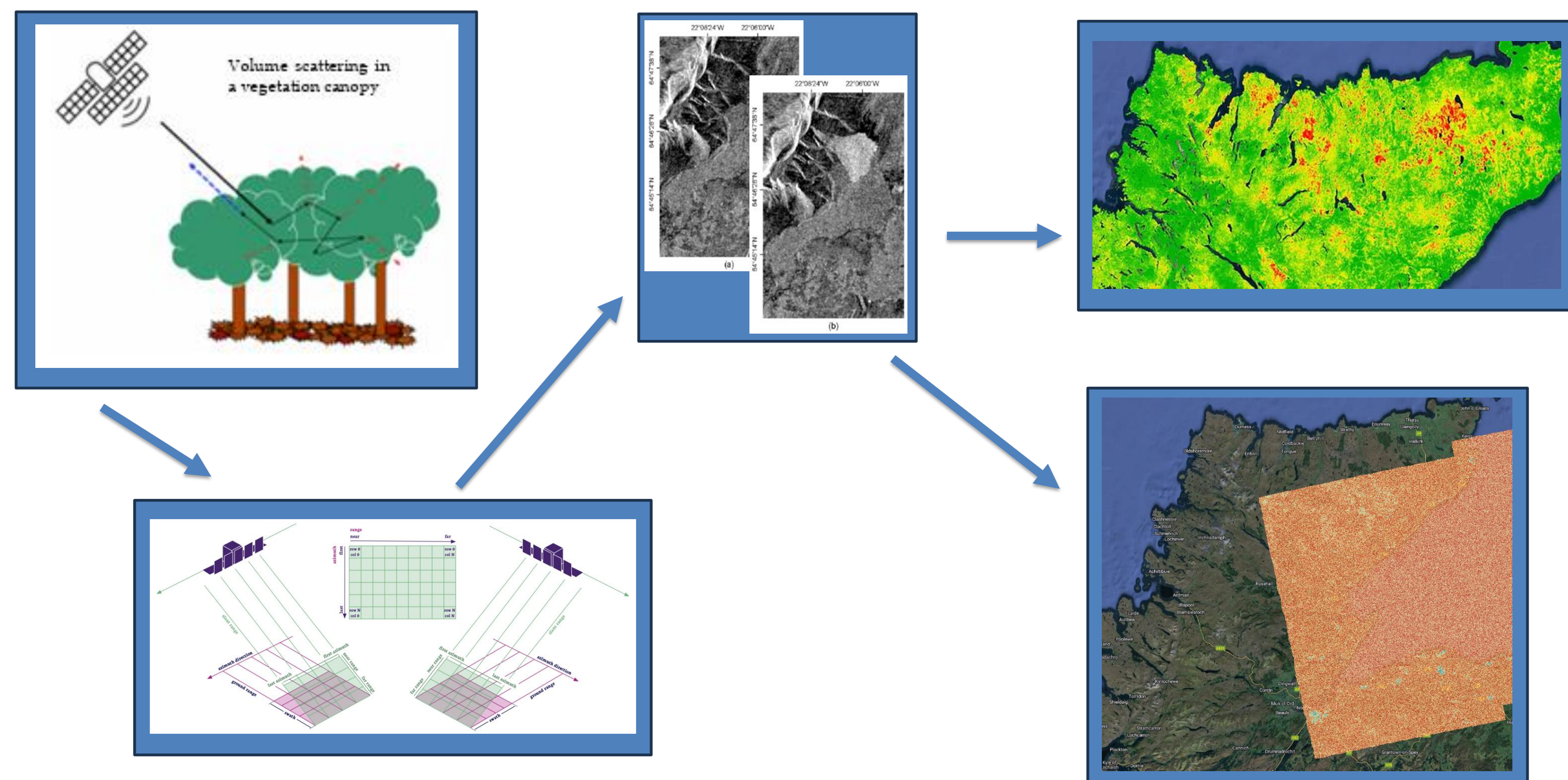


Fig1: SAR → SLC → timeseries → InSAR (phase difference) / InSAR coherence
Used in agricultural land as alternative means to estimate soil moisture

InSAR Coherence and peat

- Raised bog in Ireland
 - Soil moisture could be a key control on coherence
 - Large changes moisture cause coherence loss
- Higher coherence in peatlands
- Coherence noted to decline seasonally as groundwater table declines

Locations

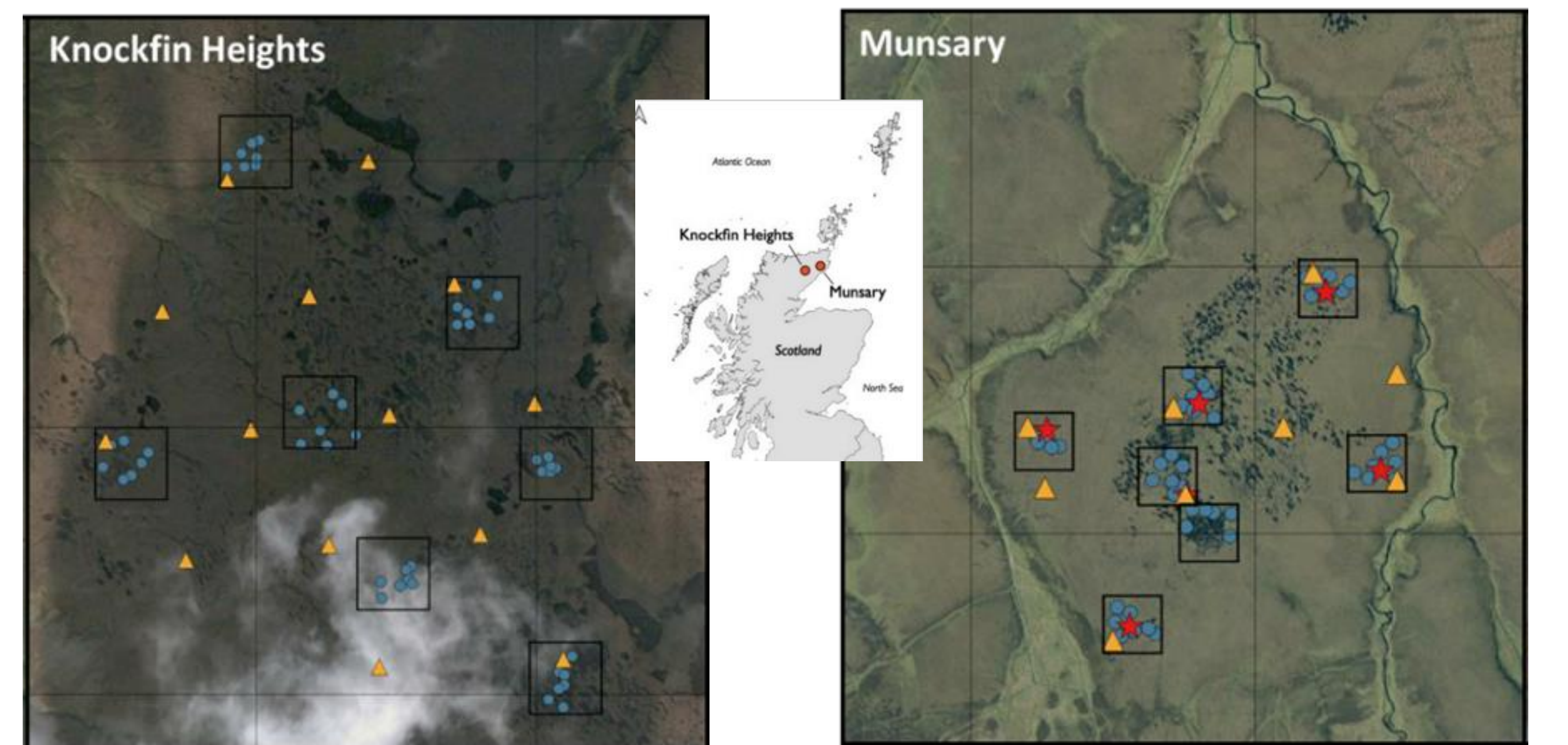
The Flow Country is the largest contiguous blanket bog in the world



Flow Country

Fig 2a: Near-natural peatland in the Flow Country

Fig 2b: Forest-to-bog restoration in the Flow Country



Ground data:
Soil Moisture (mg/g water)
Water level (m below peat surface)
Precipitation (mm)

+ Wick precipitation data
Fig 3a: Knockfin Heights (degraded)
Fig 3b: Munsary (near-natural)
Fig 3c: Location of sites in the Flow Country

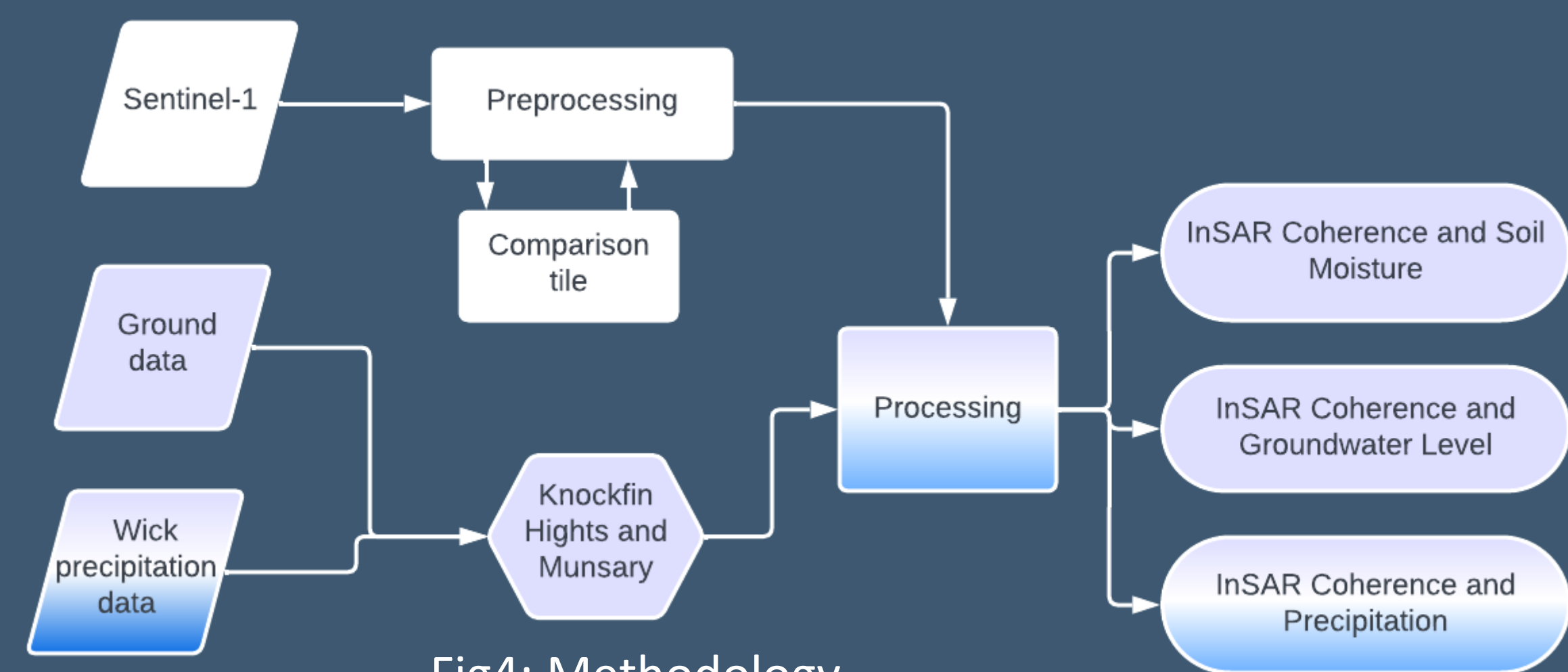


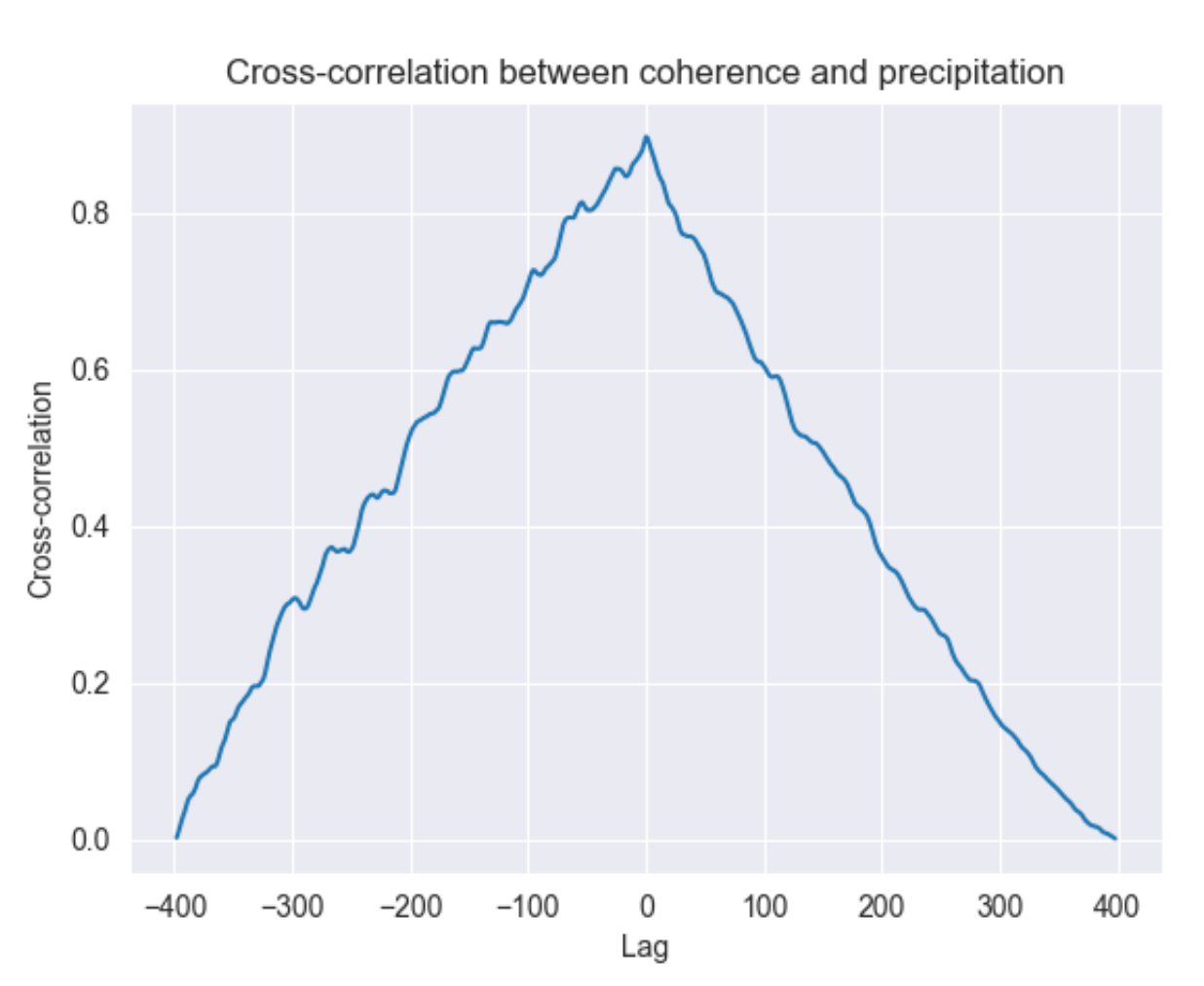
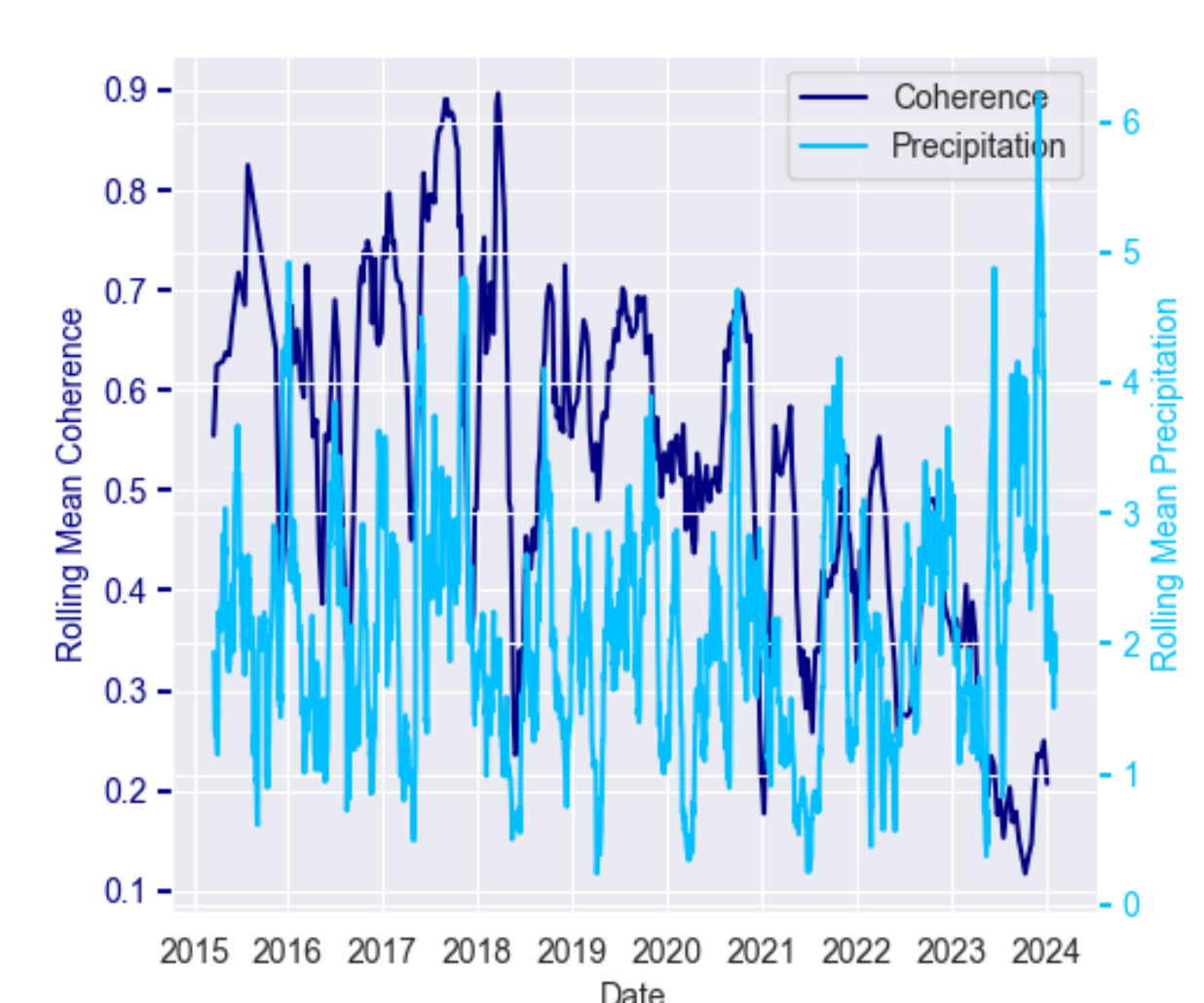
Fig4: Methodology



Preprocessing

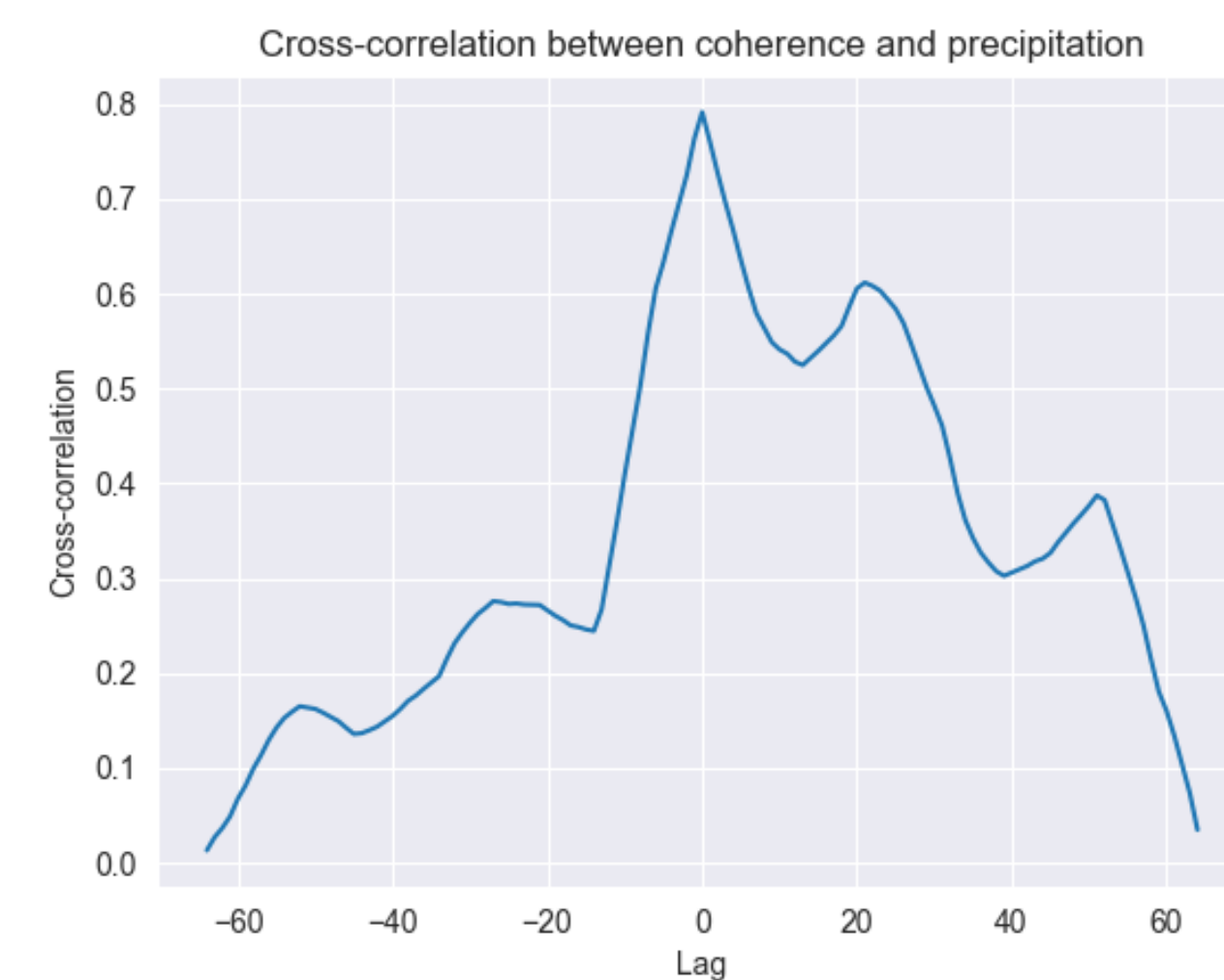
Platform: Sentinel-1
Polarisation: VV
Beam Mode: IW
Flight Direction: Ascending
Relative Orbit: 132
Granule: SLC

Water Mask: True
Looks: 10x2
Reference Image: 02/04/2018
Time Period: 2015-2024
Spatial resolution: 40 m²/pixel
Temporal resolution: 6/12 days

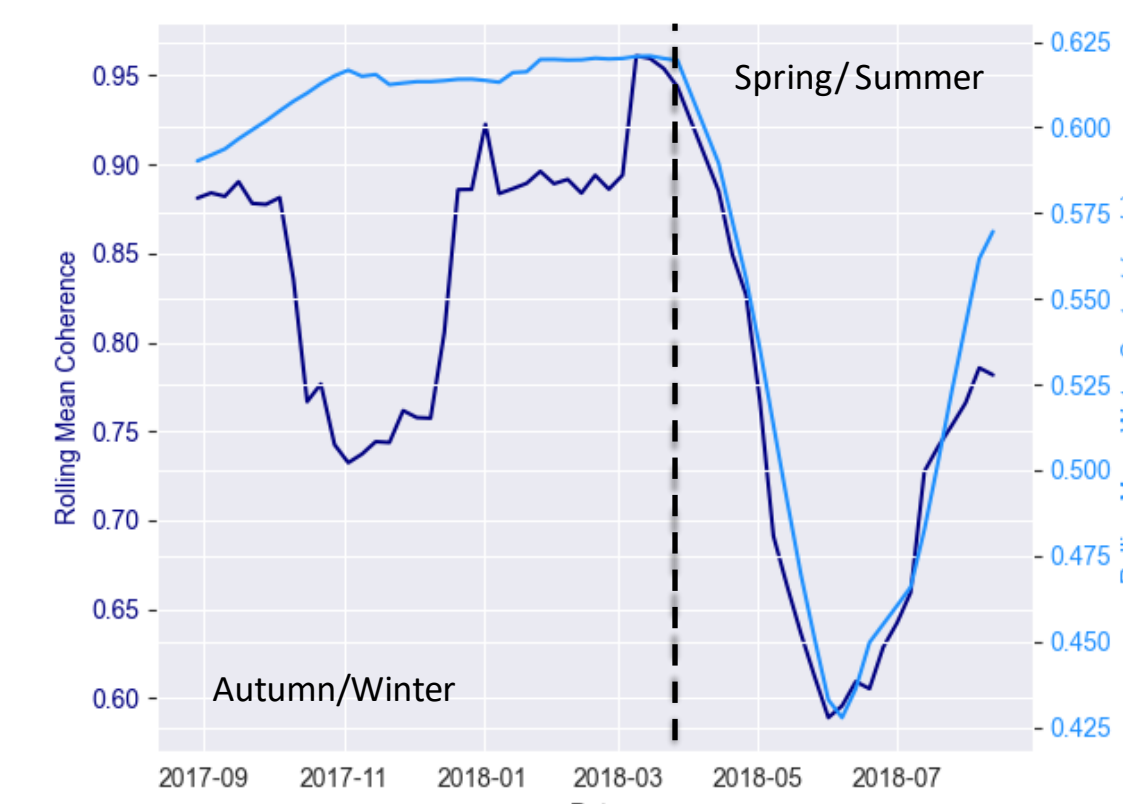


Site	Six-weeks (precipitation)	
	Generic mean CC	Focused mean CC
Knockfin Heights A-F	0.87	0.78
Munsary A-G	0.84	0.81

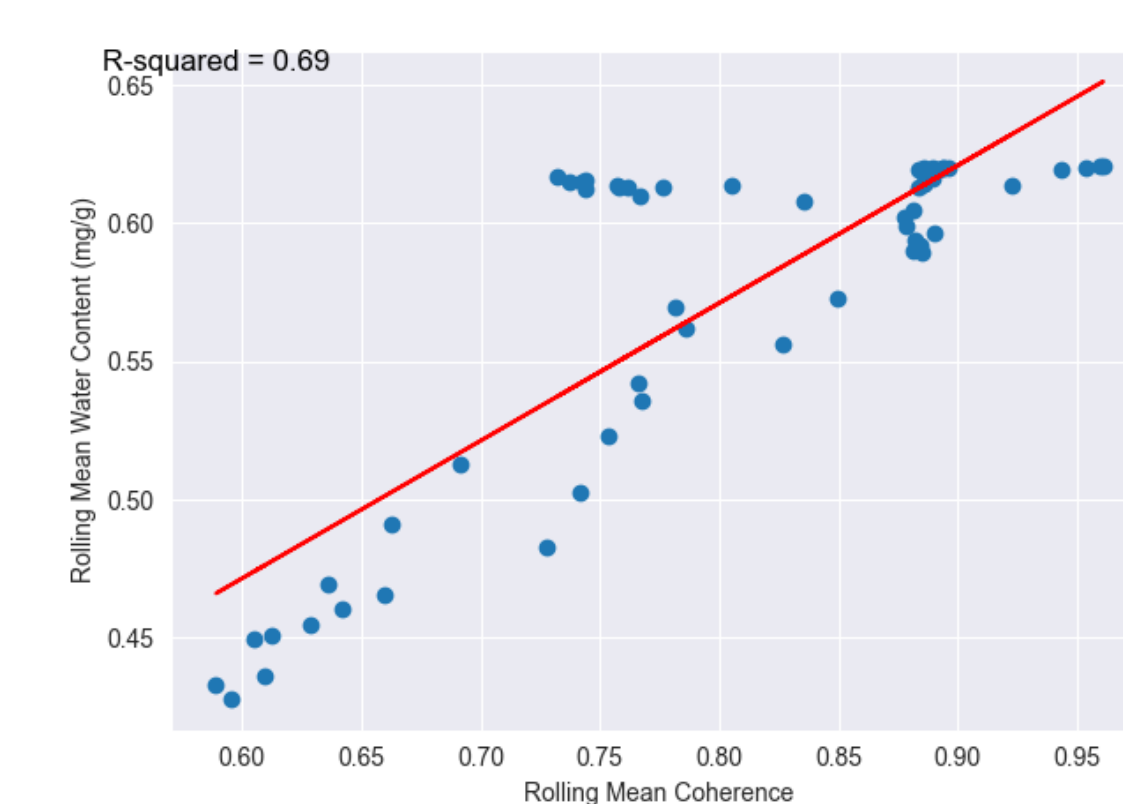
Table 1: Mean cross correlation Knockfin Heights and Munsary when applying a 6-week rolling mean
Fig 5: Knockfin Heights E precipitation and InSAR coherence (rolling means and cross correlations)



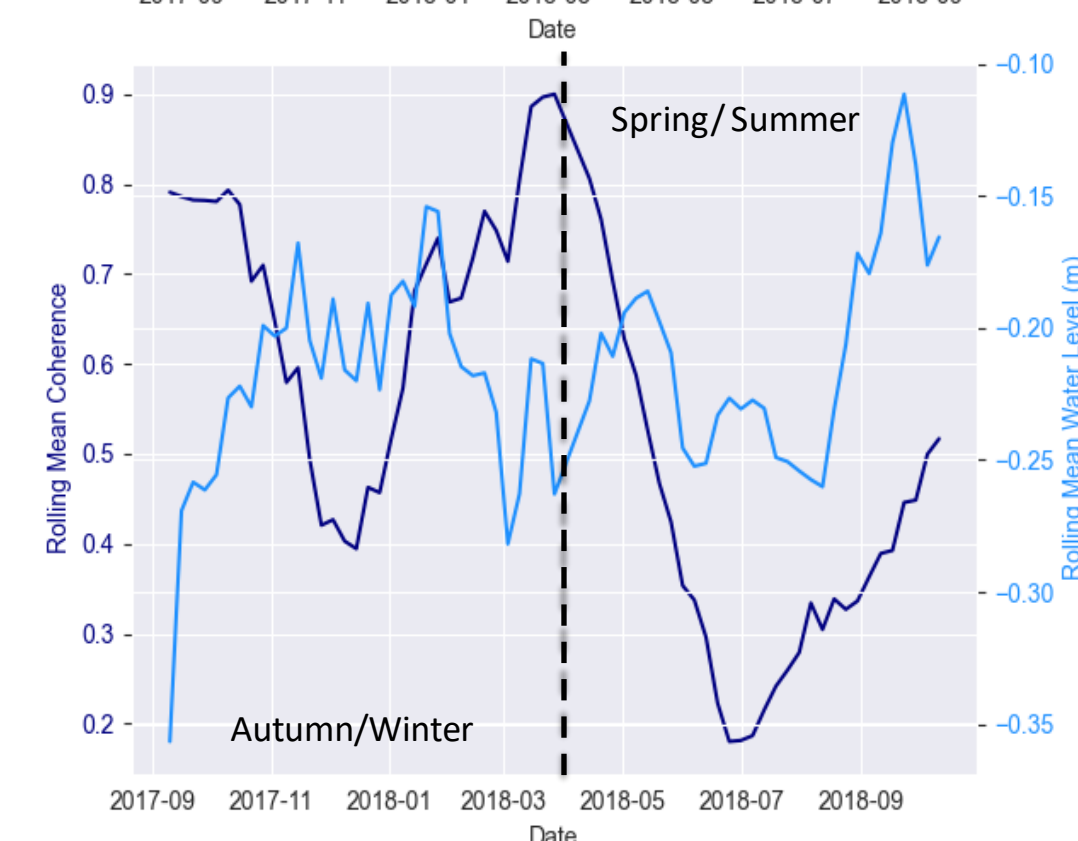
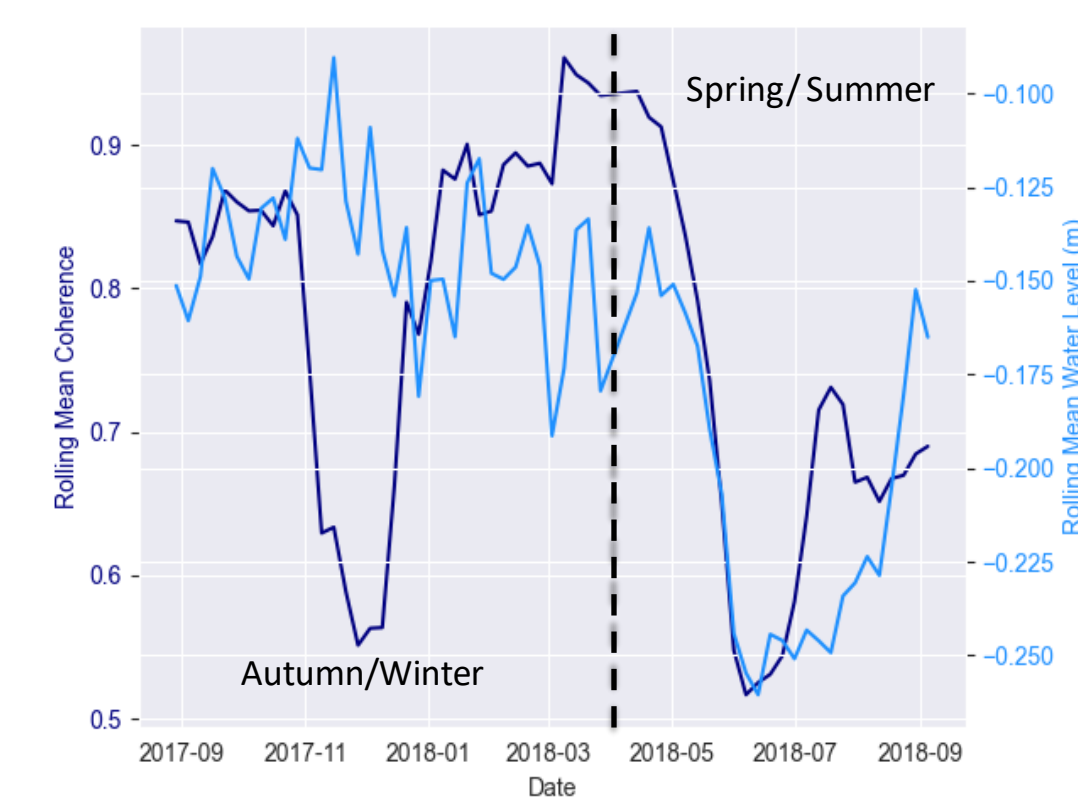
Focused was only one year and included the drought. More regular data collection.



← Fig 6a&b: InSAR coherence and soil moisture (Munsary B)



→ Fig 7: InSAR coherence and groundwater (top: Munsary D, bottom Knockfin Height D)



Site	2-months (soil moisture)		6-weeks (water level)	
	Mean CC	Mean Pearson	Mean CC	Mean Pearson
Knockfin Heights A-F	0.97	0.71	-0.89	0.36
Munsary A-G	0.97	0.87	-0.88	0.55

Conclusions

Precipitation and InSAR coherence are related in the Flow Country
Seasonal relationship between soil moisture and InSAR coherence

Potential Uses:

Proxy for soil moisture
Potential indicator for near-natural condition

Next steps:

Longer timescale ground data
Analyse for a different location and compare



Cold Recycled Asphalt

Assessing the curing evolution under early damage

Rani Bastari Alkam
Supervisors: Prof Gordon D. Airey & Dr Nick Thom

1 Introduction

- A sustainable technique for pavement rehabilitation [1], [2].
- Recycles existing pavement material at ambient temperature [3].
- Uses bituminous binders (foamed bitumen; bitumen emulsion), hydraulic binders (cement, lime, etc.), or both [4].
- Requires curing for its evolutive performance [5], [6], [7].
- Early damage from immediate traffic access can affect its critical early performance.

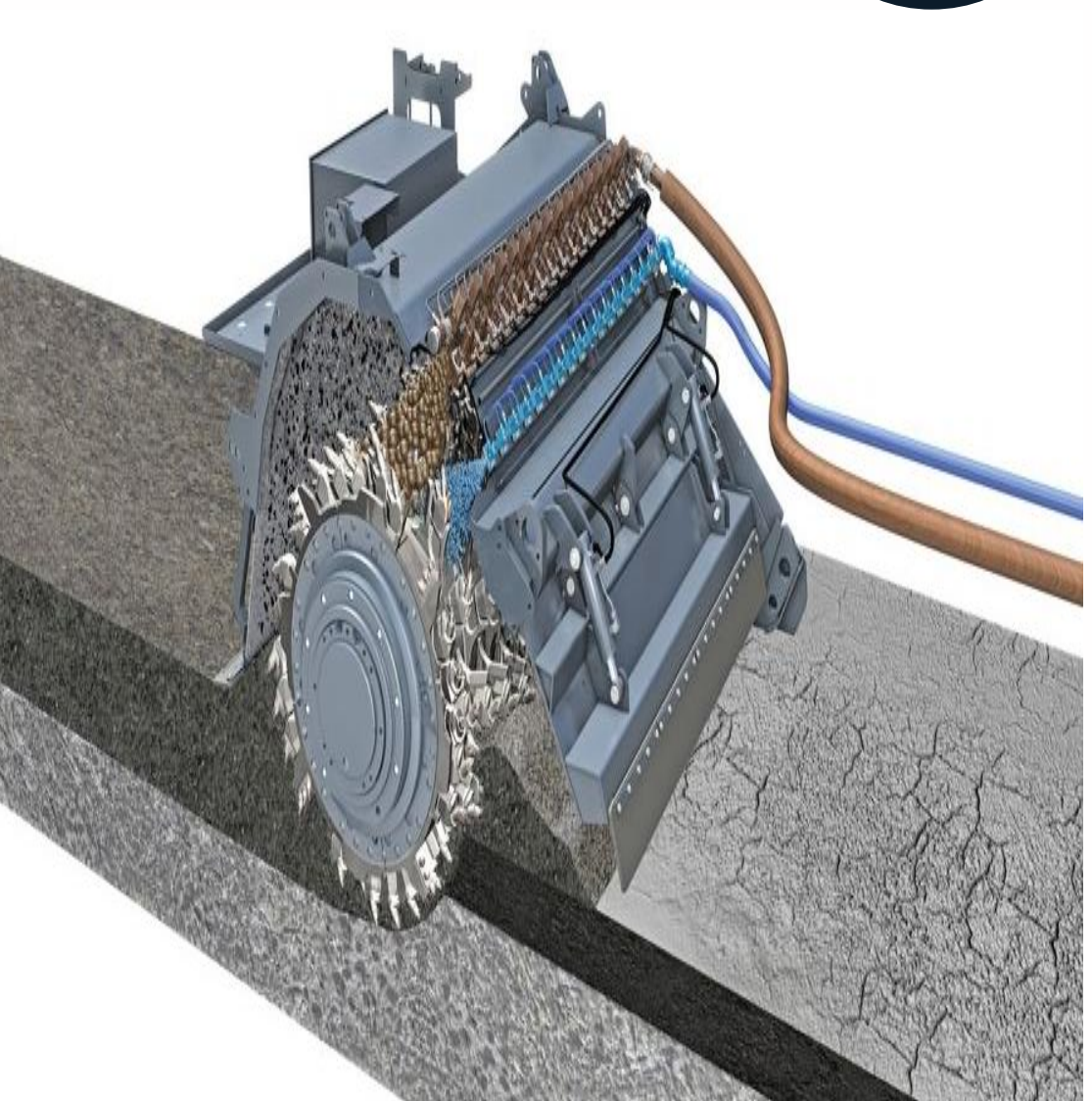


Fig 1: Asphalt cold recycling with foamed bitumen stabilisation
Source: Wirtgen GmbH, 2012 [8]

2 Research Gap

Current State
Absence of knowledge on the concurrent impacts of curing and early traffic on CRA performance.

Action Plans
Simulate curing and early damage on CRA materials using standardised testing procedures.

Desired State
Enhanced pavement design incorporating CRA, promoting sustainable road maintenance.

3 Experimental Approach

Materials

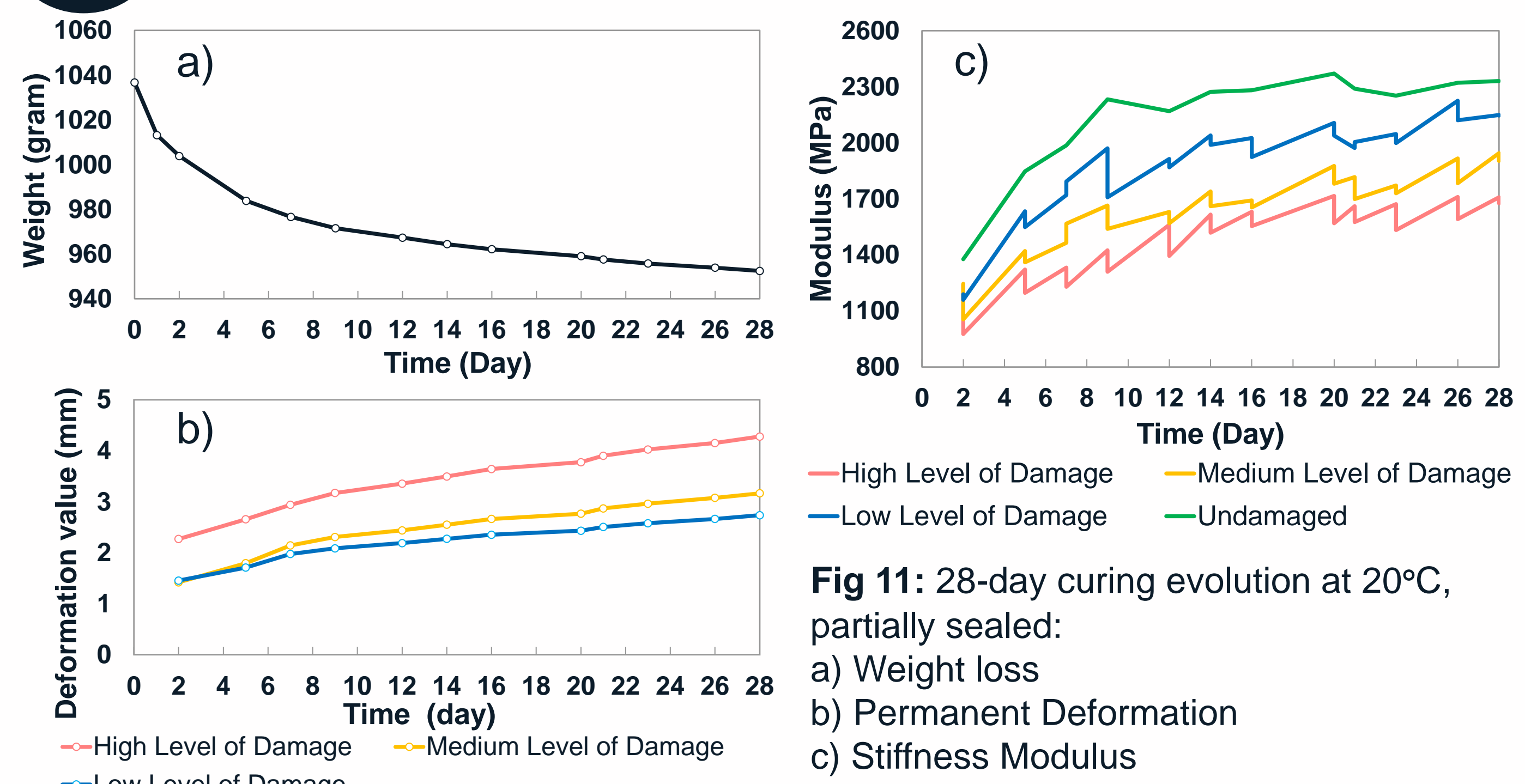
The characteristics of each material were investigated prior to their use in the mixtures.

Mixture Design

Manufacturing

Testing Protocols

4 Preliminary Results



5 Future Works

Curing Temperature Variations

Hydraulic Binder Combinations

Curing Modelling

Pavement Design

6 References

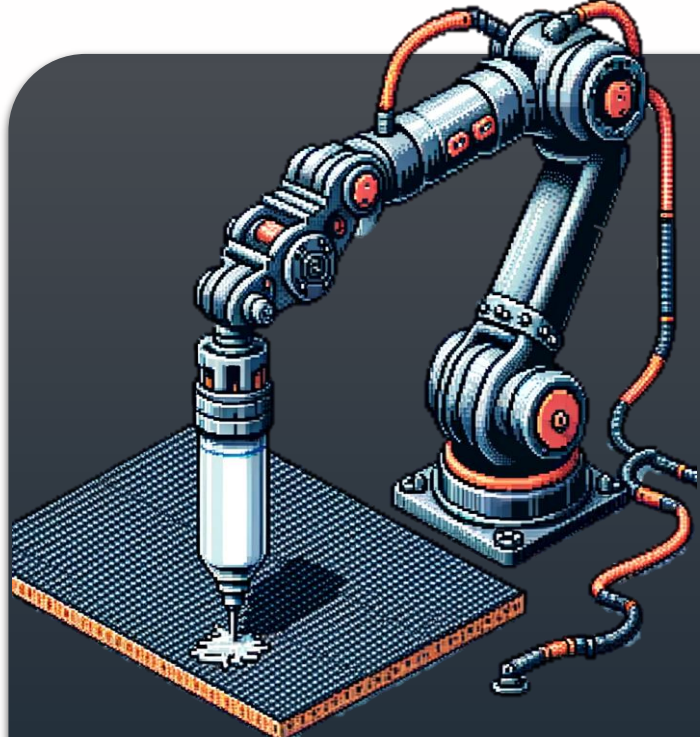
Please scan here for the references





Continual Learning-Based Adaptive Control Framework for Sealant Application

1 Background



The deposition of high viscosity sealant is a crucial process in manufacturing.

The process uses a sealant gun to precisely deposit fluid onto a substrate for the purpose of sealing leakages and preventing build-up of dirt.


Sealant application is currently done manually. This is due to the need for 1) exceptional hand eye co-ordination and 2) ability to adjust to new ambient disturbances. Currently, these tasks are difficult for industrial robots.

The persisting ongoing challenges are:

- 1) robot path planning
- 2) bead quality inspection
- 3) sealant dispenser control

To address the challenge of sealant dispenser pressure control, we need adaptive control systems capable of maintaining precision across various conditions.

2 Aims & Objectives



The **primary aim** of this study is to develop an adaptive control framework capable of robustly retraining machine learning models for use in a sealant dispensing system.

The objectives are to:

1. Propose a novel continual learning-based adaptive control framework that incorporates continual learning techniques to overcome the limitations posed by catastrophic forgetting.
2. Showcase preliminary results through the implementation of this framework on a typical feedforward parameter optimization (FFPO) module.
3. Generate a sealant flow dataset alongside the implementation of a Fully Connected Neural Network (FCNN) to demonstrate the application of the proposed framework.

3 Methodology

1. The General Adaptive Control Framework
2. Feedforward Parameter Optimization formulation
3. Data Collection and Preprocessing
4. Model Architecture and Training

3.1. The General Adaptive Control Framework

The adaptive control framework is a learning-based control system, with continual learning capability. The framework, as shown in Fig. 3.1, is composed by 5 main modules:

- (1) the feedforward parameter optimization module
- (2) a feedback control module
- (3) a monitoring module for quality monitoring and drift detection
- (4) a continual learning module and
- (5) an automated data processing module.

In learning-based control, neural networks are used to model process dynamics. These models can optimize and control parameters on-line, providing robustness to small scale disturbances such as natural temperature fluctuations in real-time. However, for larger scale changes such as context drift, an off-line continual learning approach will enable the retraining of the models, enabling robustness to large scale disturbances.

Rey Narvato, Dr. Peter Kendall, Dr. David Sanderson,
Prof. Svetan Ratchev, Dr. Giovanna Martínez Arellano,
Omnifactory Research Group
Institute for Advanced Manufacturing

3.2 Feedforward Parameter Optimization formulation

To address the complex non-linear relationships of sealant fluid dynamics, a neural network is used.

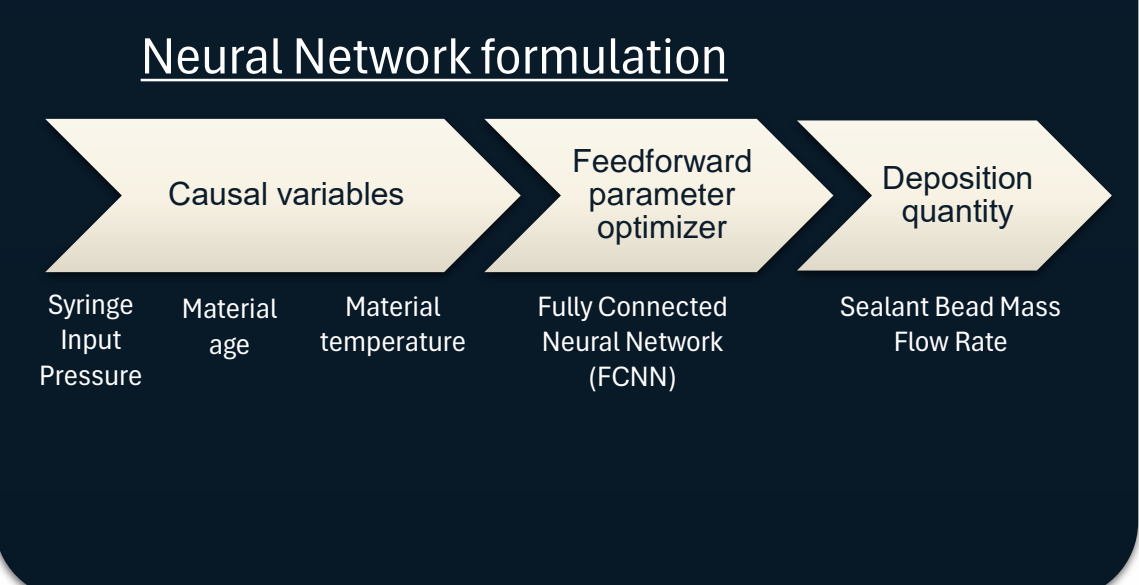
- In the data collection stage (1), an inverse model is formulated, with the aim of predicting the causal variable (syringe pressure) from an observation (mass flow rate)
- In deployment (2), this pressure will be used to drive the sealant, leading to reliable, precise mass flow rate.
- We also collect material properties to allow the model to learn material property dependent relationships.

Mathematical formulation

$$p = FCNN(m, T, t) \quad (1) \quad \begin{matrix} p = \text{syringe pressure (kPa)} \\ m = \text{bead mass (kg)} \\ T = \text{material temperature (C)} \\ t = \text{material age (s)} \end{matrix}$$

$$m = F(p, T, t) \quad (2)$$

Neural Network formulation



3.3 Data Collection and Preprocessing

To form the FFPO, pressure, age, temperature and mass data is collected to form a dataset.

1. Temperature is controlled using a Wachendorff URDR001A Controller (Fig. 3.3a)
2. Pressure is controlled by a Nordson UltimiusPlus I air regulator. (Fig. 3.3b)
3. The mass is measured using an Arduino Uno R3 (Fig. 3.3c)

Data Preprocessing

To prepare the dataset for the neural network, preprocessing is done.

1. **Data fusion** of mass flow rate, pressure, temperature, and material age data.
2. **Normalisation** using min-max scaling
3. **Data split** into train, test, validation datasets:

Interpolation split: 20% Train, 20% Test, 20% Validation, 20% Validation, 20% Validation

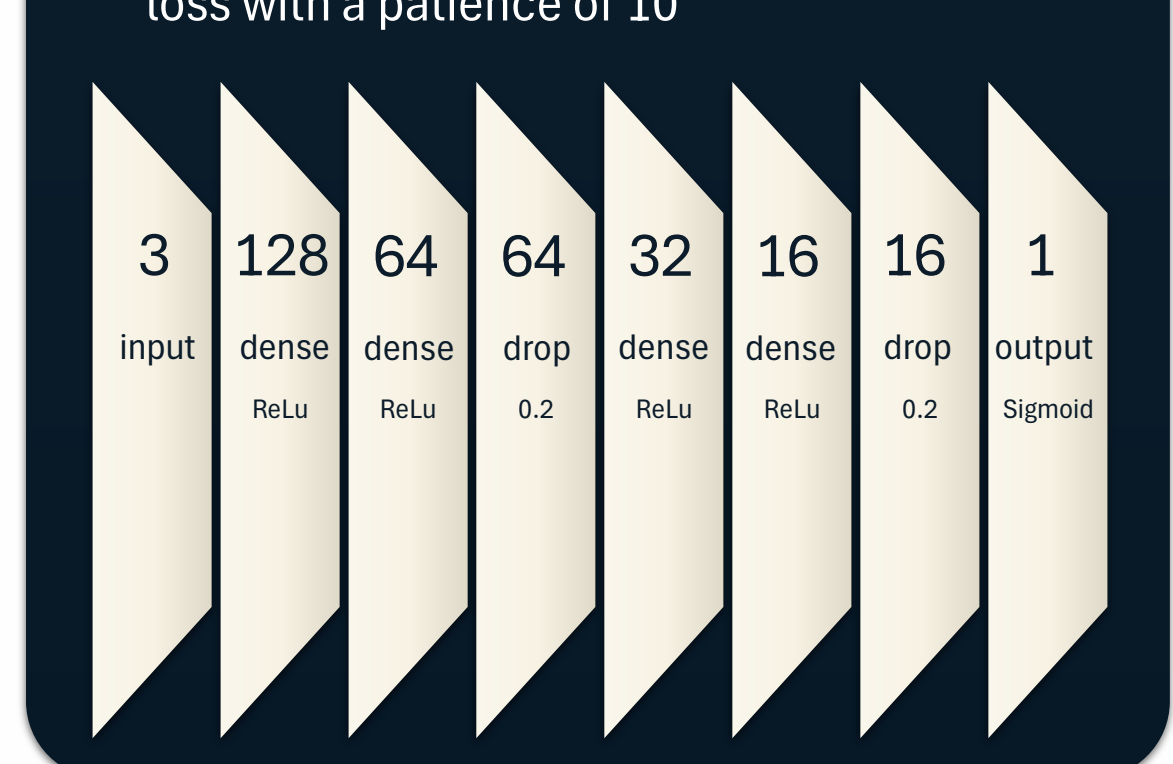
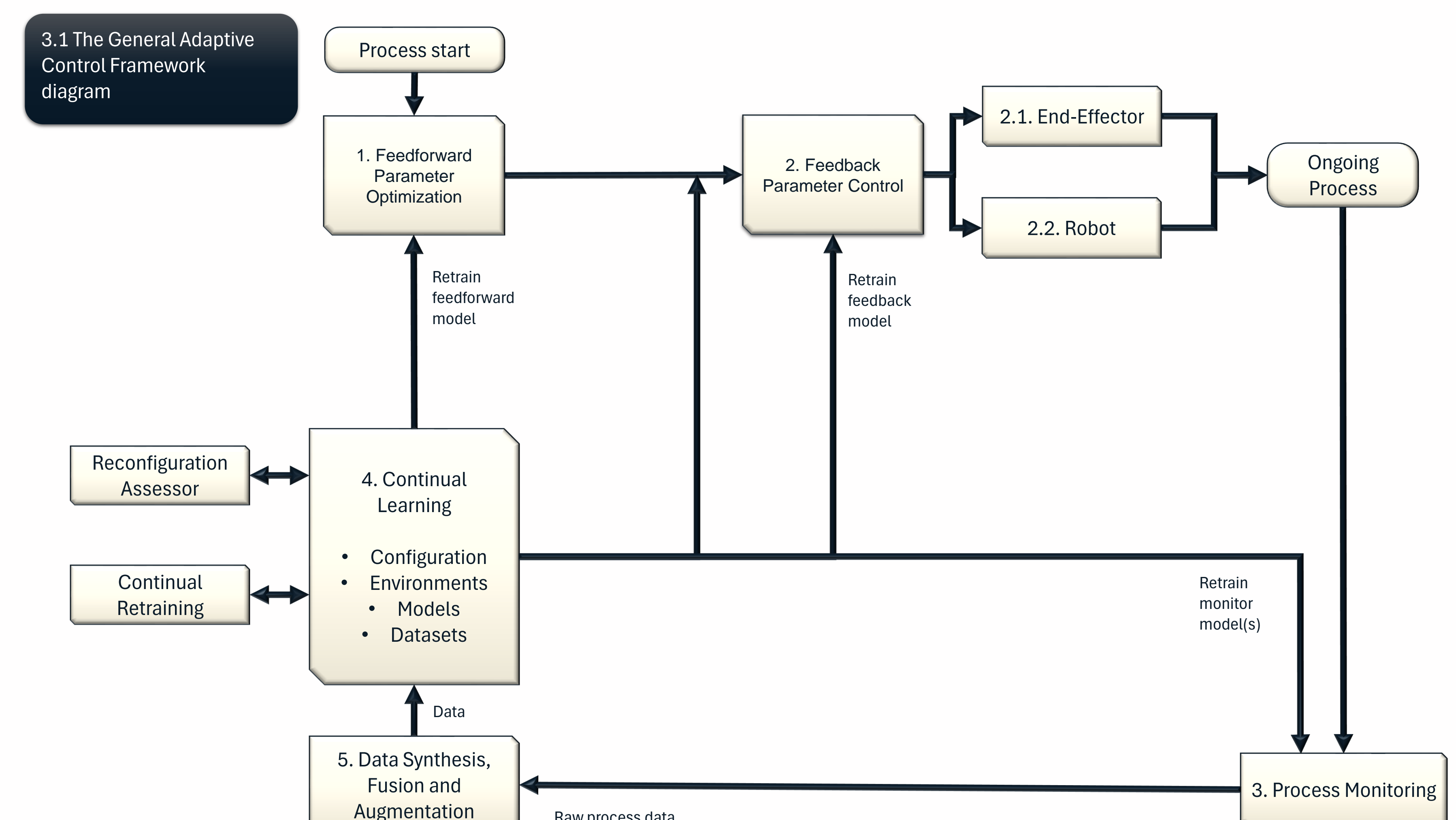
Extrapolation split: 20% Train, 20% Test, 20% Validation, 20% Validation, 20% Validation

Final Datasets: Age Interpolated, Age Extrapolated, Temperature Interpolated, Temperature Extrapolated

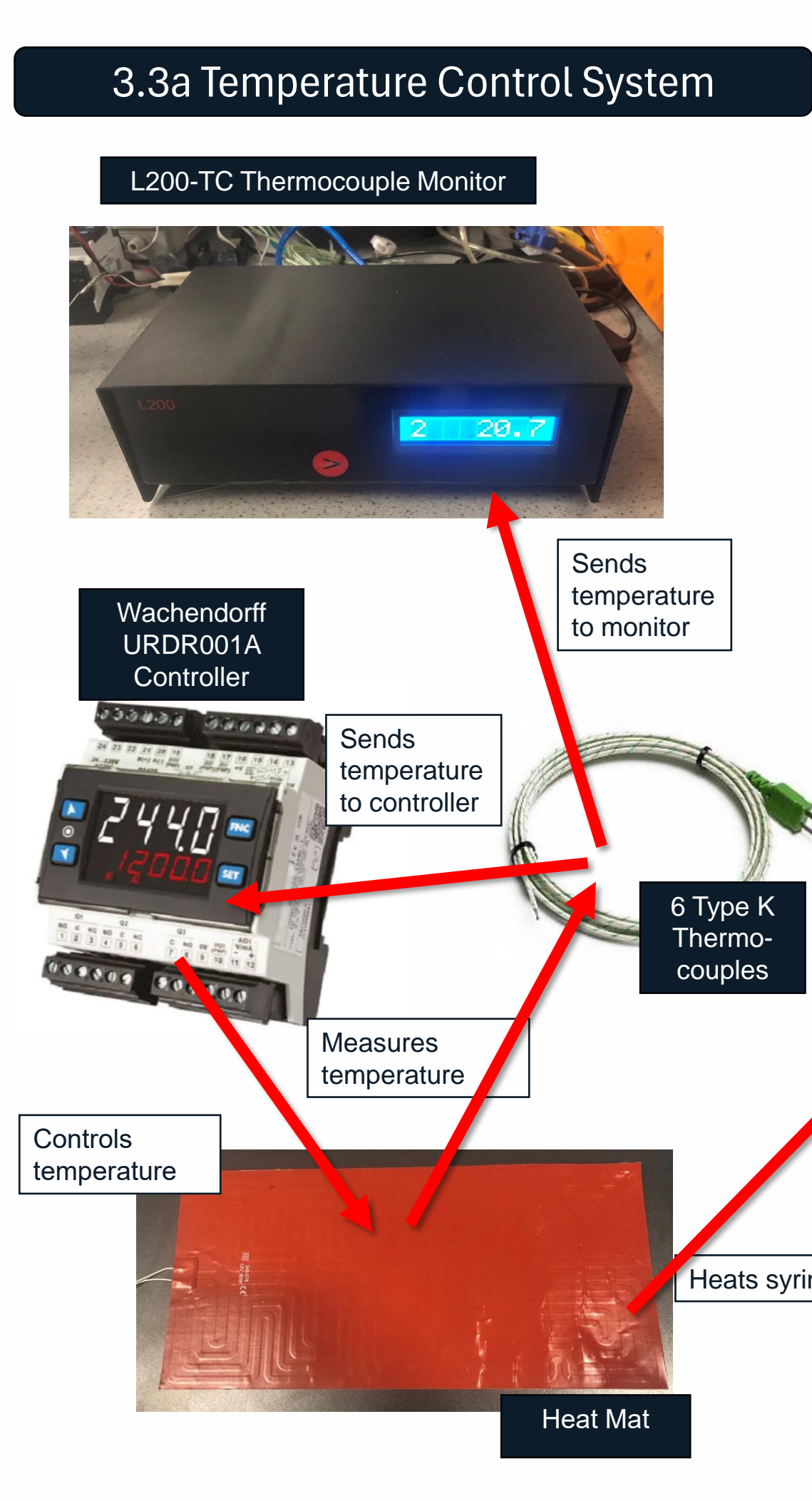
3.4 Model Architecture and Training

The FFPO uses a neural network architecture designed to receive the input variables (pressure, temperature, age). The model will then learn to predict the pressure required to achieve the mass flow rate, given temperature and age constraints. The model used for this regression task is a Fully Connected Neural Network (FCNN), consisting of:

- dense layers (ReLU activation)
- dropout layers (ratio=0.2)
- Batch size = 32 samples
- Optimizer = 'Adam' (learning rate = 0.001)
- The loss function = mean squared error
- The maximum of epochs = 500
- Early stopping criteria = minimum validation loss with a patience of 10

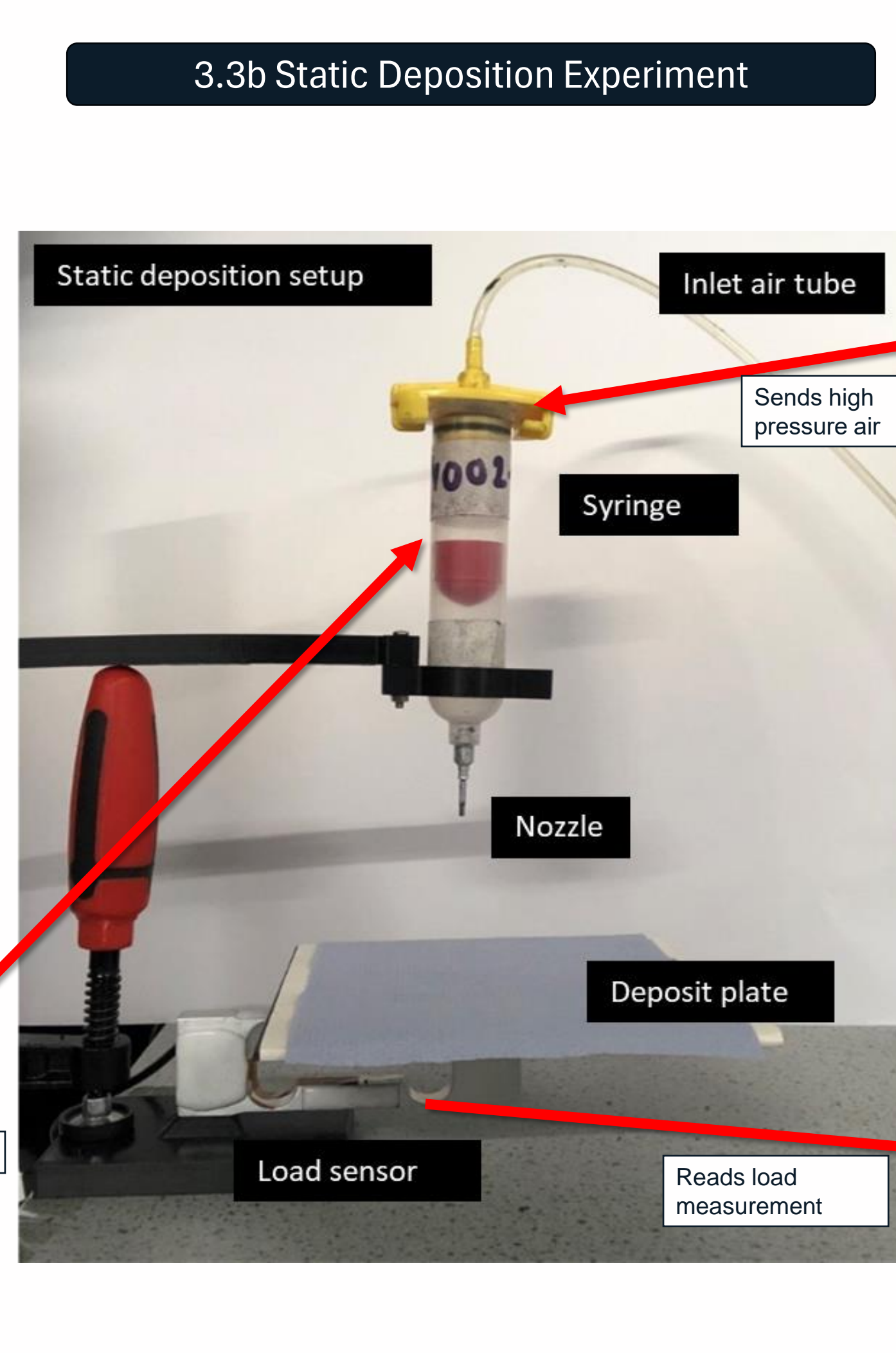



3.3a Temperature Control System



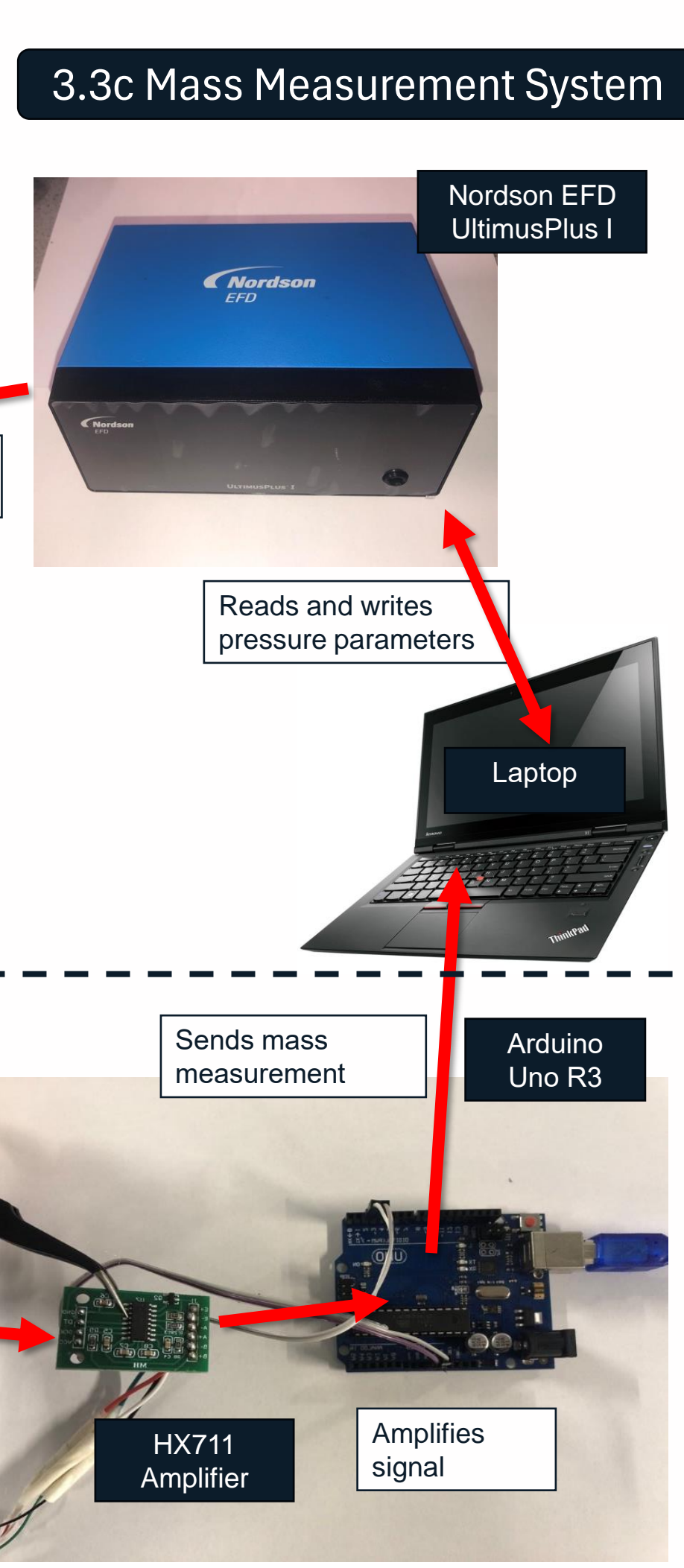
Controls temperature, Measures temperature, Sends temperature to controller, Sends temperature to monitor, Heats syringe

3.3b Static Deposition Experiment



Static deposition setup, Inlet air tube, Sends high pressure air, Syringe, Nozzle, Deposit plate, Load sensor, Reads load measurement

3.3c Mass Measurement System



Nordson EFD UltimiusPlus I, Reads and writes pressure parameters, Laptop, Sends mass measurement, Arduino Uno R3, HX711 Amplifier, Amplifies signal

4 Results

1. Error magnitude
2. Extrapolation vs Interpolation
3. Underestimation and Variability

4.1. Error magnitude

The magnitude of the error that the model achieves is around 41.5-52.7kPa MAE across all datasets.

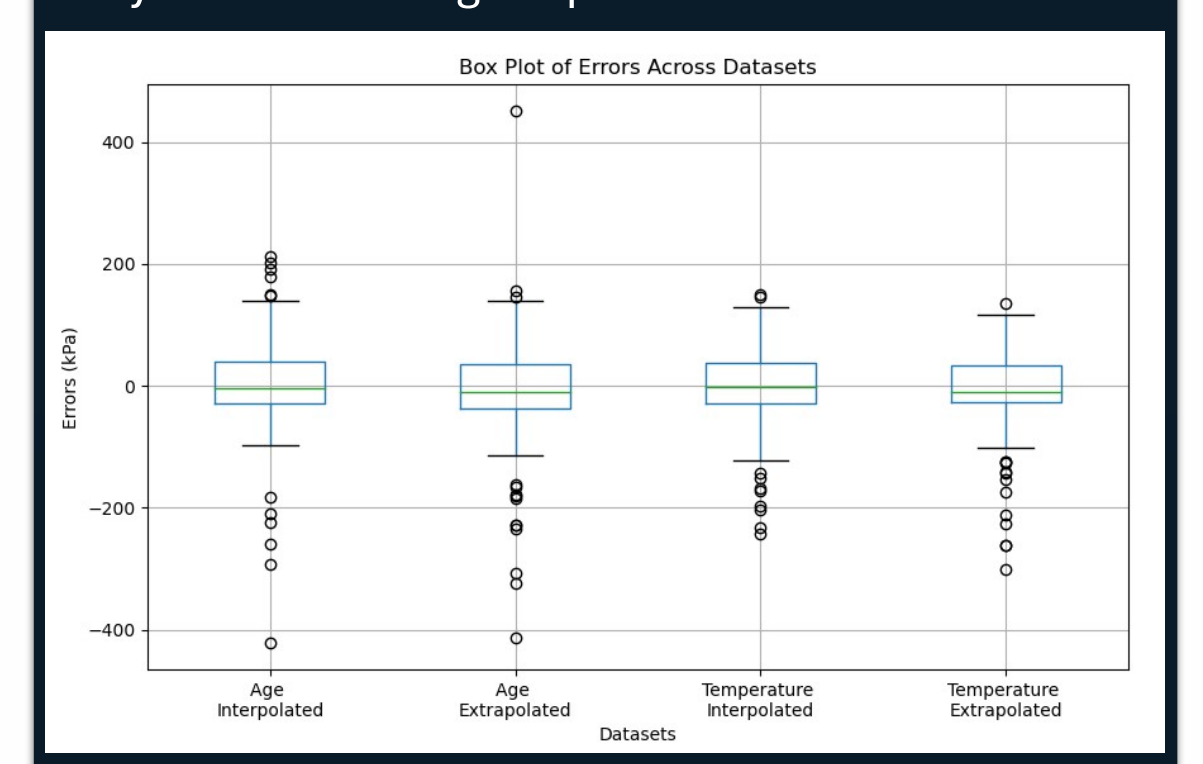
In general, it achieves 24.5-33.0% MAPE. However, these ranges shown in Table II, indicate a differential in the prediction errors across the datasets which will be explored in the following discussion.

Data Splits	Performance Metrics					
	MAE (kPa)	MAPE (%)	MSE (kPa ²)	RMSE (kPa)	Median Error (kPa)	IQR Error (kPa)
Age (Interpolated)	47.6	28.2	4920	70.1	-3.0	68.0
Age (Extrapolated)	52.7	33.0	6243	79.0	-10.0	72.5
Temperature (Interpolated)	43.6	24.5	3559	59.7	-2.7	65.1
Temperature (Extrapolated)	41.5	32.6	3673	60.6	-9.8	60.9

4.2. Extrapolation vs Interpolation

The model consistently performs better on datasets split by interpolation compared to extrapolation.

For example, in age-related splits, mean squared error (MSE) increased more significantly in extrapolation compared to interpolation, indicating challenges in model generalization beyond the training scope.



4.3. Underestimation and Variability

The model tended to underestimate across all datasets, and more so in extrapolation cases.

Variability, as measured by the interquartile range (IQR), was also higher in extrapolation, suggesting greater uncertainty in predictions outside the trained data range.

5 Future Work

- 1) **More Data Collection:** More extensive data collection should be done to improve insight into prediction error and variability
- 2) **Validation of Feedback Module:** Implement robot-guided deposition with vision-based feedback to validate the feedback parameter control module and contextualize model performance with bead quality.
- 3) **Adaptive Control Module:** Integrate and validate continual learning techniques such as rehearsal-based methods and Elastic Weight Consolidation (EWC).
- 4) **Scientific Machine Learning:** Use physics-informed neural networks for modelling thermo-fluid dynamics of sealant flow to improve data efficiency and accuracy.
- 5) **Synthetic Data Augmentation:** Employ data augmentation and computational fluid dynamics simulations to address data scarcity and generate synthetic data for model training.

Thermal Blood Flowmeter Based on Cascaded Fabry-Pérot Interferometers Improved by Enhanced Harmonic Vernier Effect

Ruirong Gong

Supervisor: Dr Ricardo Goncalves Correia, Prof Barrie Hayes-Gill, Prof Stephen Morgan, Prof Serhiy Korposh, Dr Chenyang He

Introduction

•Heat Generation:

A multi-mode optic fibre delivers light to generate heat in the fluid. The light is absorbed by the fluid, creating a localized heating effect.

•Heat Dissipation:

Fluid flow carries away the heat from the heated element. The rate of heat dissipation is proportional to the flow rate.

•Temperature Measurement:

A temperature sensor records the cooling effect caused by the fluid flow. Changes in temperature are used to calculate the flow rate.

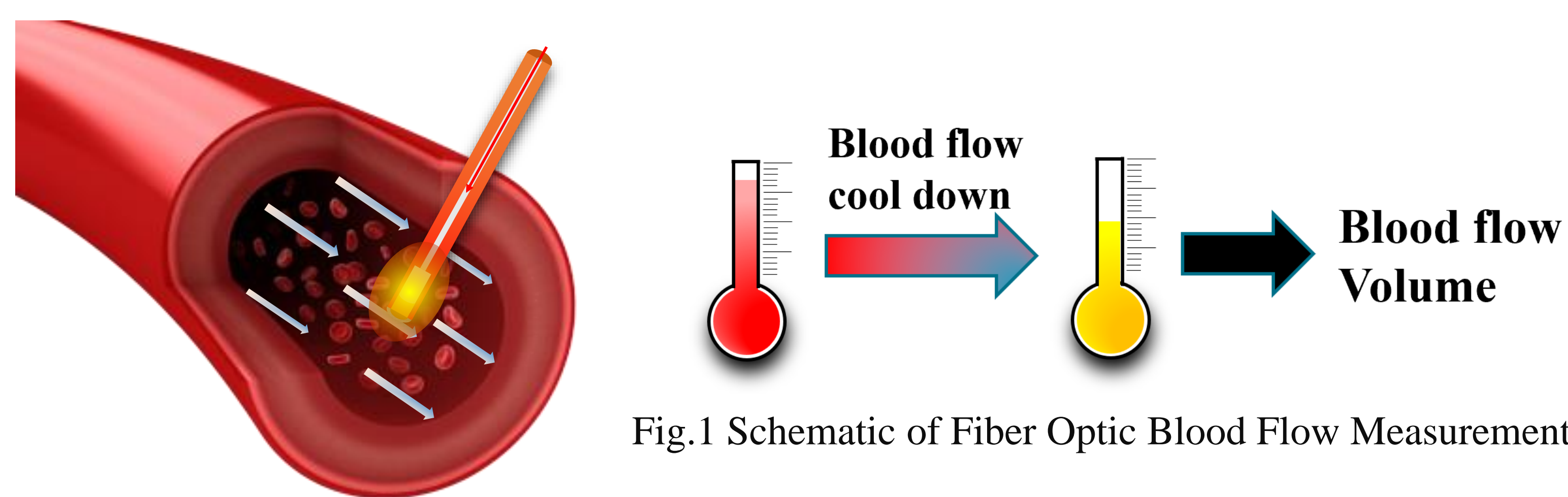


Fig.1 Schematic of Fiber Optic Blood Flow Measurement

•Real-time Monitoring:

- Continuous, real-time measurements enhance patient comfort by reducing the need for repeated interventions(Thermodilution).

•Robust and Simple Design:

- Detects minute flow changes with high precision and is less dependent on precise alignment(LDV).

•Cost-effective:

- It is more affordable than OCT and MRI, lowering healthcare costs and making it a practical choice for many facilities.

Ultra-sensitive temperature sensor

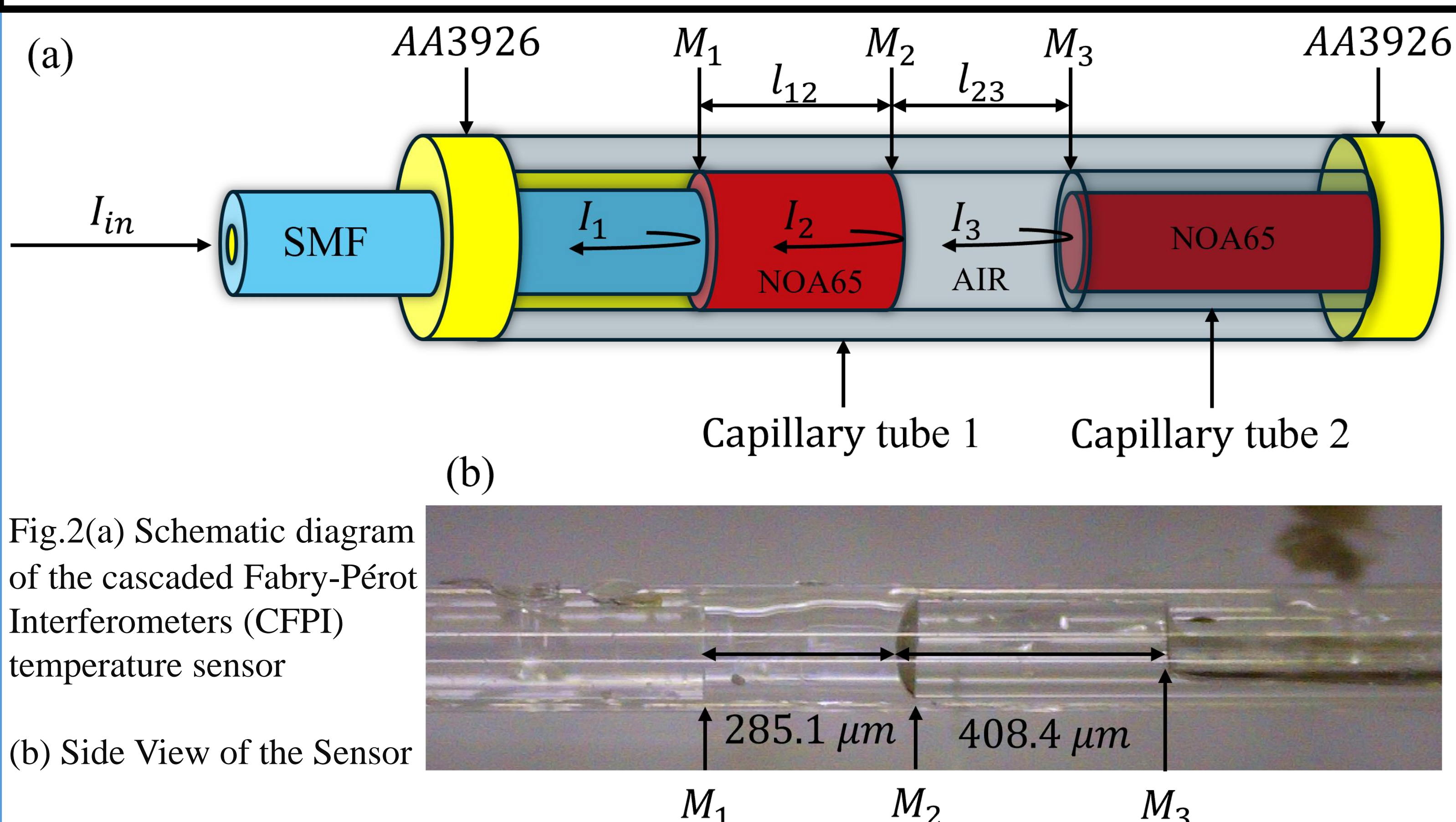


Fig.2(a) Schematic diagram of the cascaded Fabry-Pérot Interferometers (CFPI) temperature sensor

(b) Side View of the Sensor

•Enhanced Harmonic Vernier Effect

Enhances sensitivity(26.67 nm/ °C) with greater fabrication tolerance.

•Material Innovation

UV adhesives (NOA65) have outstanding thermal-expansion ability

•Biocompatibility

Fabricated by biocompatible material(optical fiber and AA3926).

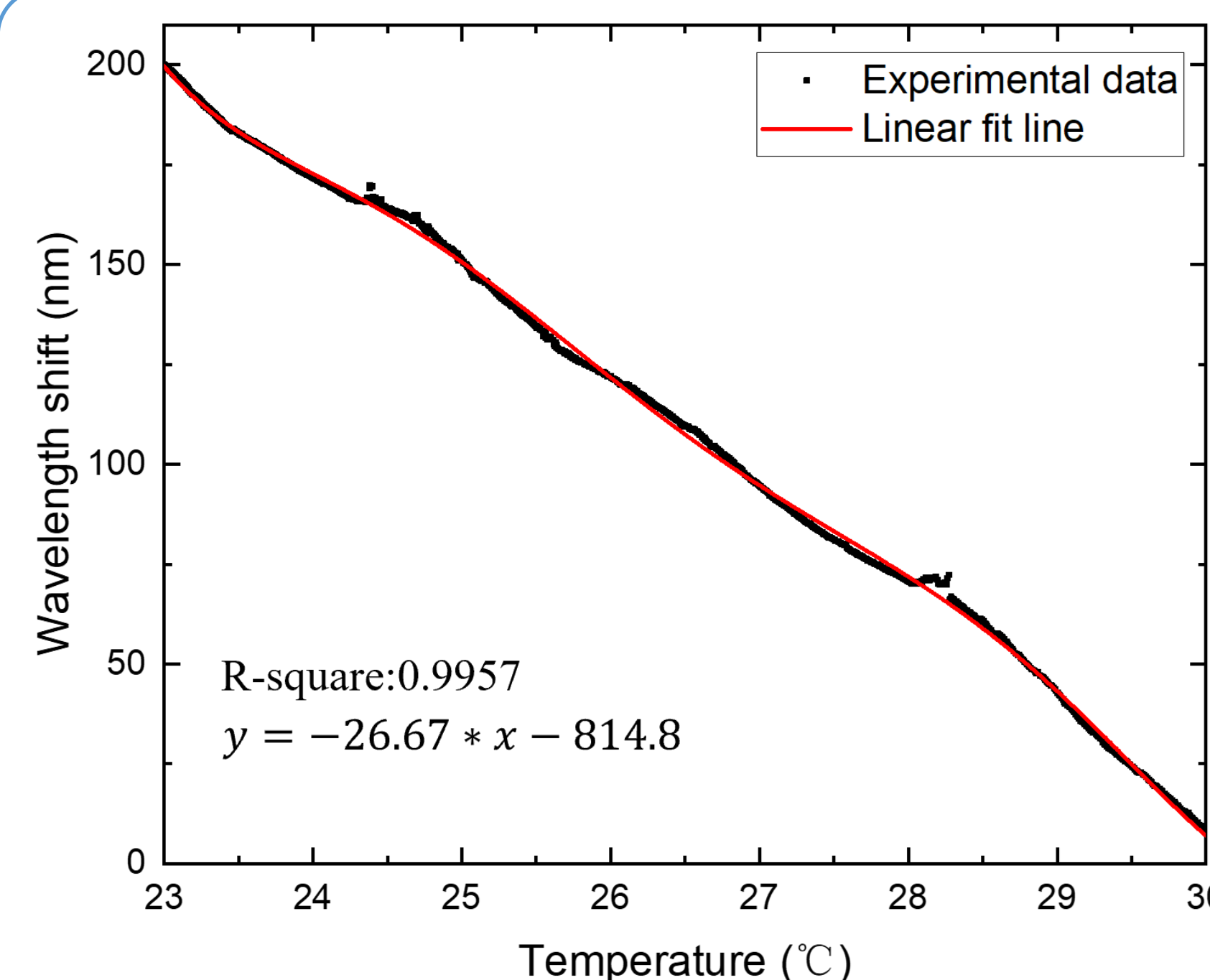


Fig.3 Temperature Sensitivity of the CFPI

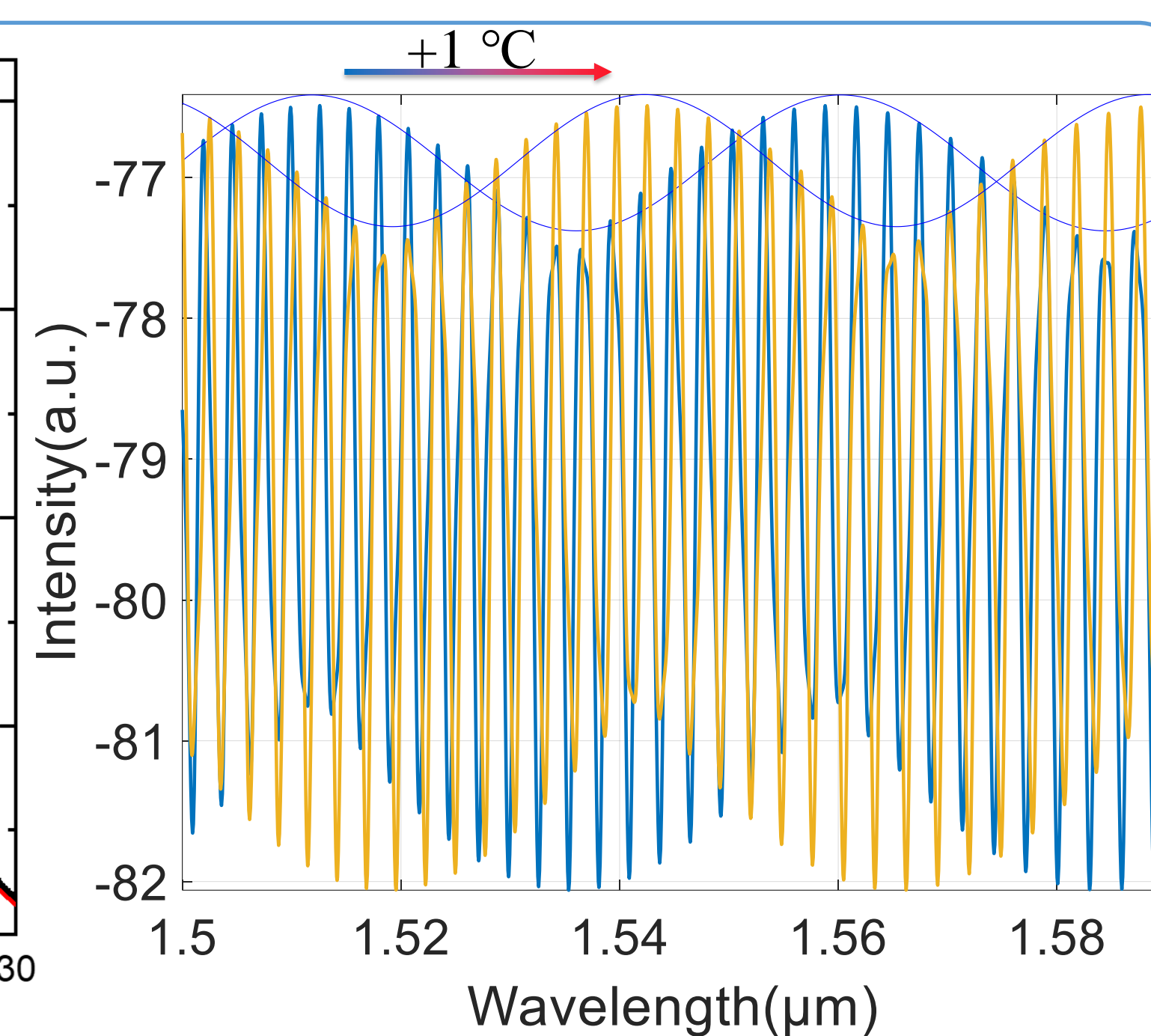


Fig.4 Spectral Variation of CFPI at Different Temperature

Configuration

Configuration	Sensitivity(nm/°C)
Fiber Bragg Grating, FBG[1]	0.027
Long Period Fiber Grating, LPFG[2]	0.1
Single polymer F-P cavity	0.62
CFPI with traditional vernier effect	8.9
CFPI with enhanced harmonic vernier effect	26.67

Blood flow measurement

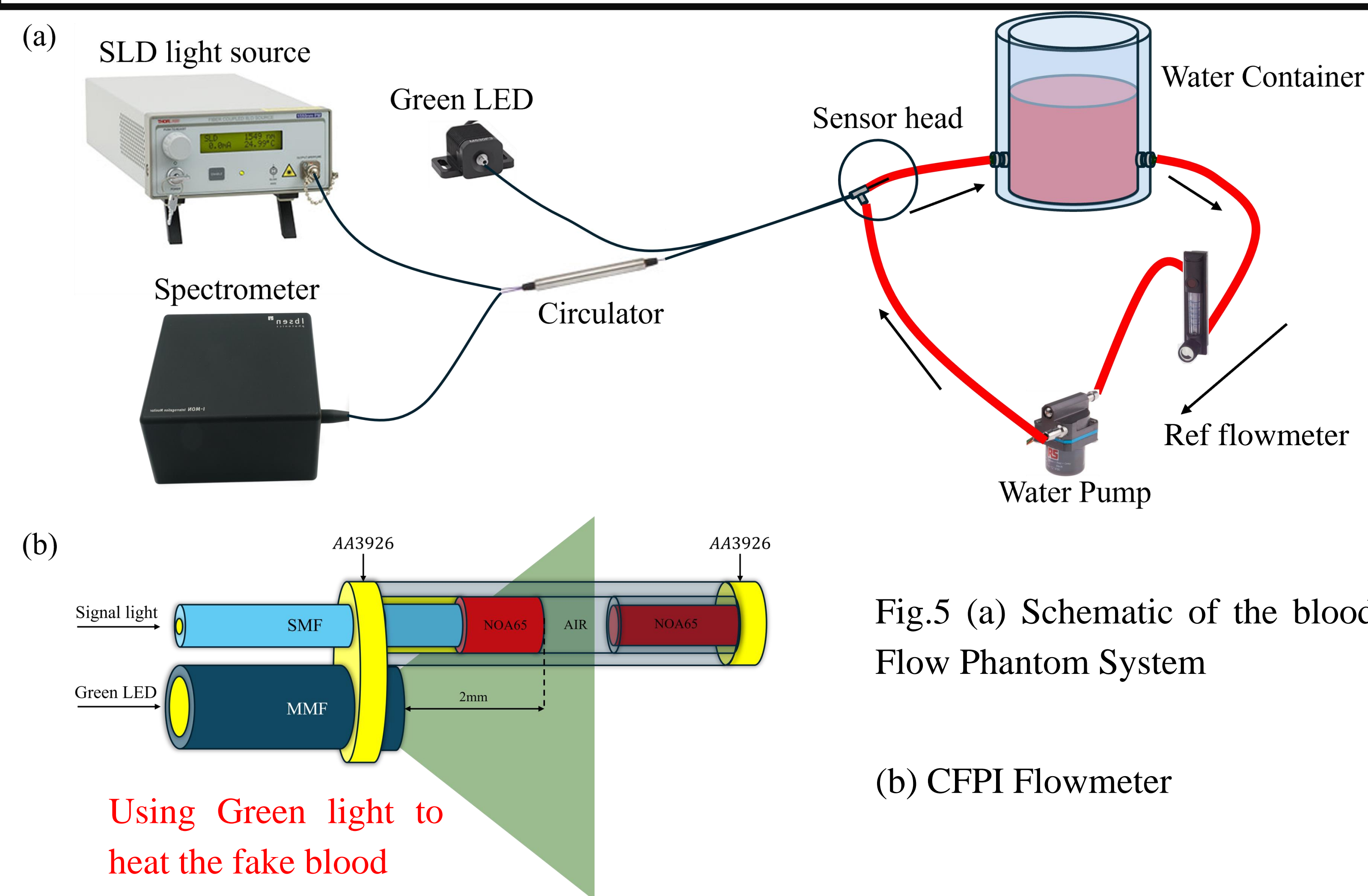


Fig.5 (a) Schematic of the blood Flow Phantom System

(b) CFPI Flowmeter

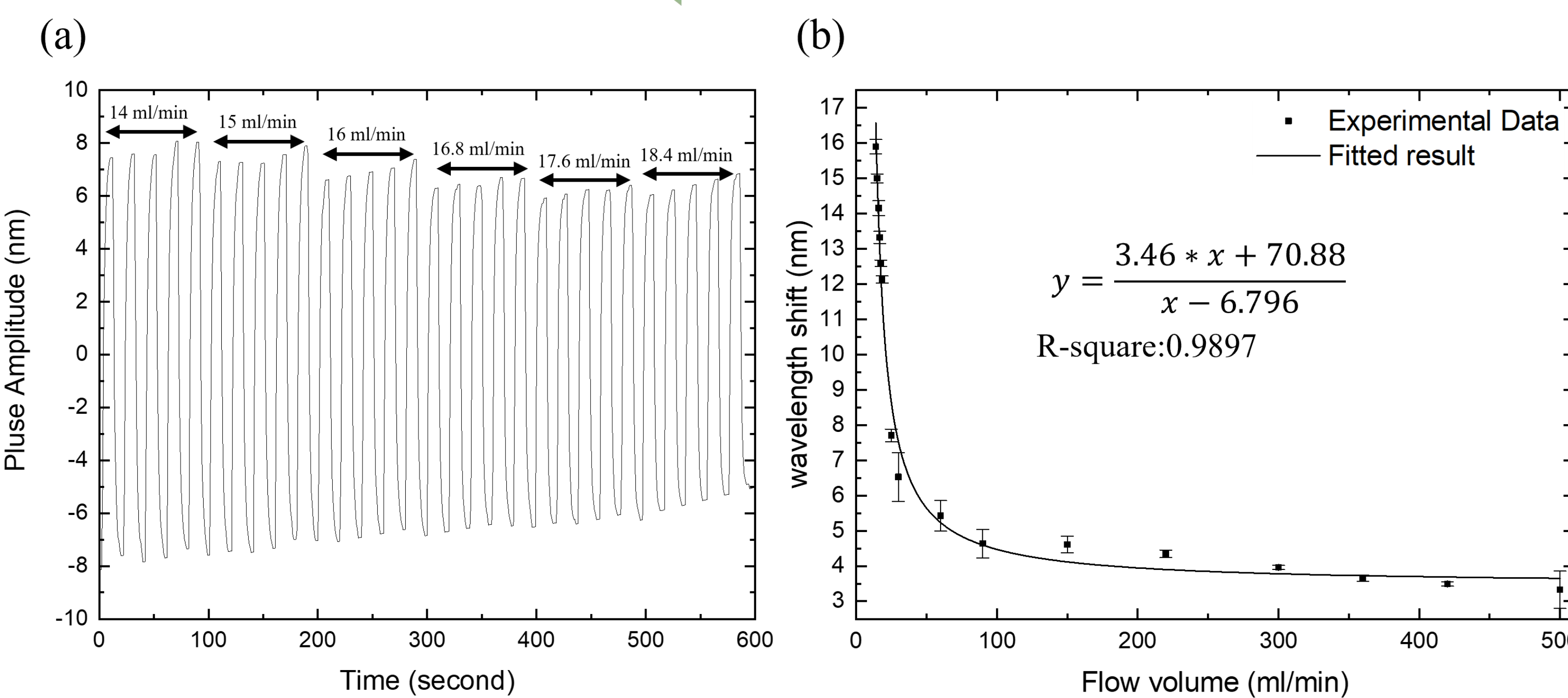


Fig.6 (a) Wavelength shift of the spectrum with different flow volume (b) Flow volume versus Wavelength Shift

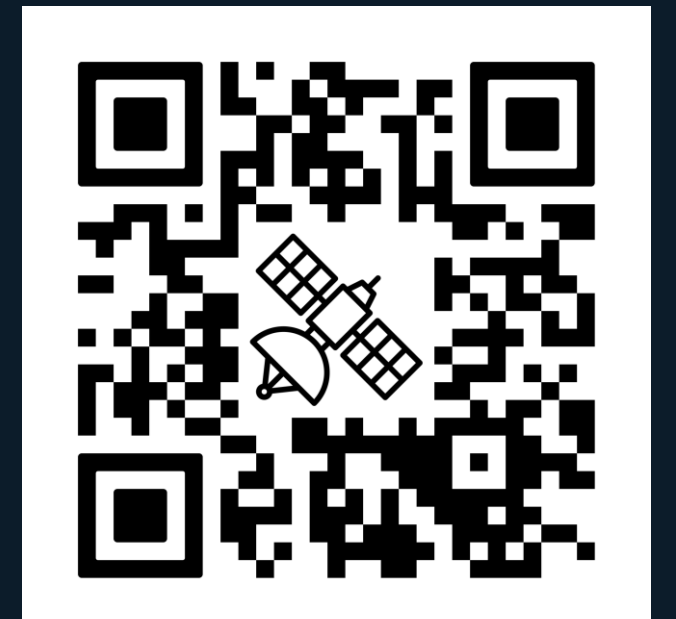
Conclusion

1. Designed an ultra-sensitive temperature sensor using the Enhanced Harmonic Vernier Effect with 26.7 nm/°C sensitivity.
2. Successfully measured blood flow volume from 14 to 500 ml/min using CFPI sensor.



A Novel RF Interference Detection and Geolocation Algorithm by LEO Satellites

Tasneem Yousif (tasneem.yousif@nottingham.ac.uk)
Supervisors: Dr. Paul Blunt; Dr. Peter Christopher



1. Introduction

Global Navigation Satellite Systems (GNSSs) have become essential for many different civilian applications, especially **space applications**. Jamming signals, spoofing signals, and multipath signals are among the major challenges that GNSS receivers face. This has led to the development of many **geolocation and detection algorithms** to address these issues.

2. Research Aims

- **Characterize and map** the interference of the GNSS for space applications.
- Assess the complexity of different interference scenarios in terms of **types, power level, and number of interferences**.
- A novel algorithm will be developed to detect the RFI by **LEO satellites** using **simulated GNSS data** and validating it against the historical raw data from **SSTL DoT-1, TDS, and CYGNSS** satellites.

3. Methods

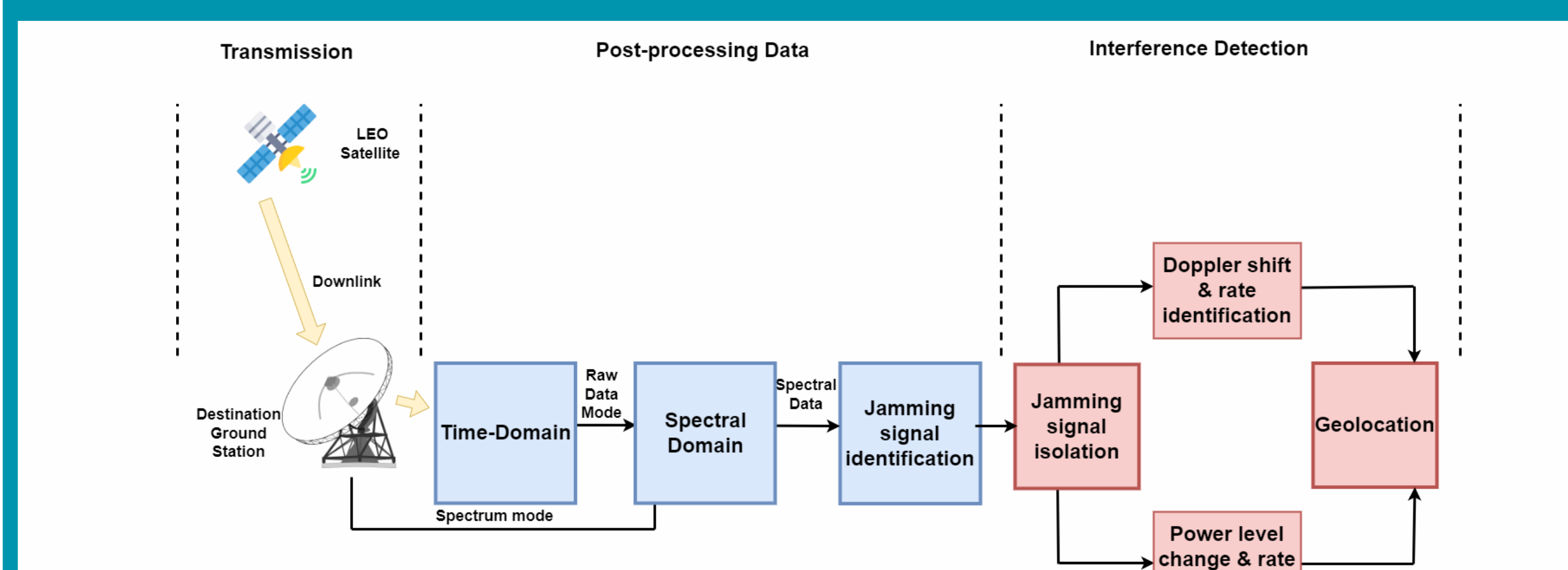


Fig.1: Ground Segment Post-Processing Methodology

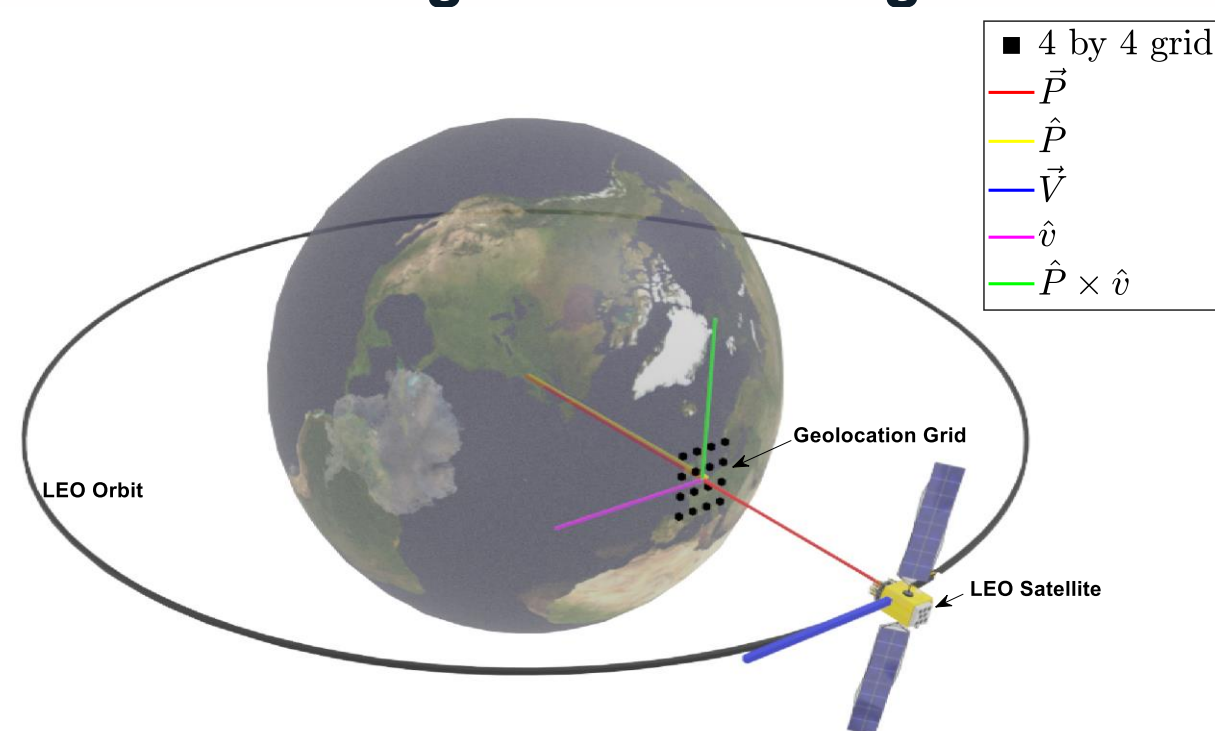
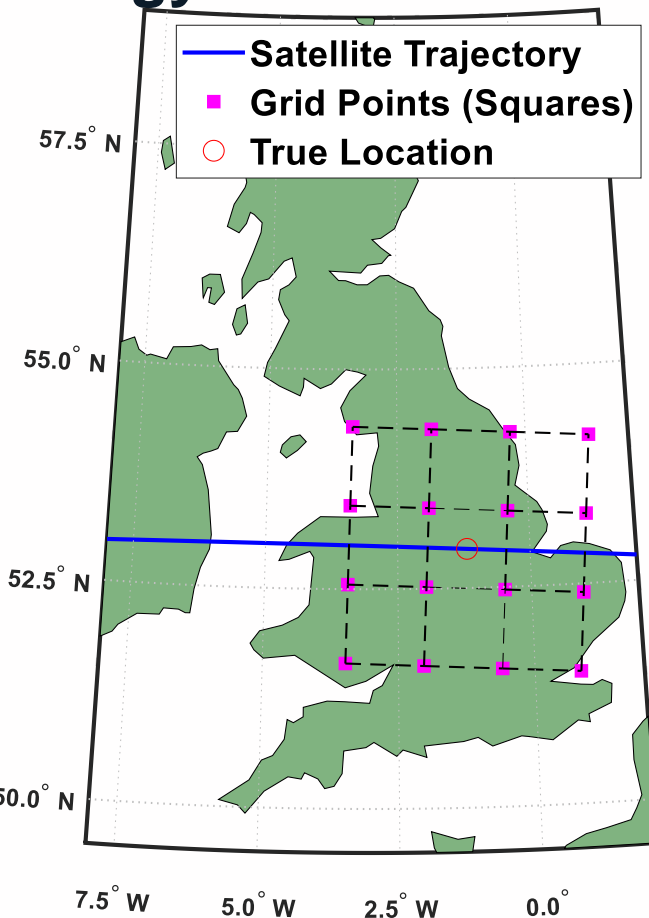


Fig.2: 3D Visualization of a LEO Satellite with the key vectors

Fig. 3: Grid points, the true location, and the satellite trajectory located at the University of Nottingham.



4. RFI Identification

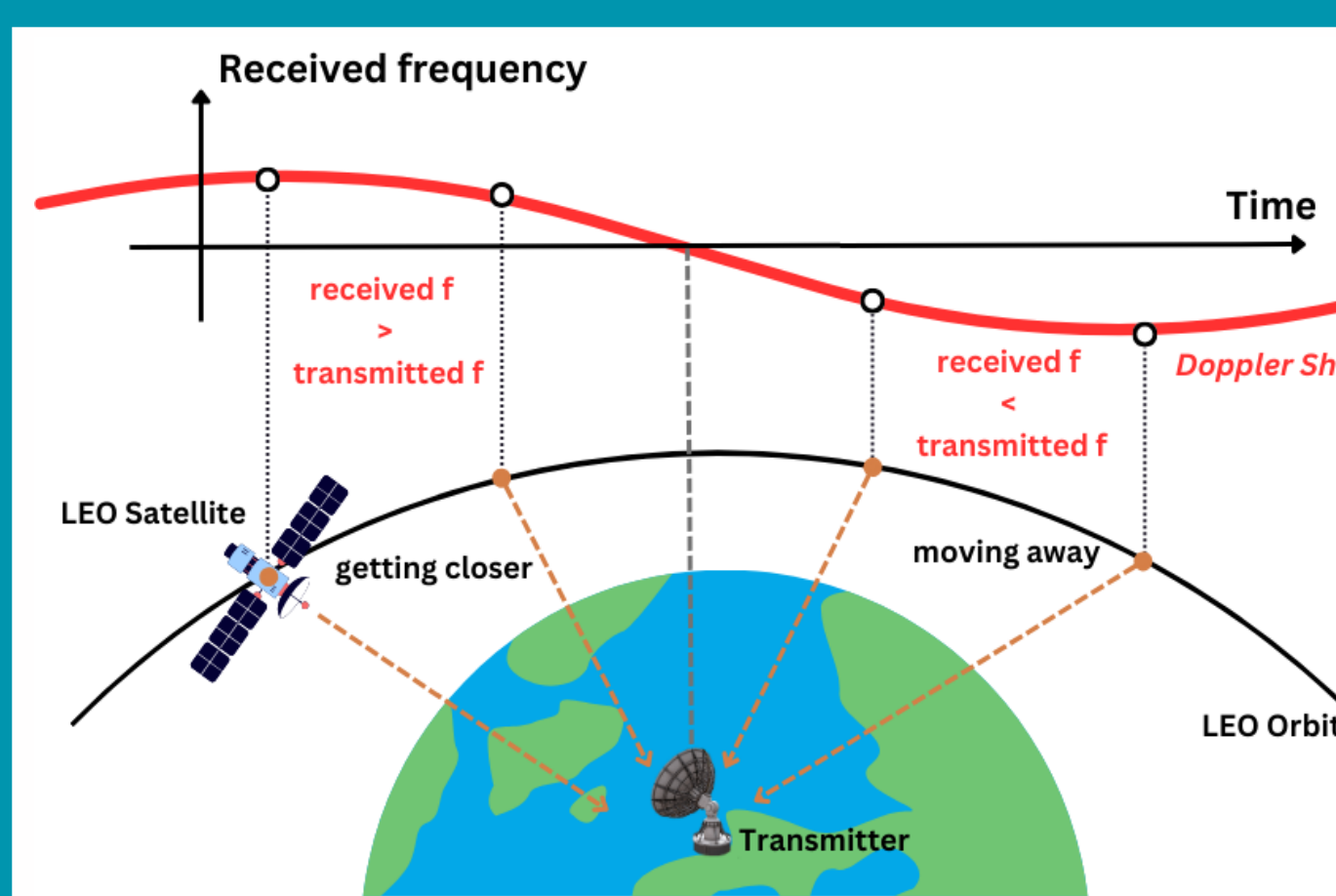


Fig.4: Overview of the Doppler Effect

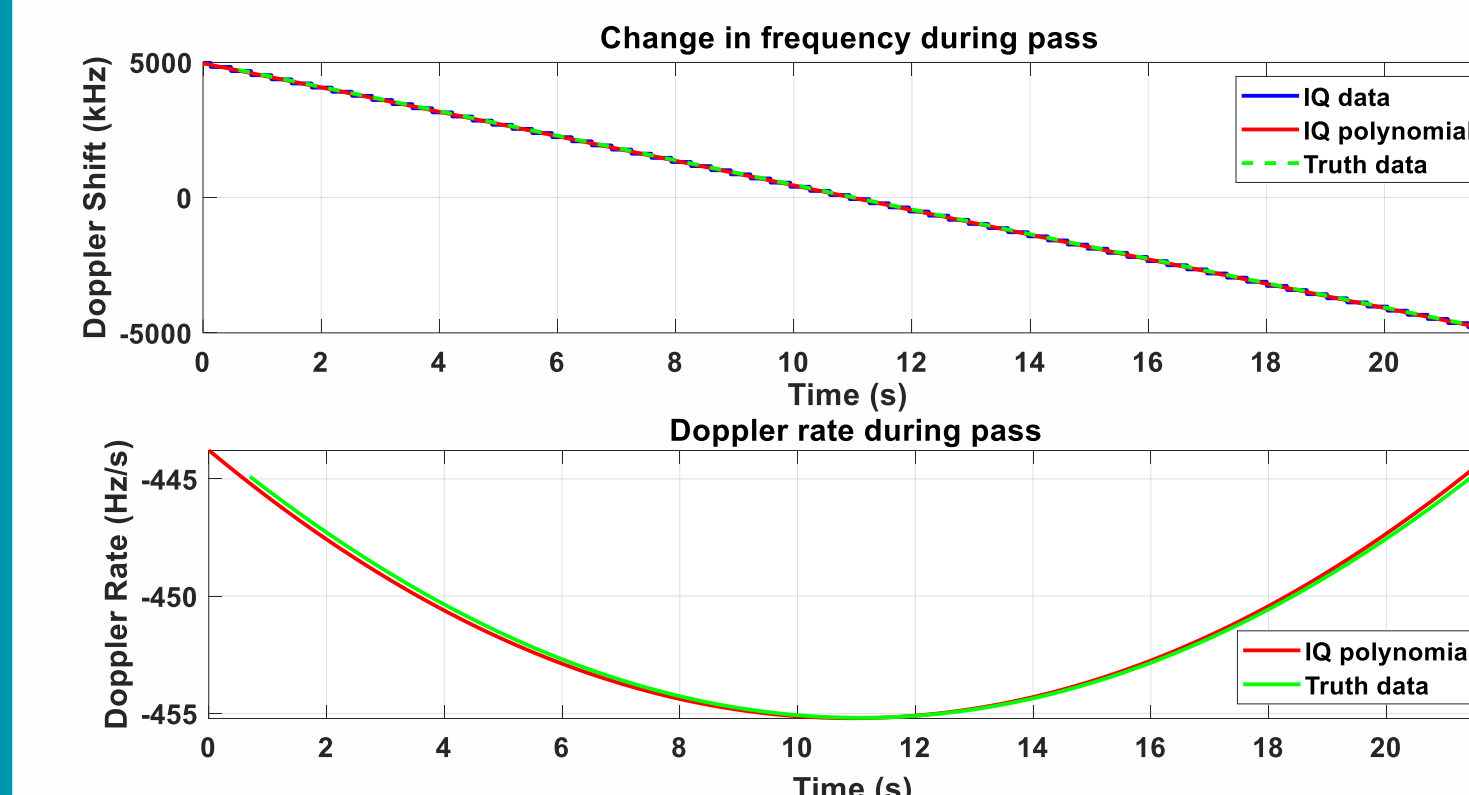


Fig. 6: Doppler shift and Doppler rate comparison for the 20-second simulated data overhead the transmitter

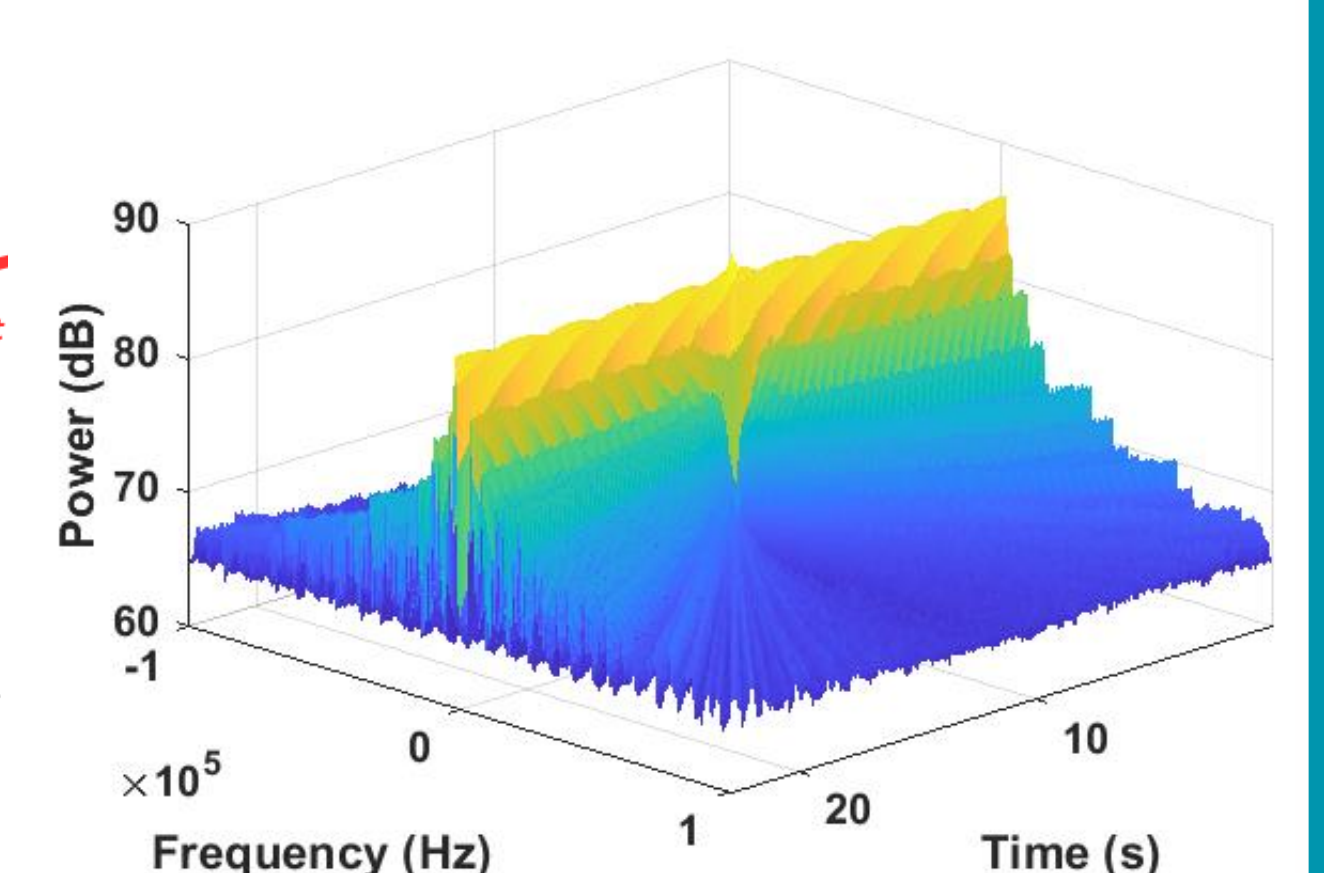


Fig.5: A 10 s extract of the CW simulation.

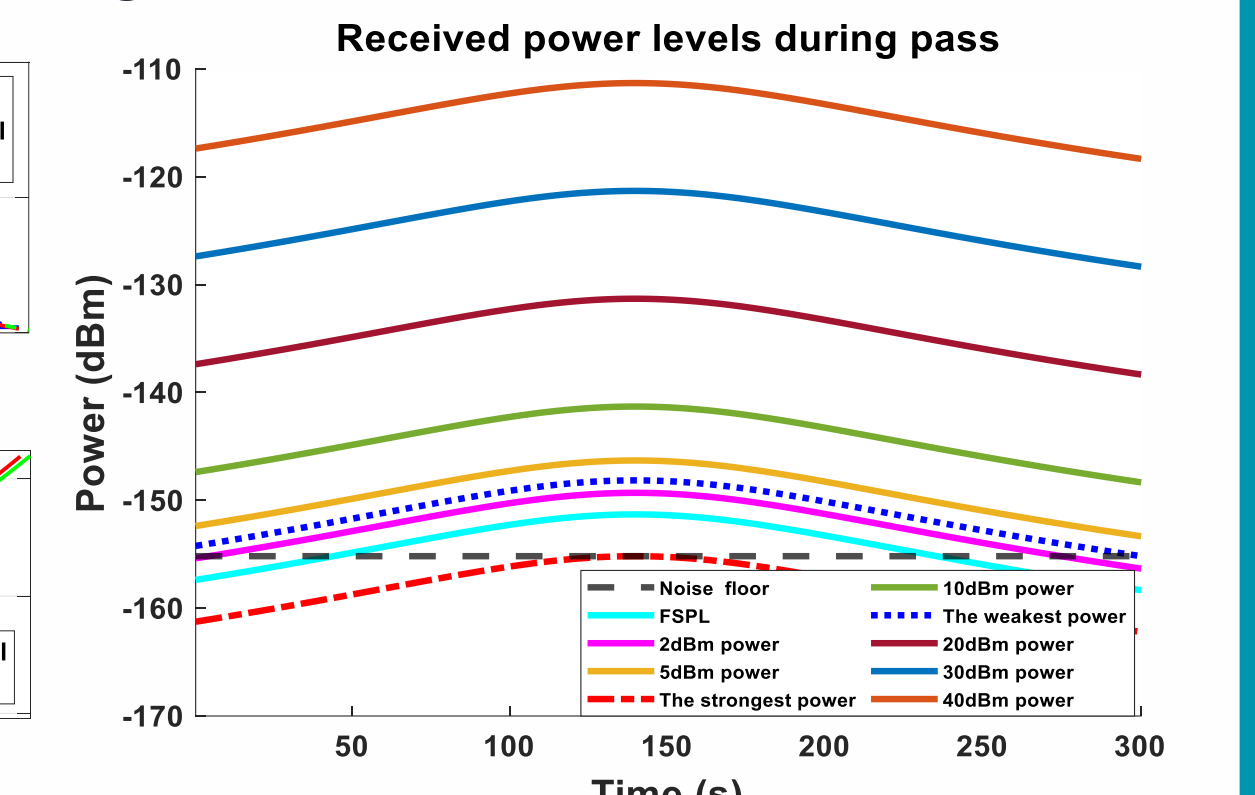


Fig.7 The received power levels of various signals

5. RFI Geolocation Results

The mean error between the ground truth Doppler rate and the measurement Doppler rate is **0.13 Hz/s**. The geolocation algorithm was utilized and performed extremely well converging within **7.6 seconds** to within approximately **1-kilometre range** of the true transmitter position over a **600 km** search space.

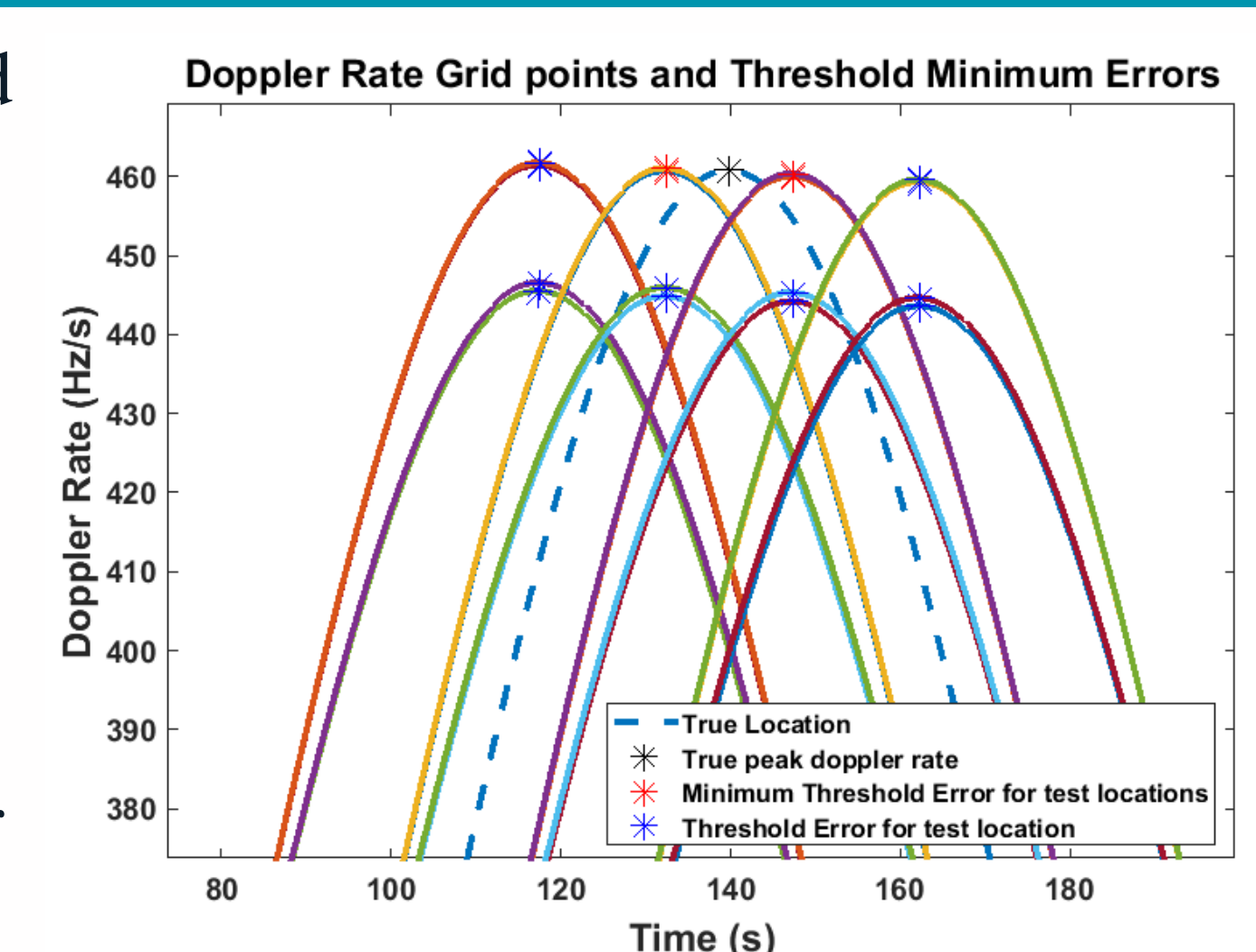


Fig.9 4 minimum errors based on the combination threshold of 16 grid positions on the peak of the Doppler rates

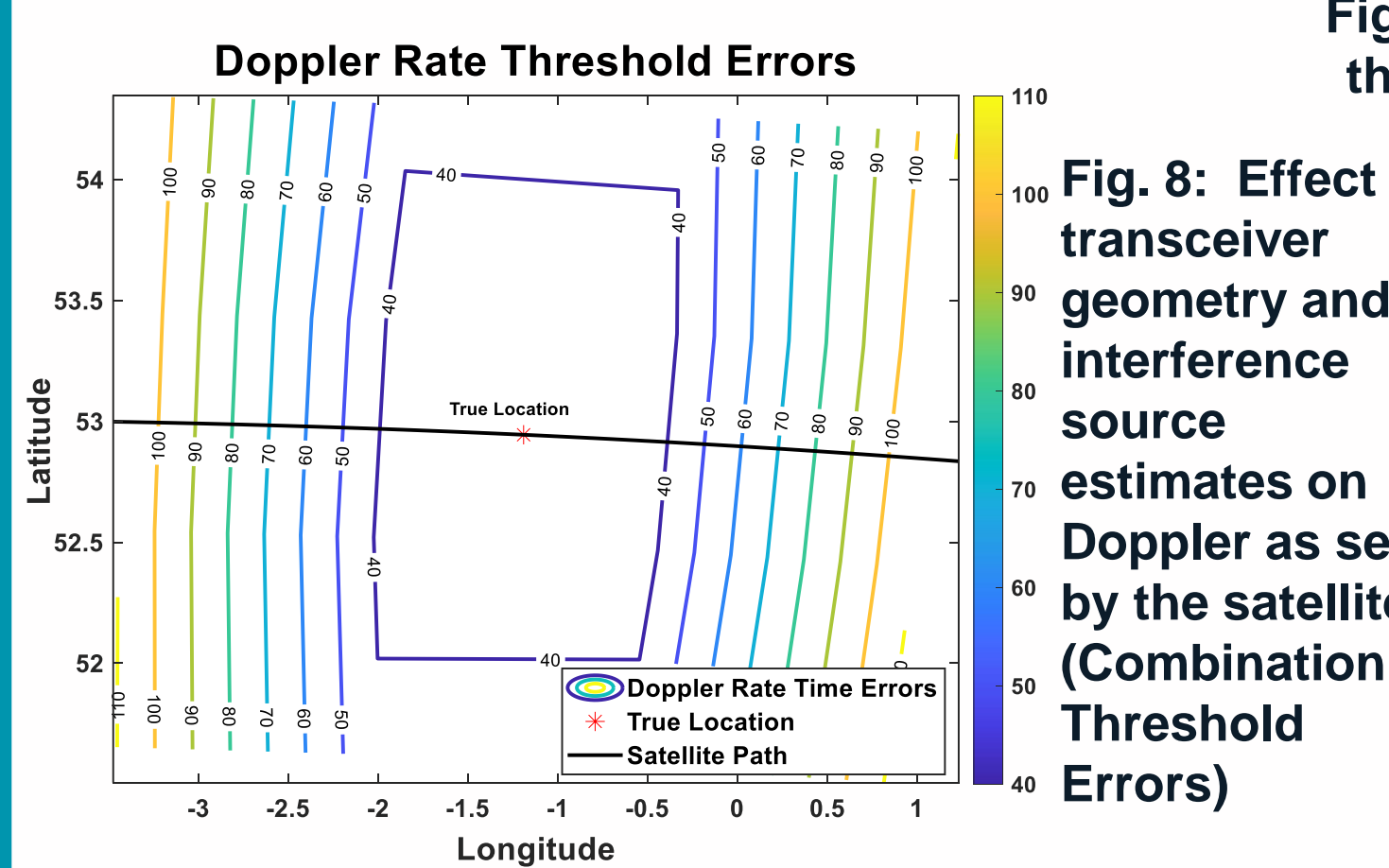


Fig. 8: Effect of transceiver geometry and interference source estimates on Doppler as seen by the satellite (Combination Threshold Errors)

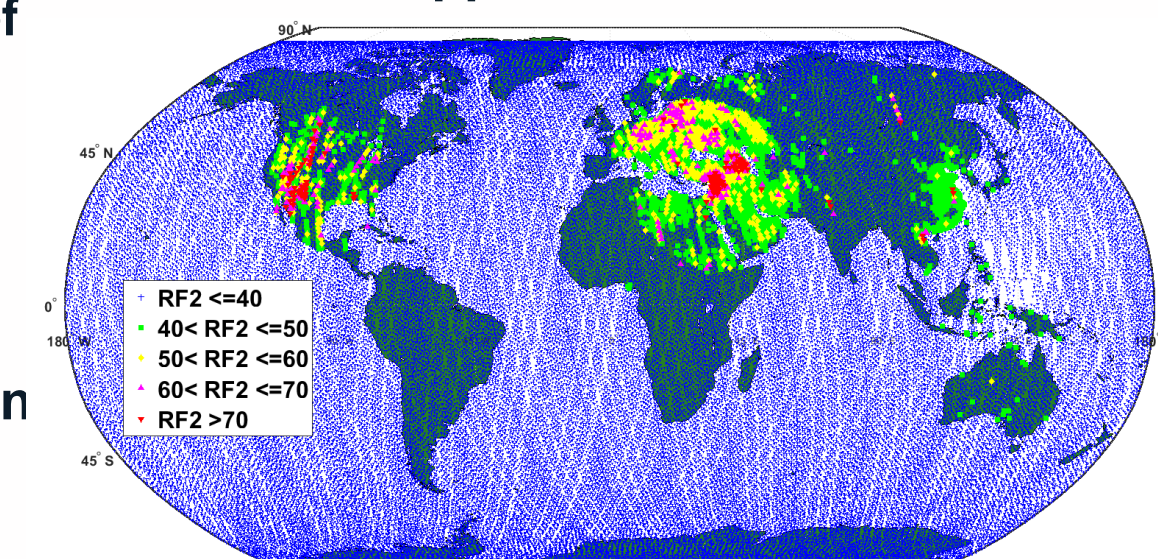


Fig. 10: Global distribution of the RF2 Magnitude % for TDS-1 Satellite.

6. Conclusion and Future Works

- A geolocation algorithm using an **estimated grid** has been developed and tested with the **Quasi-simulated RFI** and validated against the **historical data** from the **TDS-1 Satellite**.
- Developing a novel algorithm to detect and locate the RFI on the **CYGNSS** and **DoT-1** data using the geolocation grid and **Kalman filters**.

References

- [1] H. Witzgall, "A reliable Doppler-based solution for single sensor geolocation," in 2013 IEEE Aerospace Conference, 2013: IEEE, pp. 1-7.
- [2] Ellis, P., D. Van Rheeden, and F. Dowla, Use of Doppler and Doppler rate for RF geolocation using a single LEO satellite. IEEE Access, 2020. 8: p. 12907-12920.



The Politicisation of Fuel Poverty in England: Obfuscation, Metrics & Energy Justice

Torran Semple¹, email: torran.semple@nottingham.ac.uk

Supervisors: Lucelia Rodrigues¹, Mark Gillot¹, Graziela Figueredo², John Harvey³

¹Department of Architecture & Built Environment; ²School of Computer Science, ³N/LAB, Nottingham University Business School

Background

In 2019, the UK Government changed the definition of fuel poverty in England. The Low Income Low Energy Efficiency (LILEE) metric only considers a household to be fuel poor if (i) *residual household income is below the poverty line (following energy expenses)* and (ii) **the home has an EPC rating of D–G** [1]. Approximately 40% of homes in England have an EPC rating of A–C and are therefore considered *not fuel poor* by default. To date, **Study 1** of my PhD [2] provides comprehensive evidence that the LILEE metric significantly underestimates fuel poverty, particularly among EPC A–C rated properties, and is not fit for purpose. As a result, the remaining studies in my PhD are as follows:

- **Study 2** (in progress) aims to develop and validate a new fuel poverty metric on a sample of English households. To achieve this, we are collaborating with an industry partner (Experian), who will provide us with household-level data, including income and composition. Initial results suggest that a new metric should prioritise multiple dimensions of fuel poverty, including energy security (self-reported energy affordability) [3], precarity (taking account of energy cost volatility) [4] and justice (ensuring an equitable energy transition) [5].
- **Study 3** aims to forecast fuel poverty according to various metrics in different future scenarios; for example: “hypothetically, if gas boilers were phased out of the English housing stock, how would this affect fuel poverty according to the LILEE metric, our newly developed metric or other alternatives?” Exploring this type of question will allow us to better understand a fuel poverty metric’s sensitivity to inevitable changes to the housing stock and will also aid the co-occurrence of fuel poverty’s alleviation and the decarbonisation of housing.

Study 1: Key findings (two-stage analysis of LILEE fuel poverty)

- **Stage 1** involved a spatial analysis of London, where we found unexpectedly pronounced deviations between deprivation and LILEE fuel poverty rates. This suggests that LILEE undercounts fuel poverty in low-income homes (see **Figure 1**). Following this, we used income, employment and energy efficiency data to estimate the number of financially vulnerable homes that are erroneously omitted from LILEE fuel poverty statistics; we found that **171,091 households (4.4% of London homes)** fitted this description.
- **In Stage 2**, we collected survey data (n=2887) to gauge the energy security (self-reported ability to afford sufficient energy) of London residents. The survey data showed that (i) the rate of energy insecurity is around 145% higher than the LILEE fuel poverty rate for London (11.5%) and (ii) is still experienced by those in EPC A–C rated homes.

Study 1: Policy implications & next steps

Study 1 showed that the government’s approach to measuring fuel poverty is not fit for purpose because of the indiscriminate omission of EPC A–C rated homes. As a result, we suggest that energy efficiency should not be an *essential* fuel poverty measurement criterion. We also recommend that further work be done to develop a metric that can more accurately identify all English homes that are unable to afford adequate warmth.

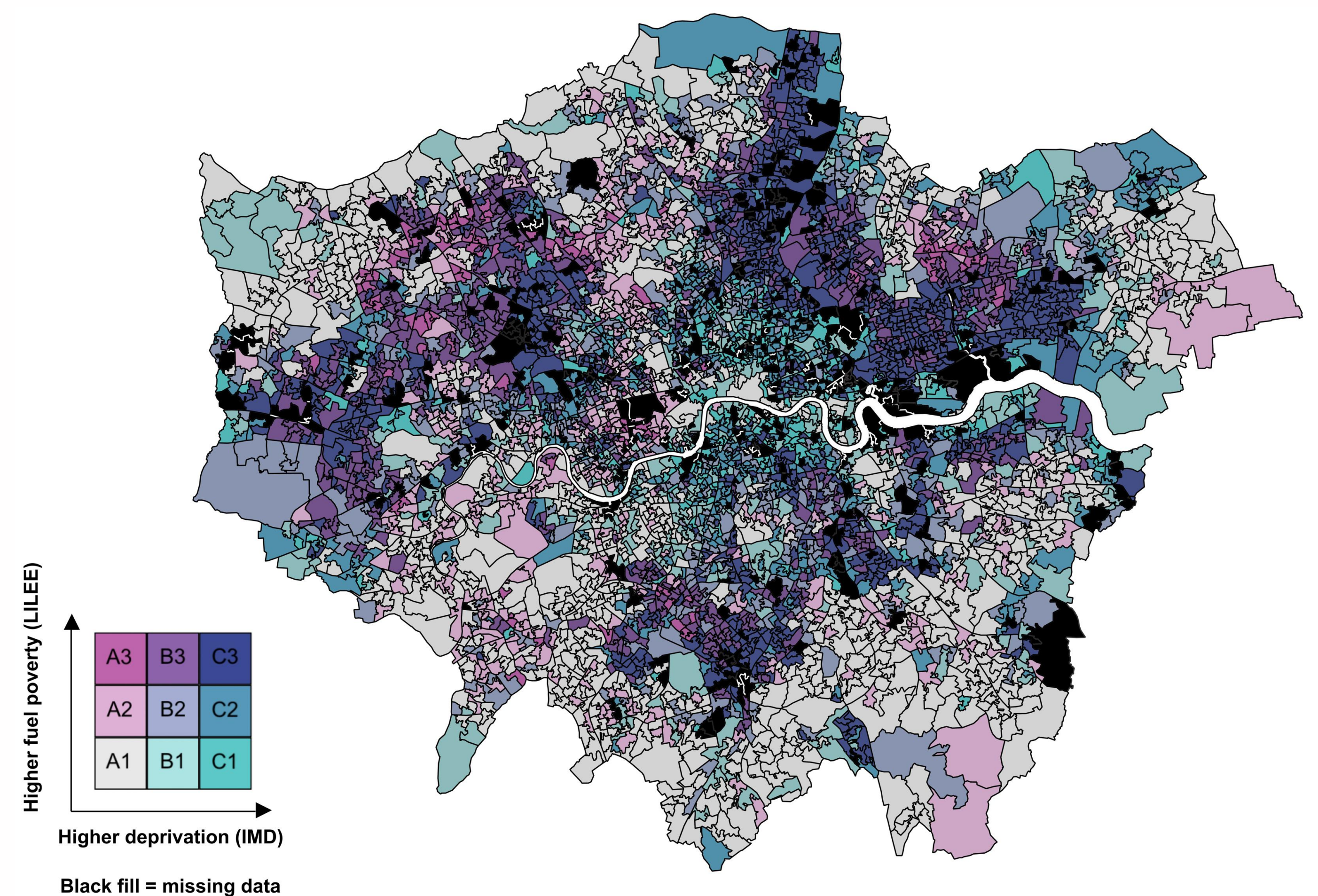


Figure 1. Bivariate choropleth map of Greater London: fuel poverty (LILEE) vs index of multiple deprivation (IMD)

Study 2: A new or amended fuel poverty metric in England

To date, an extensive literature review of existing deprivation and fuel poverty metrics was conducted to aid design considerations for a new English metric. So far, the Scottish and European Parliament fuel poverty definitions have provided inspiration. Both are significantly different from LILEE, as they do not place much focus on energy efficiency and include a clause to ensure minimum living standards. Also salient, are incipient concepts of energy precarity and justice.

The next stage of Study 2 will involve the testing and validation of contending metrics on a real sample of English households, supplied by the industry partner. In the meantime, a pilot analysis of potential fuel poverty metrics is being conducted on synthetic household income distributions for Nottingham.

Study 3: Energy justice and the eradication of fuel poverty

Study 3 will provide high-level forecasts of fuel poverty according to our new metric, as well as alternatives, with the aim of showing (i) the effect of hypothetical decarbonisation strategies on fuel poverty rates; and (ii) exploring routes to the eradication of fuel poverty. Stage (i) can help policymakers ensure that housing decarbonisation strategies do not exacerbate fuel poverty further, while Stage (ii) looks to reintroduce the notion of fuel poverty’s eradication to the discourse – as it was in the 2000s and 2010s, with the failed 2016 eradication target.

References

- [1] BEIS, 2021. Sustainable Warmth: Protecting Vulnerable Households in England. [Online] Available at: <https://www.gov.uk/government/publications/sustainable-warmth-protecting-vulnerable-households-in-england>
- [2] Harker Steele, A. J. & Bergstrom, J. C., 2021. “Brr! It’s cold in here” measures of household energy insecurity for the United States. *Energy research & social science*, Volume 72, p. 101863.
- [3] Semple, T. et al., 2024. An empirical critique of the low income low energy efficiency approach to measuring fuel poverty. *Energy Policy*, Volume 186, p. 114014.
- [4] Petrova, S., 2018. Encountering energy precarity: Geographies of fuel poverty among young adults in the UK. *Transactions - Institute of British Geographers* (1965), Volume 43, pp. 17-30.
- [5] Sovacool, B. K., 2015. Fuel poverty, affordability, and energy justice in England: Policy insights from the Warm Front Program. *Energy* (Oxford), Volume 93, pp. 361-371.

Machine Learning Estimation the Optical Properties of Tissues

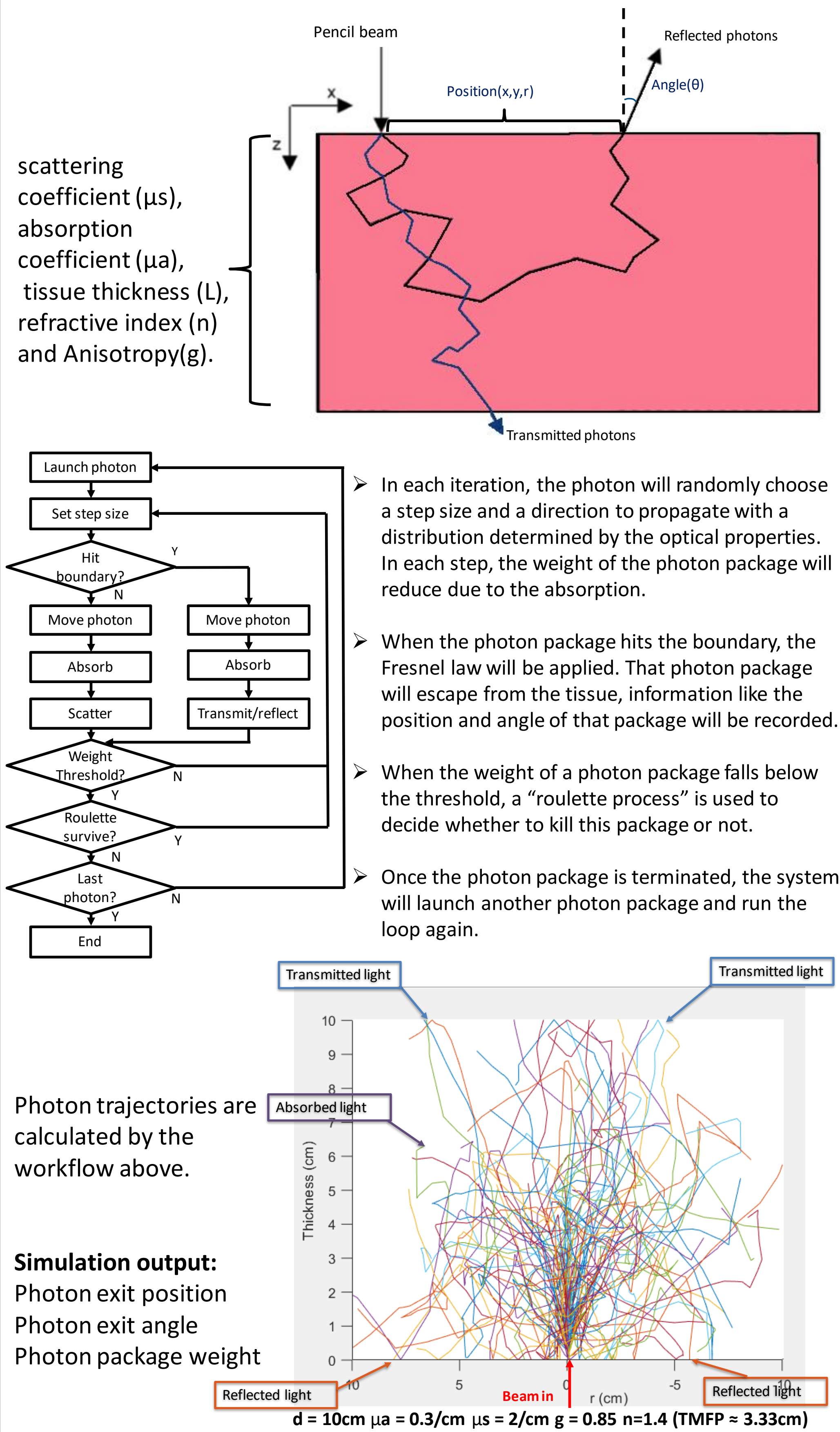
Yihan Zhang, Bowen Deng, Amanda J. Wright, Michael G. Somekh, Andrew Parkes, Michael Pound

Optics and Photonics Group, Faculty of Engineering, University of Nottingham, NG7 2RD, United Kingdom

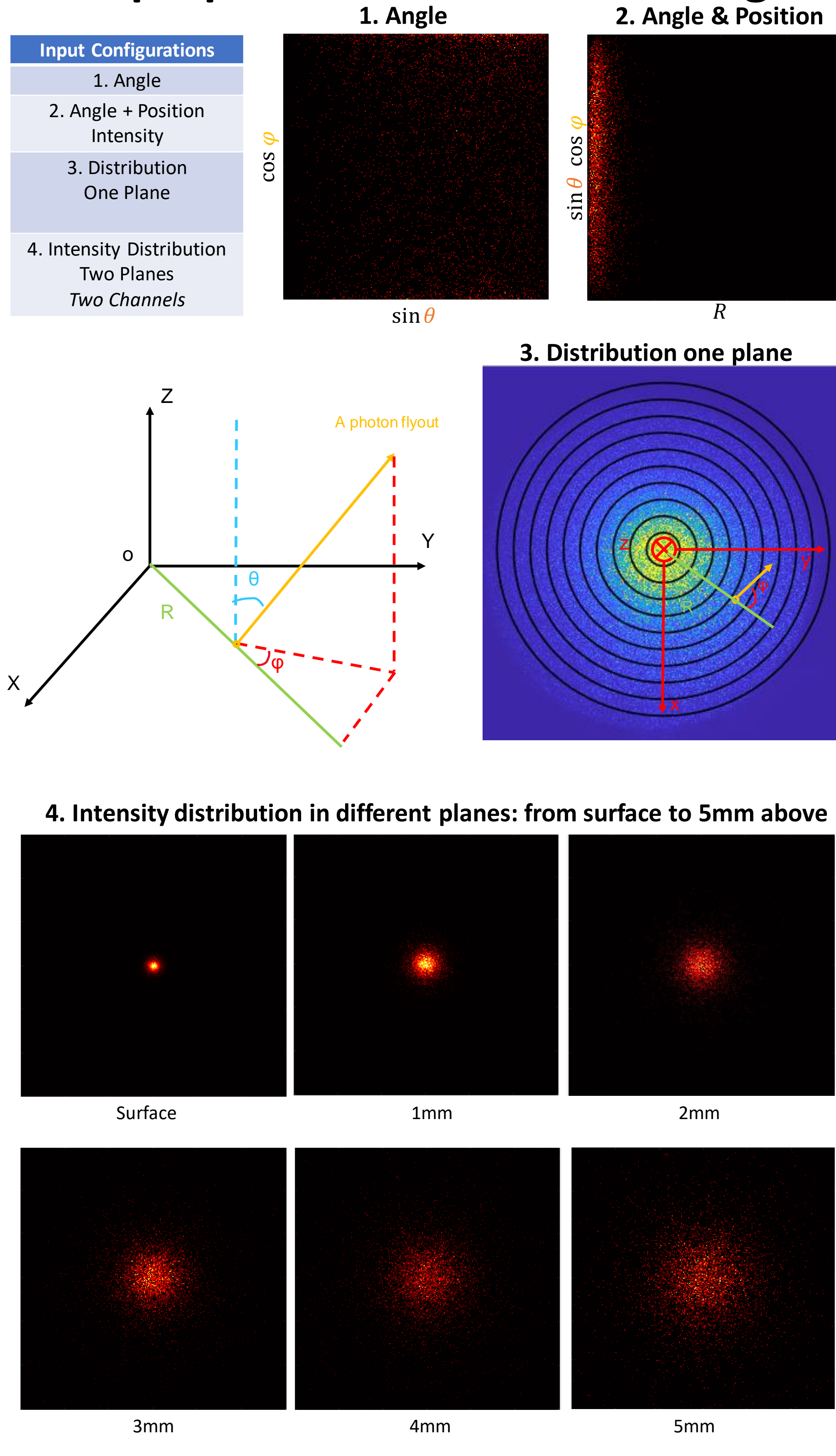
Motivation

- Understanding the **scattering** and **absorption** properties of biological tissue is crucial for achieving deep imaging. This is because for deep imaging wavefront correction is required to correct for scattering a produce a good focus.
- Current techniques to measure scattering and absorption coefficients, such as diffuse reflectance spectroscopy and spatial frequency domain imaging, require calibration and are only applied over limited regimes. Also, they require fitting a model to experimental data and make a series of assumptions. These techniques usually suffer from disadvantages such as poor estimation, long measurement time and requirements on the target material to be measured[1].
- This research aims to develop a fast and accurate in-vivo measurement method by **combining Monte Carlo simulation and machine learning**. We are training the neural network from the Monte Carlo generated light scattering pattern and aim to **separately measure the scattering coefficient, anisotropy and absorption coefficient**.

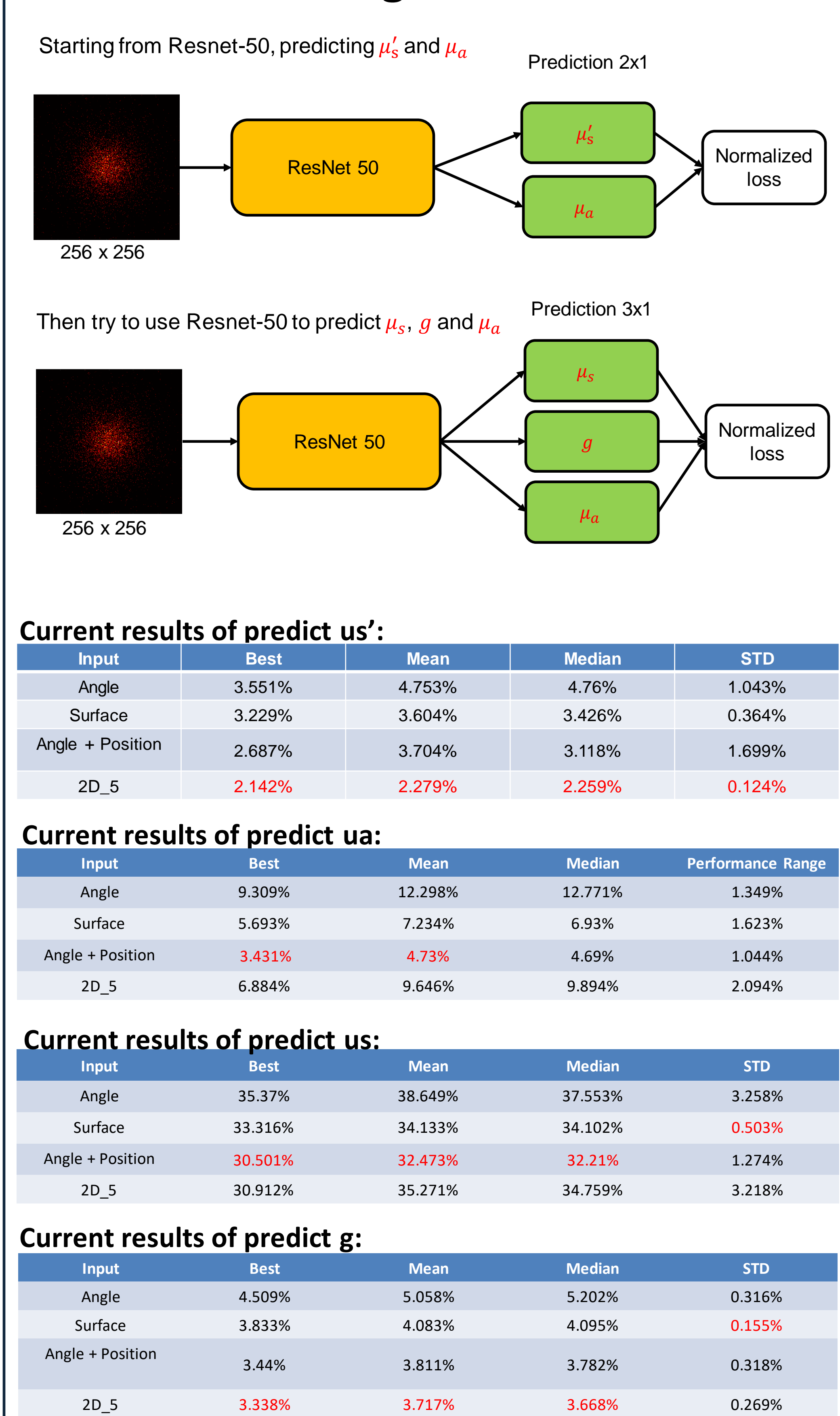
Monte Carlo Simulation



Data preparation – Transmitted light



Machine Learning



Conclusion

- A Monte Carlo was used to calculate the photon trajectories in a single-layer simulated tissue. 50,000 Monte Carlo simulation results have been generated with different optical properties and each simulation includes 40,000 photons.
- Simulation results are processed to train the neural network. The angle & position format including the most information and can let the network get the best performance. But the angle information is hard to measure in the lab. Two-intensity distributions then become the first choice because it not only produce a good training result but also easier to be measured in the lab.
- The currently worked-out model is based on Resnet-50 which can predict the reduced scattering coefficient within a 2.14% error and predict the absorption correction within a 3.43% error.

Future work

- Improve the network performance of separate predict μ_s' , μ_a and g .
- Block the photons on the edge of the image (limited the field of view) and check the network predicted performance.
- Collect and train the network based on the back scattering light.

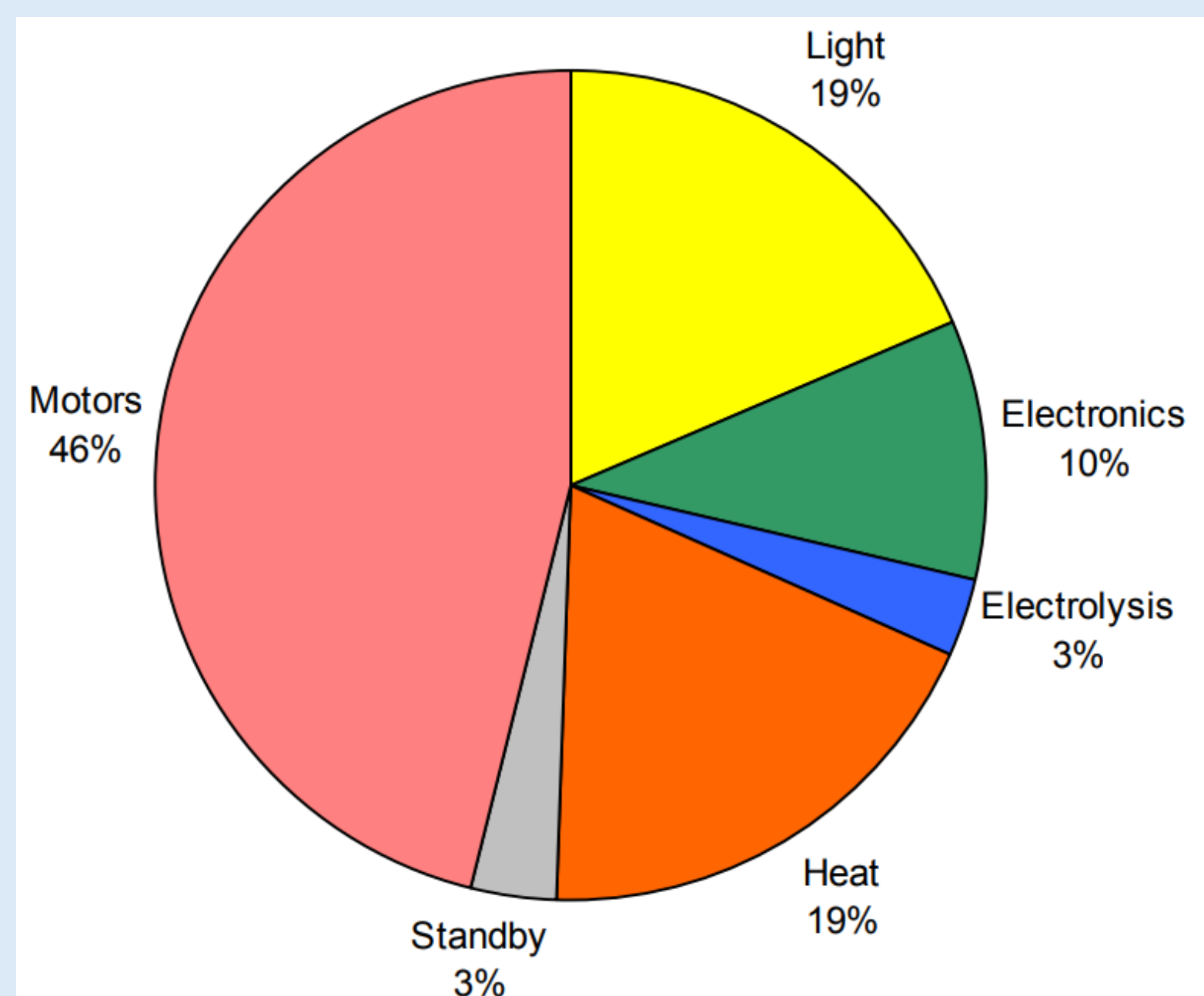
Reference

- [1] K. Setchfield, A. Gorman, A. H. R. W. Simpson, M. G. Somekh, and A. J. Wright, "Relevance and utility of the in-vivo and ex-vivo optical properties of the skin reported in the literature: a review [Invited]," *Biomedical Optics Express*, vol. 14, no. 7, 2023, doi: 10.1364/boe.493588
- [2] D. Wamcke, E. Lewis, S. Lochmann, and M. Leahy, "A neural network based approach for determination of optical scattering and absorption coefficients of biological tissue," *Journal of Physics: Conference Series*, vol. 178, 2009, doi: 10.1088/1742-6596/178/1/012047
- [3] X. Z. Lianshun Zhang, "Measurement of the Optical Properties Using Genetic Algorithm Optimized Neural Networks," *IEEE*, 2011.
- [4] M. Jager, F. Foschum, and A. Kienle, "Application of multiple artificial neural networks for the determination of the optical properties of turbid media," *J Biomed Opt*, vol. 18, no. 5, p. 57005, May 2013, doi: 10.1117/1.JBO.18.5.057005.
- [5] B. H. Hokr and J. N. Bixler, "Machine learning estimation of tissue optical properties," *Sci Rep*, vol. 11, no. 1, p. 6561, Mar 22 2021, doi: 10.1038/s41598-021-85994-w.



ADVANCING SUSTAINABLE PRACTICES IN ELECTRIC MOTOR DRIVE SYSTEMS TO DRIVE GLOBAL ENERGY EFFICIENCY

1. GLOBAL ENERGY CONSUMPTION SCENARIO¹



- Electric motors generate **over 6000 Mt** of CO₂ emissions annually.
- End-user expenditure is projected to increase to **\$900 billion** by 2030 from \$565 billion.

3. PROPOSED IDEA!!!

- **Boost system efficiency** by using advanced semiconductors
- Enable **smaller system sizes** through efficient electrical operation.
- Resulting in an **efficient** integrated drive

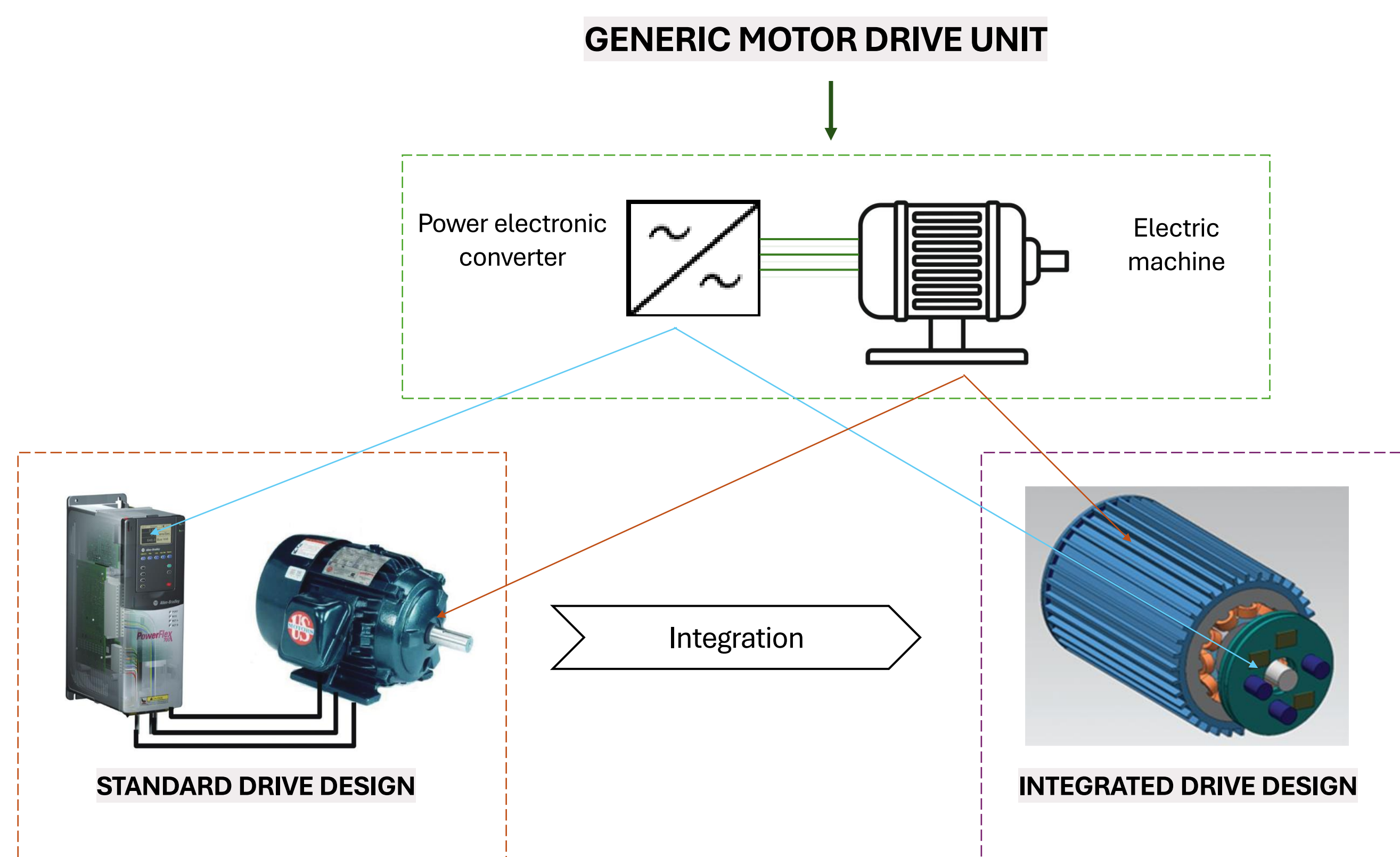
4. OUTCOMES

- Application in manufacturing, **automotive, aerospace** and **renewables** sectors.
- **Decreased** manufacturing cost.
- **Reduction** in carbon footprint.
- Improvements in **through-life efficiency**.
- **Easing adoption** of IMD in the UK.
- Assisting in fulfilment of the UK's **Paris climate commitments**.

1. Waide, P. and Brunner, C.U., 2011. Energy-efficiency policy opportunities for electric motor-driven systems.

2. WHY DO WE NEED EFFICIENT MOTOR DRIVE SYSTEMS¹?

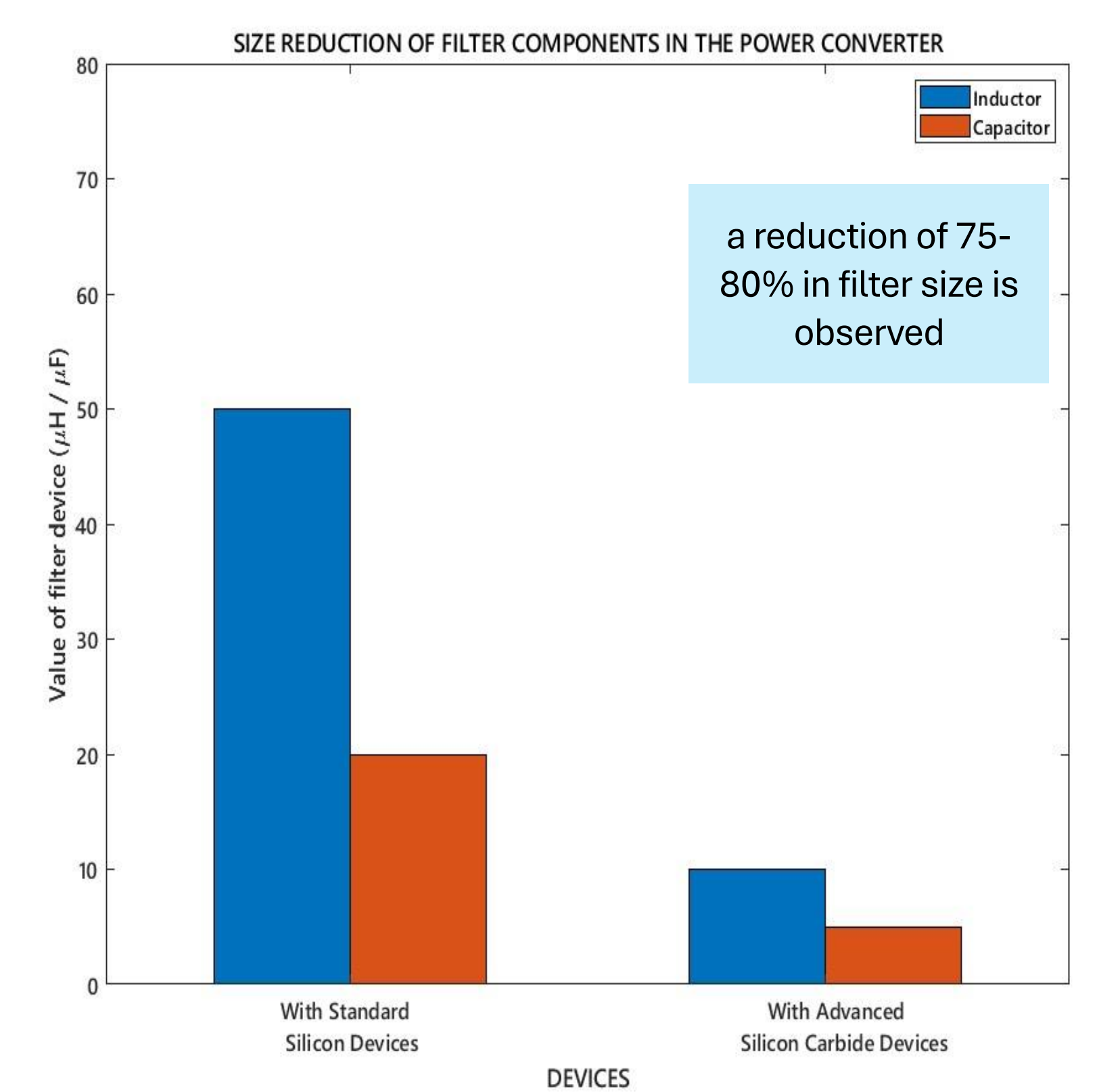
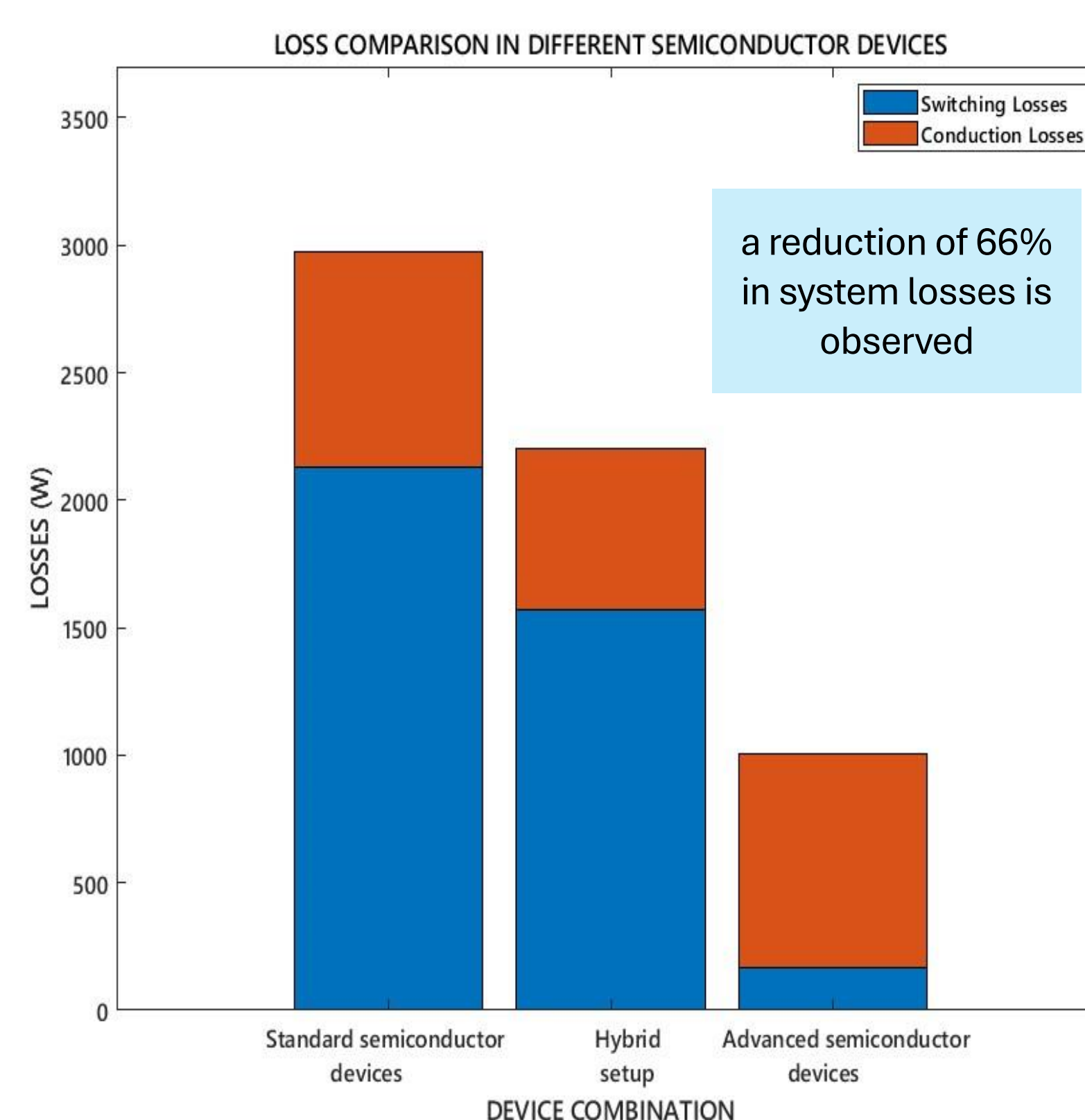
- There is a potential to achieve a **20-30% gain in efficiency** enhancement by utilising efficient motors.
- The expected outcome of above is to see a **10% reduction** in global electricity demand.



KEY ADVANTAGES:

- Increased space saving
- Enhanced operational efficiency
- Streamlined maintenance
- Reduced raw material usage

5. RESULTS



6. CONCLUSION

